2008

# Off-line MALDI mass spectrometry of bioaerosols

Jae-Kuk Kim
*Louisiana State University and Agricultural and Mechanical College*, jkim13@lsu.edu

# OFF-LINE MALDI MASS SPECTROMETRY OF BIOAEROSOLS

A Dissertation

Submitted to the Graduate Faculty of the
Louisiana State University and
Agricultural and Mechanical College
in partial fulfillment of the
requirements for the degree of
Doctor of Philosophy

In

The Department of Chemistry

by
Jae-Kuk Kim
B.S., Changwon National University, 1997
M.S., Changwon National University, 1999
August 2008

## DEDICATION

To my parents,

Soonyoung Choi and the late Inwhan Kim

and

My lovely wife, Hyeok Choi

and

My beloved two sons, Dohyung and Matthew

## ACKNOWLEDGMENTS

First of all, I would like to express my sincere gratitude to Prof. Kermit Murray for giving me an opportunity to do research in his lab and for his priceless guidance and advices during my doctoral degree. Without his guidance, I would not have been able to accomplish my work toward a doctoral degree. I am also thankful to my graduate committee for their invaluable suggestions in fulfilling my goal. I am grateful to the Mass Spectrometry Facility (MSF) of LSU and the facility personnel, Tracy McCarley and Michelle Beeson, for giving me an opportunity to learn and troubleshoot a number of mass spectrometers and for offering an opportunity for me to experience a variety of real sample analyses. I would also thank to the Louisiana State University Socolofsky Microscopy Center and Machine shop for providing microscopy services and fabricating numerous parts for mass spectrometer instrumentation.

I would also like to thank the former and current Murray group members, Nichole Bell, Sucharita Bhattacharya, Lancia Darville, Jianan Dong, John Dugas, Xing Fan, Juaneka Hayes, Fan Huang, Shelley Jackson, Jorge Laboy, Jehoong Lee, Mark Little, Harrison Musyimi, Damien Narcisse, Yohannes Rezenom, Udaya Rodrigo, David Rousell, Yichuang Xu, and Xia Zhang, who have helped me in completing this dissertation. Special gratitude goes to Mark Little and Shelley Jackson for their friendships, for all the good times and for their collaborative efforts with the Murray group projects. My appreciation is also extended to my friends, Jongtae Yang and Kyukwang Kim, who had graduated in this department, for their friendship and encouragement.

I would like to thank my pastor's family and all my church members at Korean Baptist Church of Baton Rouge for their invaluable spiritual support and encouragement. Especially, they had helped my family when we had been troubled with my kid's illness. Thanks to God for everything You blessed us with.

The most sincere thanks and appreciations go to my lovely wife, Hyeok Choi. She always gave me her encouragement and endless love. Without her love and devotion, I could not have accomplished my study here. I would also like to thank my beloved sons, Dohyung and Matthew, and express my deepest love to them.

Finally, I would like to sincerely acknowledge my mother, Soonyoung Choi, brother, Jaeha Kim, and sister, Mihyun Kim in Korea. They always gave me their unconditional love and support.

## TABLE OF CONTENTS

## LIST OF TABLES

## LIST OF FIGURES

## LIST OF ABBREVIATIONS

| | |
|---|---|
| AC | alternating current |
| ACN | acetonitrile |
| Ara | arabinose |
| ARD | Arizona road dust |
| BSA | bovine serum albumin |
| CA | 3,4-dihydroxy-cinnamic acid, caffeic acid |
| CDC | Centers for Disease Control and Prevention |
| CE | capillary electrophoresis |
| CEM | channel electron multiplier |
| CHCA | -cyano-4-hydroxy-cinnamic acid |
| CI | chemical ionization |
| CID | collision induced dissociation |
| Da | dalton |
| DCM | dichloromethane |
| DE | delay extraction |
| DG | delay generator |
| DHB | dihydroxybenzoic acid |
| DIOS | desorption/ionization on silicon |
| EI | electron ionization |
| EM | electron multiplier |
| Er:YAG | erbium-doped yttrium aluminium garnet |
| ESI | electrospray ionization |
| FA | trans-hydroxy-3-methoxycinnamic acid, ferulic acid |
| FAB | fast-atom bombardment |
| FT-ICR | Fourier-transform ion cyclotron resonance |
| FWHM | full width at half maximum |
| Gal | galactose |
| GPIB | general purpose interface bus |
| HPLC | high performance liquid chromatography |
| HV | high voltage |

| | |
|---|---|
| Hyp | hydroxyproline |
| IM | ion mobility |
| IMS | ion mobility spectrometry |
| IR | infrared |
| IT | ion trap |
| LDI | laser desorption ionization |
| MALDI | matrix-assisted laser desorption/ionization |
| MCP | microchannel plate |
| MS | mass spectrometry |
| MW | molecular weight |
| *m/z* | mass-to-charge ratio |
| Nd:YAG | neodymium-doped yttrium aluminium garnet |
| Nd:YLF | neodymium-doped yttrium lithium fluoride |
| OA | orthogonal array |
| o-TOF | orthogonal time-of-flight |
| ppm | part per million |
| psi | per square inch |
| RF | radio frequency |
| RSD | relative standard deviation |
| SA | 3,5-dimethoxy-4-hydroxycinnamic acid, sinapinic acid |
| SEM | scanning electron microscopy |
| Si | silicon wafer |
| S/N | signal-to-noise ratio |
| SS | stainless steel |
| Succinic acid | 1,2-ethanedicarboxylic acid |
| TDC | time-to-digital |
| TFA | trifluoroacetic acid |
| TOF | time-of-flight |
| UV | ultraviolet |

## ABSTRACT

Matrix-assisted laser desorption/ionization time-of-flight mass spectrometry was used for off-line analysis of bioaerosols. The overall goal of the work is to develop methods and instrumentation to minimize sample treatment and maximize sensitivity and selectivity for bioaerosol analysis. This work is divided into three parts: sample preparation, test bioaerosol analysis, and instrument development. Untreated silicon wafer substrates were used as an alternate to conventional stainless steel targets and proved to be excellent substrates for large molecule analyses as well as small molecule analyses with excellent spot-to-spot and shot-to-shot reproducibility, which is useful for high-throughput and automated sample analysis. MALDI sample preparation was optimized by the $L_9$ ($3^3$) orthogonal array of Taguchi's systematic approach using the effects of various parameters such as matrices, solvents, and deposition methods. Test bioaerosol particles were generated from a nebulized bacterial suspension and were collected onto bare or matrix pre-coated MALDI targets placed in an impactor for off-line analysis. The MALDI matrices or solvents were added on the target afterward by pipette or spraying to obtain signals similar to the dried droplet method. Finally, two novel MALDI mass spectrometers were constructed to test new bioaerosol ionization approaches. A transmission geometry MALDI-MS, in which the laser irradiates samples from back side of the target, enabled a tight laser focusing by coupling a microscope objective lens outside of the vacuum. The instrument is applicable to the analysis of single deposited bioaerosol particles. A UV and IR MALDI ion mobility mass spectrometer was used for the analysis of complex bioaerosol mixtures by two-dimensional separation of ions according to their shapes and masses. The instrument separates the complex bioaerosol mixtures into different classes on trend lines that simplify the analysis. These trend lines include lipids, peptides/proteins, and oligonucleotides.

# CHAPTER 1. INTRODUCTION

## 1.1. Aerosols

Aerosols are any particulate matter, solid or liquid particles suspended in a mixture of gases that has some stability against gravitational settling. Examples of aerosols include smoke, fog, dust, smog, and pollen. The aerodynamic diameter of aerosol particles ranges from 1 nm to 100 μm but particles on either end of the distribution do not generally persist for long.[1] Typically, ambient aerosol particles are divided into three modes by their sizes (see Figure 1-1).[2] Particles less than approximately 0.1 μm belong to the nucleation mode and mainly consist of particles created from gas-to-particle conversion and direct emission. They may also be formed by the condensation of gases. These tiny particles do not generally persist for a long time because condensation and coagulation cause them to grow rapidly.

Particles between about 0.1 and 2.5 μm are considered to be part of the accumulation mode, representing a region of particle growth mainly due to coagulation and condensation. These particles include sulfate, nitrate, ammonium, and carbon. Particles in the accumulation mode persist for much longer periods of time because they grow relatively slowly and are not rapidly removed by other means. Particles in both nucleation and accumulation modes pose great health risks to humans because of their innate ability to deposit deep in the lungs.

Larger, coarse mode aerosols greater than 2.5 μm are mechanically generated, such as sea salt particles from the ocean, dust particles, or pollen particles. Atmospheric lifetimes of nucleation mode and coarse mode particles are relatively short due to dry deposition mechanisms of Brownian motion and gravitational settling, respectively. Figure 1-1 shows a common urban aerosol showing plots of number, surface, and volume distributions. This illustrates that the majority of particles are located in the nucleation mode and the greatest surface area occurs in

the accumulation mode while aerosol mass is divided between the accumulation and coarse modes.

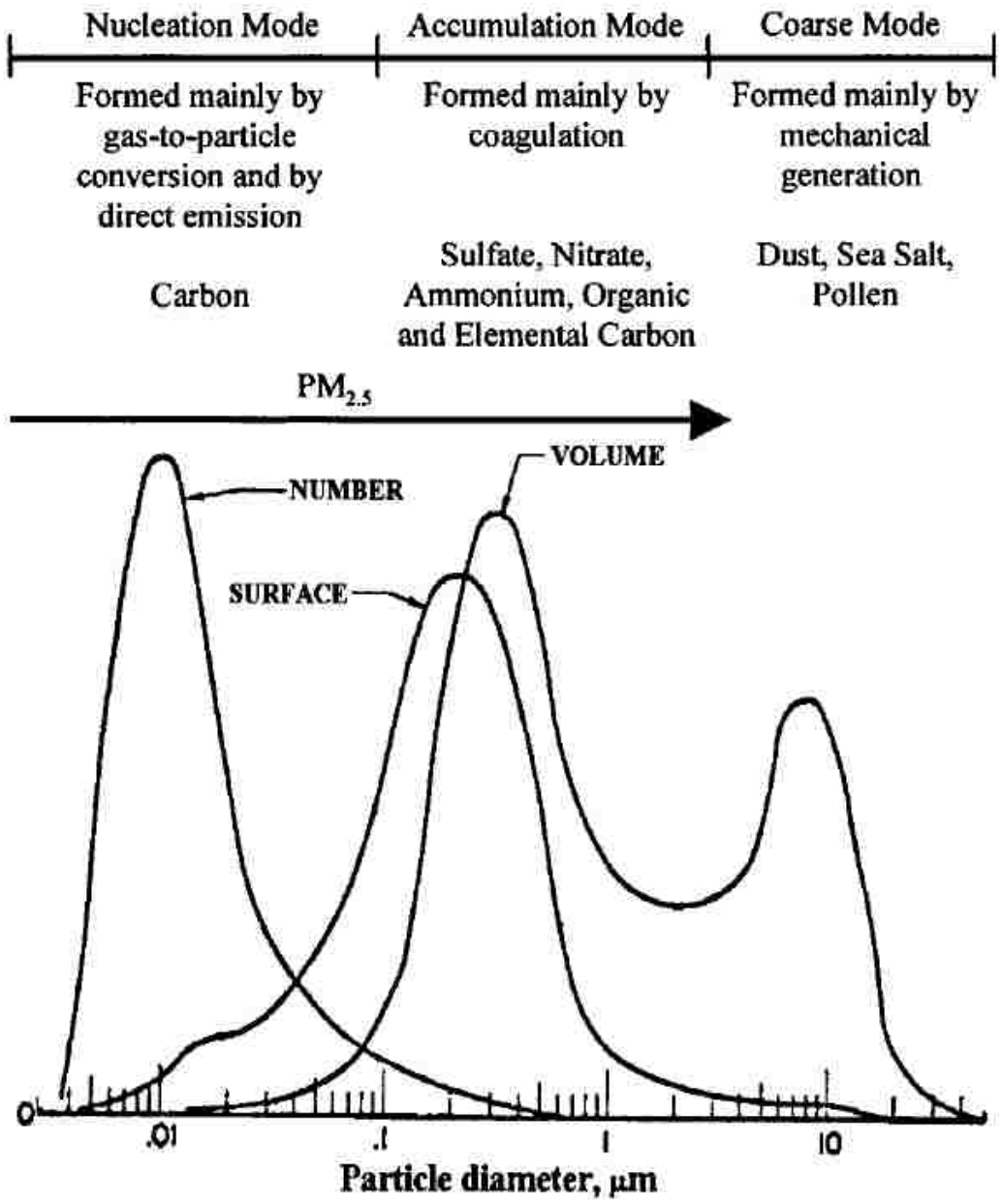


**Figure 1-1.** Common urban aerosol distribution presented in number, surface, and volume distributions. The three common aerosol modes (nucleation, accumulation, and coarse) along with their main processes of formation, common sources, and constituents are shown. (Reproduced with permission from © American Chemical Society from Ref 2.)

## 1.2. Bioaerosols

Bioaerosols are airborne particles with the sizes ranging from 10 nm for viruses to 100 μm for pollen grains that are living, contain biologically active compounds or were released from living organisms. The range from 300 nm to 10 μm is particularly dangerous for respiratory tract deposition.[3] Examples of bioaerosols include bacteria, virus, fungal spores, pollen, animal dander, insect emanations, microbial endotoxins, and human skin scales. These particles are a public health concern because they can cause infection, allergic or toxic and pharmacological reactions in humans. Bioaerosols have also been implicated as a cause for sick building syndrome, which includes non-specific symptoms such as headache, fatigue, and throat irritation.[4]

Many biological warfare agents such as anthrax, brucellosis, plague, tularemia, Q-fever, viral encephalomyelitis, botulinum toxin, and small pox are disseminated as bioaerosols.[5] The Centers for Disease Control and Prevention (CDC) Category A bioterrorism agents and diseases are listed in Table 1-1.[6] Biological warfare agents are living organisms or toxins derived from living organisms and are particularly dangerous weapons due to the following factors: they are simple and difficult to detect by the senses, easy to weaponize,[7,8] relatively inexpensive to produce compared to conventional weapons, can be self replicating, exhibit targeted physiological effects, and the repercussions of their use may not be detected for days.[3,8] They can be manufactured in small laboratories that can be concealed, transported, or disguised as pharmaceutical or food production facilities. Dispersal of biological agents is typically through an aerosol spray, but sabotage of food, water, or public spaces by dispersal of material is also possible. Biological agents are not detectable with the naked eye or by smell; hence, their effects are not observed for hours or days after exposure. They are psychologically threatening and thus particularly effective weapons of terror.

Biological agents consist of either pathogens or toxins. Pathogens are disease-causing organisms such as viruses, bacteria, or fungi. Toxins are poisons that are created by the biological reactions in organisms. Examples of toxins include botulinum, tetanus, ricin, and tetrodotoxin. These biological agents are especially difficult to detect from ambient particles due to their low infective doses: approximately 10,000 spores for bacterial agents and 1 to 100 organisms for viral agents.[5] The optimal size for aerosol delivery of biological agents is 1 to 5 μm,[3] because particles with this diameter will deposit in the lower respiratory tract and are not detected by the senses. Thus the threat of global health concerns and biological warfare agents associated with bioaerosol had led to an essential need for rapid bioaerosol detection methods.[9-14]

**Table 1-1.** CDC Category A Bioterrorism Agents/Diseases. CDC Category A bioterrorism agents and diseases are believed to pose the greatest potential threat because of their ease of dissemination or transmission from person to person, high mortality rate and potential to cause panic and social disruption.

| Agents | Incubation period | Mortality | Dissemination method |
|---|---|---|---|
| Anthrax (*Bacillus anthracis*) | 1-4 days | 25-100% | Aerosol |
| Botulism (*Clostridium botulinum* toxin) | 1-3 days | 8-50% | Aerosol |
| Plague (*Yersinia pestis*) | 2-3 days | 50-100% | Aerosol Vector |
| Smallpox (variola major) | 7-17 days | 30-90% | Aerosol |
| Tularemia (*Francisella tularensis*) | 1-10 days | 30-40% | Aerosol |
| Viral Hemorrhagic Fevers (Ebola, Marburg, Lass, etc.) | 4-21 days | 40-90% | Aerosol |

### 1.3. Detection Methods for Bioaerosols

The development of techniques for the detection of biological agents is challenging. The

sensitivity of a biological agent detector must be high because of the high toxicity relative to the mass. In addition, the detector must be selective and able to discriminate against an ambient background that includes a high level of naturally occurring particulates. Development of analytical instrumentation for biological agent detection has followed two general paths:[15] the adaptation of existing analytical instruments, and the development of affinity sensors that are based on biochemical selectivity.[16,17] In both cases, particles are typically collected prior to analysis. Affinity based sensors are small, fast, inexpensive and highly specific, but this specificity limits their applicability to systems for which affinity targets have been developed.[17]

Classical methods for bioaerosol detection involve collection of particles with later culturing and counting.[18] The important consideration for bioaerosol analysis is that microorganisms in the bioaerosol are viable or non-viable. The non-viable microorganisms cannot be cultured in the lab; hence, the culturing method cannot be used. The major disadvantages to these methods are that they are time-consuming, expensive, and may require multiple tests for proper identification. Thus, there is a pressing need for the rapid detection and characterization of bioaerosols in the environment. Mass spectrometers are particularly promising analytical instruments for biological agent detection because they are sensitive, specific, and selective as with affinity methods, but at the same time they are generally applicable. The main challenge for biological agent detection by mass spectrometry is to ionize the relatively large molecules that are indicative of biological agents without excessive fragmentation.

### 1.4. Mass Spectrometry

Mass spectrometry is an important analytical tool that determines the molecular weight and structural information of chemical or biological compounds by separating ions according to their mass-to-charge ratio ($m/z$).[19] Mass spectrometry has become the primary analysis method in

proteomics because of its high throughput, sensitivity and high mass accuracy.[20] Proteomics is an experimental approach to explain the information contained in genomic sequences in terms of the structure, function, and control of biological processes and pathways.[20] Proteomics is the comprehensive study of biological processes by the systematic analysis of the proteins expressed in cells or tissues.

A mass spectrometer consists of three fundamental parts: ion source, mass analyzer, and detector. A simplified schematic of a mass spectrometer is shown in Figure 1-2. Mass spectrometry involves the ionization of molecules using various ionization sources such as electrons or photons and the separation of the molecules based on their mass-to-charge ratio in a mass analyzer. The ions are generated by ionizing a neutral molecule through protonation, deprotonation, cationization, charge transfer, electron ejection, or electron capture from a gas or condensed sample phase ejected into the gas phase.[19]

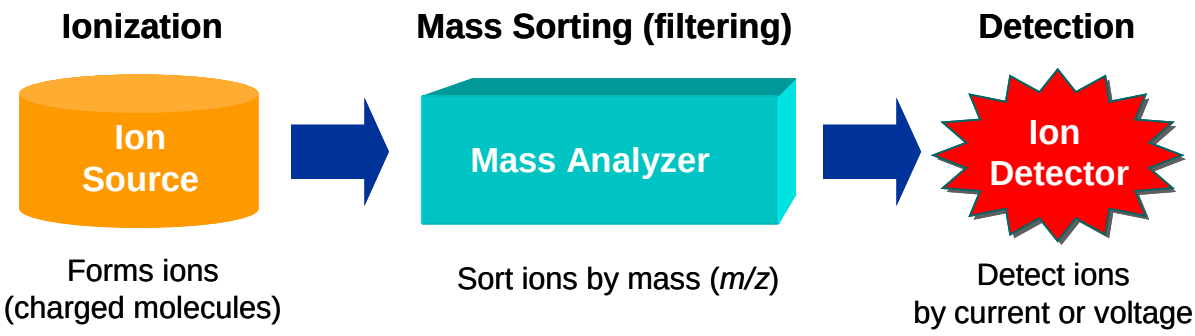


**Figure 1-2.** Simplified schematic of a mass spectrometer.

Formation of gas phase ions is an essential prerequisite to the mass separation and detection processes that occur in a mass spectrometer. The gas phase ions are extracted and separated into the mass analyzer according to their mass-to-charge ratios (*m/z*). The separated ions are collected by a detector. In the detector, the ion flux is converted to an electrical current.

The current signal is amplified and sent to a data system where the magnitude of the electrical signal is recorded as a function of *m/z*, and this information is converted into a mass spectrum. The mass analyzer and detector (and sometimes the ion source) are maintained under high vacuum to allow ions to travel from one end to the other without any hindrance from air molecules.

### 1.4.1. Ionization Sources

A number of ionization techniques are available and each has its own advantages and disadvantages. These include electron ionization (EI), chemical ionization (CI), laser desorption ionization (LDI), fast-atom bombardment (FAB), electrospray ionization (ESI), and matrix-assisted laser desorption/ionization (MALDI). Prior to the 1980s, EI was the primary ionization source for mass analysis.[19] The EI plays an important role in the routine analysis of small, hydrophobic, thermally stable molecules and is still widely used. In the EI source, ions are generated by bombarding the gaseous sample molecules with a beam of energetic electrons. The EI usually generates numerous fragment ions; however, the fragmentation information is useful for a library searching in compound databases. The CI uses gas or spray samples but ionizes with less fragmentation.[21] It also uses gas phase ion-molecule reactions with a reagent gas such as methane, isobutane, or ammonia within the vacuum of the mass spectrometer to produce ions from the sample molecules.[21] The major limitations of EI and CI are their inability to handle nonvolatile compounds and restricted mass range below 1000 Da due to extensive fragmentation.[21]

The FAB was introduced in 1981 by Barber and co-workers[22] and was a major breakthrough in the analysis of condensed phase samples. The FAB ionization technique typically uses a high energy beam of Xe atoms, $Cs^+$ ions, or massive glycerol-$NH_4^+$ clusters to sputter the sample and a liquid matrix from the probe surface. The matrix is a nonvolatile solvent

in which a sample is dissolved. Two common FAB matrices are *m*-nitrobenzyl alcohol (NBA) and glycerol. Although the mass range as high as 35 kDa has been observed for CsI clusters, 4,000 Da can be considered to be an upper mass limit for a routine operation of FAB.[21]

Soft ionization methods such as MALDI and ESI are suitable for achieving the goal of identification and structural determination of peptides, proteins, oligonucleotides, lipids, and synthetic polymers. Until the introduction of soft ionization methods, mass spectrometric analysis of molecules was limited to volatile compounds with small molecular weights of a few thousand daltons (Da).[21] Proteins are nonvolatile and have molecular weights that range from thousands to several hundred thousand Da. In the MALDI method, analyte molecules are imbedded in an excess solid matrix and irradiated with pulsed laser to form protonated molecules in positive mode[23,24] or deprotonated molecules in negative mode.[24,25] The ESI method involves the use of an electric field to create a fine spray of highly charged droplets containing the analyte molecules.[26] Evaporation of the solvent results in highly charged analyte molecules. Both methods enable large biomolecules to be ionized with little or no fragmentation.

### 1.4.2. Mass Analyzers

The function of a mass analyzer is to separate the ions that are generated in the ion source according to their *m/z*. The first mass analyzers, made in the early 1900's, used magnetic fields to separate ions according to their radius of curvature through the magnetic field.[27] Modern mass analyzers, including variations of the early magnetic methods, offer high accuracy, high sensitivity, high mass range, and an ability to give structural information. The most widely used mass analyzers are magnetic sector, quadrupole, ion trap, time-of-flight (TOF), and Fourier-transform ion cyclotron resonance (FT-ICR).[19,21]

A magnetic sector separates ions according to their radii of curvature; therefore, only ions of a given *m/z* are able to reach a detector at any given magnetic field. Ions of larger *m/z* follow

larger radius paths than ions of smaller *m/z*, so ions of differing *m/z* are separated in space. The double-focusing magnetic sector has two distinct parts, a magnetic sector and an electrostatic sector for energy selection. It has the advantages of high mass range, high mass resolution (~ 100,000), high mass accuracy, reasonable scan speed, and high dynamic range but has the disadvantages of high cost and low ion transmission efficiency.[21]

The quadrupole mass analyzer is one of the most widely used[21] and separates ions solely by electric fields. The quadrupoles function as a mass filter. As the field is imposed, ions moving into the field region oscillate depending on their *m/z* and on the radio frequency (RF) field, and thus, ions of particular *m/z* can pass through the filter. The *m/z* of an ion is therefore determined by correlating the field applied to the quadrupoles with the ion reaching the detector. The quadrupole mass analyzer has a mass resolving power of up to 4,000 and a mass limit of up to *m/z* of 4,000, which is useful because electrospray ionization of proteins and other biomolecules commonly produce charge distributions from *m/z* 1,000 to 3,500.[19,21] The quadrupole mass analyzer has advantages of low cost, high scan speed, high transmission, increased sensitivity, mechanical simplicity, and linear mass range.[21] However, in contrast to magnetic sector, it is inferior with respect to upper mass range, mass resolution, and mass accuracy.

The ion trap mass analyzer stores and manipulates ions in time rather than in space with a radio frequency quadrupole field.[21] The quadrupole ion trap consists of a ring electrode and two hyperbolic end-cap electrodes. The motion of the ions induced by the electric field on the electrodes allows ions to be trapped or ejected from the ion trap. A useful feature of ion traps is that it is possible to isolate one ion species by ejecting all others from the trap. The isolated ions can subsequently be fragmented by collisional activation and the fragment ions detected. The primary advantage of the quadrupole ion trap is that multiple collision induced dissociation (CID) experiments can be performed quickly without having multiple analyzers, thereby,

enabling a real-time LC-MS/MS routine. Other important advantages of the quadrupole ion trap is the compact size, ease of coupling with ESI and MALDI, and the ability to trap and accumulate ions to provide a better ion signal.

The time-of-flight mass analyzer is the simplest mass analyzer and has the potential of unlimited mass range. Mass resolving power of the linear TOF-MS is usually less than 500 but increases to more than 20,000 coupled with delayed extraction[28-,30] and reflectron ion mirror techniques.[31,32] The TOF is commonly combined with MALDI and used for the analysis of macromolecules such as proteins, carbohydrates, oligonucleotides, and synthetic polymers with high sensitivity. The time-of-flight mass analyzer will be discussed in detail in Chapter 2.

Lastly, the FT-ICR analyzer has the highest mass resolving power ($> 10^5$) as well as the highest mass accuracy (< 5 ppm) of the existing mass analyzers.[19,21] FT-ICR is based on the principle of monitoring ion cyclotron motion in a magnetic field. In this technique, ionization, mass analysis, and detection take place in the same region, generally in a small cell that is placed in a strong (3 to 16T) magnetic field. Ions are typically formed outside of the cell and trapped in the cell by applying a few volts of electric potential. An excitation pulse is applied where ions whose cyclotron frequency matches the excitation pulse, absorb energy from the external pulse. Finally, the image current that is induced when ions are in close proximity of the receiving plates is detected. The image current generated by all of the ions can then be Fourier-transformed to obtain the component frequencies of the different ions, which correspond to their *m/z*.

### 1.4.3. Ion Detectors

After the ions are separated by the mass analyzer, they arrive at a detector, which generates a current signal from the incident ions. A commonly used detector is the electron multiplier (EM),[19] which converts the kinetic energy of incident ions into secondary electrons. The electron multiplier is made up of a series of dynodes maintained at ever-increasing potentials.

The discrete and continuous dynodes are both in common use. Ions strike the dynode surface, resulting in the emission of electrons. The secondary electrons are then attracted to the next dynode where more secondary electrons are generated, ultimately resulting in a cascade amplification of electrons.

Various designs of the particle multipliers include discrete, continuous, and channel electron multiplier. The channel electron multiplier (CEM) is constructed from a special type of glass, which has either heavily doped with lead or its inner surface coated with beryllium.[21] The CEM is more compact and less expensive than a discrete EM, and provides gains as high as $10^8$. Microchannel plates (MCP) is a multichannel version of CEM.[33] It consists of small diameter (~ 12 μm) channels with approximately 15 μm center-to-center channel spacing.[34] The gain of each individual channel is much higher than the conventional CEM because of the significant increase in length to diameter ratio of the tube. Usually, two MCPs are arranged in a chevron configuration to provide a sufficiently large directional change so as to inhibit positive ions produced at the output of the rear plate from reaching the input of the front plate.[34] The MCP detectors are typically used in a TOF-MS and were employed in all mass spectrometers used in this dissertation research.

### 1.5. Matrix-Assisted Laser Desorption/Ionization

MALDI mass spectrometry was first introduced in 1985 by Karas and Hillenkamp[35] and thereafter has been widely used for mass spectrometric analysis of large, nonvolatile, and thermally labile compounds–such as peptides, proteins, oligonucleotides, and oligosaccharides–due to its inherent simplicity, low sample consumption, and high sensitivity. Karas and Hillenkamp discovered the highly efficient MALDI process using nicotinic acid as a solid organic matrix with a 266 nm UV laser to analyze proteins up to 67 kDa.[36,37] Meanwhile, Tanaka *et al*. in 1988 found that it is possible to soft desorbs large molecules (proteins and

polymers up to *m/z* 100,000) mixed with a matrix of ultrafine cobalt powder, finely dispersed in glycerol by irradiation with a 337 nm nitrogen UV laser.[38] Today, a typical MALDI mass spectrometer uses a 337 nm nitrogen laser and solid organic acid as the matrix.

Matrix-assisted laser desorption/ionization is a modification of the laser desorption/ionization technique in which the samples of interest are dispersed in a chemical matrix consisting of a solid or liquid that is a strong absorber of the laser light.[19] The matrix plays a key role in this technique by absorbing the laser energy and causing the matrix to vaporize into the gas phase with analyte. In early mass spectrometry using pulsed lasers, the sample was irradiated directly by the laser. This is termed laser desorption/ionization (LDI).[39] In this case, the extent of energy transfer is difficult to control and often leads to excessive thermal degradation and fragmentation. Another problem is that not all compounds absorb radiation at the laser wavelength. As a consequence, LDI is applicable to a limited number of compounds, which absorb the laser wavelength and have a molecular mass of less than 1,000 Da.[21] The incorporation of matrix overcomes these problems by several means. First, the laser energy is strongly absorbed by the matrix and transferred to the nonvolatile analyte molecules, enabling them to enter the gas phase without thermal degradation and fragmentation. Second, the matrix reduces analyte-analyte intermolecular contact thereby reducing the necessary desorption energy. Third, the matrix acts as a protonation (positive ion detection) or deprotonation (negative ion detection) agent, and is therefore essential in the ion formation process. Once the sample molecules are vaporized and ionized they are transferred electrostatically into a mass analyzer where they are separated by their mass-to-charge ratio.

MALDI is a soft ionization technique, meaning that it can be used to create ions from large biomolecules without degradation or fragmentation. MALDI has significantly increased the upper mass limit for the mass spectrometric analysis of biomolecules to over 500,000 Da[40,41] and

has enabled the analysis of large biomolecules easy, accurate, and sensitive. But the accuracy, sensitivity, and resolution typically drop in the mass region over 100 kDa.[41,42] Furthermore, the MALDI process itself may have an upper mass limit conditional upon the nature of the analyte.[41] This limit can be affected by the chemistry and photochemistry of analytes, matrices, solvents and ionization reagents. MALDI has evolved over the past decade into a standard method of biomolecule analysis that competes successfully with gel electrophoresis for mass analysis of biomolecules.

### 1.6. Mass Spectrometry of Bioaerosols

Mass spectrometry has shown particular promise for the rapid analysis of biomolecules contained in microorganisms.[9,10] One of the most widely used methods for microorganism identification is pyrolysis mass spectrometry in which the sample is heated and the resulting volatile molecules are ionized by electron impaction[43] or chemical ionization.[44] Pyrolysis MS has been used to identify mass spectral biomarkers associated with bacteria,[43-45] fungi,[46] and viruses.[47] On-line pyrolysis MS has been used to analyze aerosol particles composed of single bacteria,[48] and a field-portable instrument with *in situ* thermal hydrolysis and fatty acid methylation has been developed.[49,50] This technique is limited to small molecule constituents that will not decompose prior to volatilization. A separation by gas chromatography can also be used in conjunction with pyrolysis mass spectrometry.[51]

In the proteomics approaches to bacteria identification, experimentally determined protein molecular weights or sequence tags are compared directly to known protein sequences[52] and various databases.[53] Although the proteomics approach does not require the development of fingerprint libraries, the identification of proteins from intact molecule mass spectra requires mass spectra with good mass resolution and signal-to-noise ratio. In a more general approach, the mass spectra can be used as a fingerprint to identify the bacteria. With this approach, a library of

specific biomarker peaks is obtained from mass spectra of test samples. Mass spectra of unknowns are compared to the fingerprint library using a comparison algorithm. These procedures have been developed for the creation of fingerprint libraries and the identification of bacteria in relatively complex mixtures.[54] A drawback to the mass spectral fingerprinting approach is that it often requires bacterial incubation under controlled conditions in order to generate reproducible mass spectra that are not affected by growth stage or other conditions.

In these proteomics approaches, the techniques of soft laser desorption, particularly MALDI, and ESI, has enabled the analysis of those large biomolecules and extended the scope of mass spectrometry into many new biological areas.[55] Before the advent of these two techniques, mass spectrometric analysis of intact biomolecules was limited to species of at most several thousand daltons due to thermal degradation and could not be used to detect large biomolecules such as peptides, proteins, and nucleic acids contained in whole cells.[21] Together with electrospray ionization, MALDI forms the basis for the systematic introduction of MS as an analytical tool in biological research.

### 1.7. Research Objective

The objective of the research presented in this dissertation is to develop methods and instruments for the analysis of bioaerosols based on MALDI and matrix-free soft laser desorption ionization. There are two main approaches of bioaerosol detection using laser desorption ionization methods. With on-line methods, particles are ionized without matrix or after matrix addition by condensation.[56] With off-line methods, particles are collected, matrix is added, and ionization is accomplished in a standard MALDI mass spectrometer.[12,57] In all cases, the key to detecting fingerprint biomolecules is the presence of a suitable matrix material, whether exogenous or endogenous. The focus of this research is on the optimization of off-line

analysis of collected bioaerosol particles and biological samples by sample preparation and instrumentation.

This research work is divided into three parts: sample preparation, test bioaerosol analysis, and instrument development for off-line analysis of bioaerosols. In Chapters 3 and 4, MALDI substrates and sample preparation were characterized systematically, and the typical MALDI limitations were overcome. Test bioaerosol particles were generated from a nebulizer and collected on a MALDI target by an impactor to analyze the simulated bioaerosol particles by off-line mass spectrometry described in Chapter 5. A transmission geometry MALDI TOF-MS and an ion mobility (IM) MALDI orthogonal-TOF-MS were evaluated for the analysis of biological samples described in Chapters 6 and 7, respectively.

# CHAPTER 2. EXPERIMENTAL

## 2.1. Overview of Time-of-Flight Mass Spectrometry

A time-of-flight mass spectrometer is one of the simplest mass analyzers and is commonly used with MALDI ionization. The recent successes of TOF-MS can be attributed to the development of MALDI, high-speed data processing devices, and microchannel plate detectors.[21] Unlike other mass analyzers such as sectors, quadrupoles, and ion traps, an entire mass spectrum can be obtained at once. The acquisition speed is limited by storing the data and the time it takes for the ions to traverse the flight tube, typically within hundreds of microseconds.[58] For MALDI, the TOF is also limited by the laser repetition rate.

In a TOF instrument, the ions formed in the ion source are accelerated in an electric field and thereafter propagate through a field-free region where they are separated based on their mass-to-charge ratio before reaching the detector. When entering the field-free region, all ions of the same charge state have obtained approximately the same kinetic energy, which is defined by the acceleration voltage. Hence, low mass ions travel faster and hit the detector before heavier ions. The length of the flight tube is based on the desired ion separation resolution over a given mass range. The arrival time of ions at the detector is dependent upon their mass ($m$) through the equation,

$$E_{KE} = \frac{1}{2} mv^2 = zeV \qquad (1)$$

where $E_{KE}$ is the kinetic energy, $v$ is the velocity of the ion, $z$ is the charge number of the ion, $e$ is the charge of an electron, and $V$ is the acceleration voltage. Since the velocity ($v$) of the ion is the field-free length of the flight tube ($d$) divided by the flight time ($t$), equation (1) can be

rearranged to solve for the flight time ($t$) as follows given a singly charged ion (neglecting time spent in the ion source and post-acceleration at the detector):

$$t = \left[\frac{m}{2eV}\right]^{\frac{1}{2}} d \tag{2}$$

Mass resolving power ($R$) is the ability of a mass spectrometer to distinguish between ions of different mass-to-charge ratios and can be calculated by:

$$R = \frac{m}{\Delta m} = \frac{t}{2\Delta t} \tag{3}$$

where $m$ is mass of the peak and $t$ is the flight time, $\Delta m$ and $\Delta t$ are mass and time at the full width at half maximum (FWHM) of the peak, respectively. The quantities of $\Delta m$ and $\Delta t$ can be estimated manually or computationally.

The mass accuracy is a measurement of a mass error involved in assigning a mass to a given ion signal. Mass accuracy can be expressed as a percent (%) or part per million (ppm).

$$\%\ Mass\ accuracy = \frac{(M_t - M_0)}{M_t} \times 100\% \tag{4}$$

where $M_t$ is the theoretical mass and $M_0$ is the observed mass.

### 2.1.1. Linear Time-of-Flight Mass Spectrometer

The linear TOF mass spectrometer operates on the principle described above and is the least complex mass spectrometer. A schematic of the linear time-of-flight mass spectrometer is shown in Figure 2-1. In a linear TOF-MS, ions are accelerated by the same applied electric field (typically 20-30 kV) and allowed to drift in a field-free region where they will traverse this region in a time that depends upon their $m/z$.[59] The length of the acceleration region is usually less than a few cm.[59] The accelerated ions enter a field-free flight tube and reach the detector at the end of the flight tube. The length of the flight tube is usually less than 2 m.[59] Ions with

different *m/z* traverse the field-free region with different velocity and reach the detector at different times. The time that it takes for the ions to reach the detector at a known distance is measured, and depends on the *m/z* of the ions. From this time, *m/z* of the ions can be calculated by internal or external calibration. Typical flight times range from a few μs to several 100 μs.[58] The linear TOF can analyze ions without mass range limitation theoretically; however a resolution of up to 1,000 and a mass range up to 350 kDa are typical for linear TOF-MS.[60]

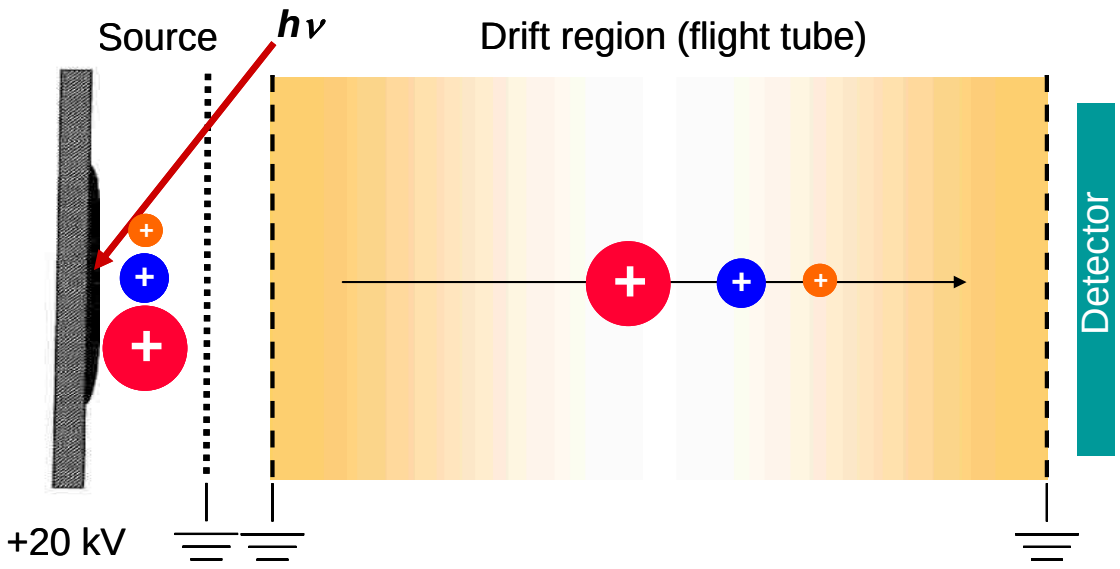


**Figure 2-1.** Diagram of a linear time-of-flight mass spectrometer.

## 2.1.2. Reflectron Time-of-Flight Mass Spectrometer

One disadvantage of the linear time-of-flight mass spectrometer is its relatively low mass resolution and accuracy. In order to distinguish the isotopic peaks of ions, higher mass resolution and accuracy are required. During the ionization process, the initial velocities and positions of the ions in the acceleration field are not the same and the ions with the same *m/z* enter the field-free drift tube at different times and velocities. This initial velocity distribution contributes

directly to broaden peak band width and decreases the mass resolving power of a single ion species.[59]

Improved mass resolving power and accuracy in TOF-MS can be obtained using a reflectron ion mirror located at the end of the flight tube.[31,32] The reflectron compensates for the difference in flight times of the same *m/z* ions with slightly different kinetic energies with an ion reflector shown in Figure 2-2. The reflectron uses an electrostatic field to reflect the ion beam toward the detector, which is located on the opposite side of the reflectron. The same *m/z* ions with higher initial kinetic energy have a higher velocity and therefore a shorter flight-time in the linear TOF-MS. This leads to a broadening of the peaks and thus decreased resolving power. In the reflectron TOF-MS, ions of the same *m/z* entering the field-free region with higher kinetic energy penetrate deeper into the reflectron and take a slightly longer path to the detector than ions with lower kinetic energy. Consequently the ions with lower initial kinetic energy catch up and hit the detector simultaneously with the ions with higher initial kinetic energy. The detector is placed at the focal point where the ions of different energies, focused by the reflectron, strike the detector at the same time. By adjusting the reflectron voltages it is possible to achieve a time-focusing plane.

In an ideal case, the resolving power of the peaks in the mass spectrum is dependent on the time-width of ion formation. In practical case, there are a number of time-broadening parameters that can degrade resolving power. These include spatial and initial-energy distributions and metastable ion formation during the desorption process.[61-63] An additional advantage to the reflectron arrangement is that nearly twice the flight path is achieved in a given length of instrument. The maximum resolution achieved in the reflectron TOF-MS is up to 35,000 and the mass range is up to 12 kDa.[59,60]

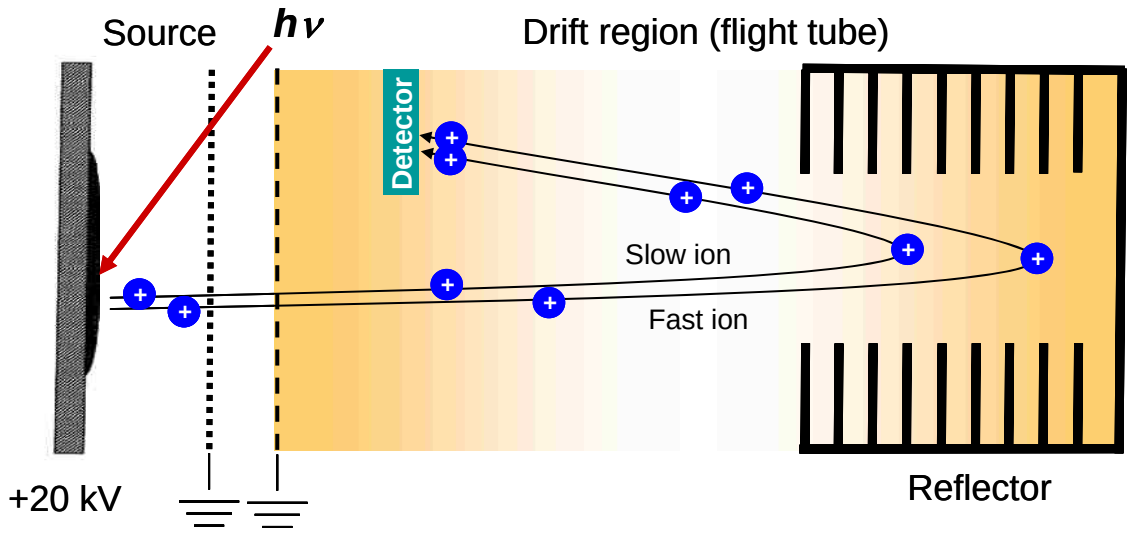


**Figure 2-2.** Diagram of a reflectron time-of-flight mass spectrometer.

### 2.1.3. Orthogonal Extraction Time-of-Flight Mass Spectrometer

Continuous ion sources such as ESI are generally interfaced to the TOF mass analyzer by orthogonal ion extraction in which the ions are introduced into the mass analyzer in a direction perpendicular to the ion source trajectory (Figure 2-3).[64,65] Ions that are produced between each duty cycle of mass analysis are introduced to the accelerating field, and then, a short pulse of an orthogonal accelerating potential is applied to eject those ions into the flight tube. This improves duty cycle and sensitivity by analyzing a slice of ions instead of a packet of ions. The orthogonal acceleration also removes problems arising from the initial kinetic energy and spatial distribution in the axis perpendicular to the direction of ion flight. The ion beam entering the orthogonal extraction region is focused to a small diameter by ion guides and the reflectron to minimize the spatial distribution of the beam in the direction of ion flight. A minimal temporal dispersion is also achieved with a short accelerating pulse. The mass resolution and accuracy can be greatly enhanced for orthogonal TOF-MS, and a mass resolving power of up to 35,000 and a mass accuracy of ~20 ppm were reported.[66,67]

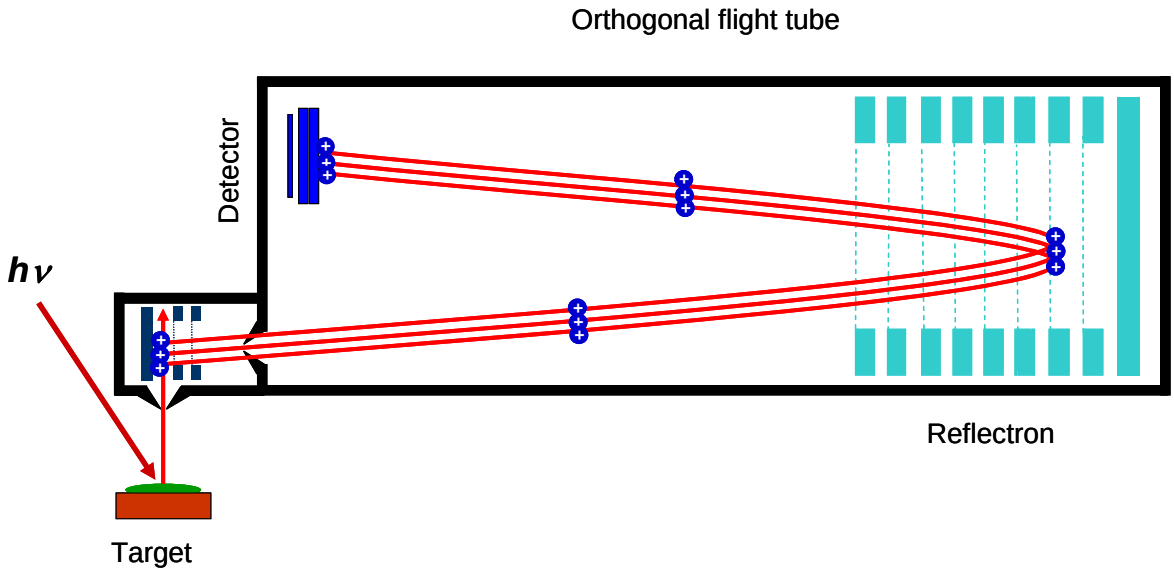


**Figure 2-3.** Diagram of an orthogonal extraction reflectron time-of-flight mass spectrometer. The ions from a continuous or discrete ionization source are accelerated into the field free region by a high voltage pulse.

## 2.1.4. Delayed and Pulsed Ion Extraction

The primary contribution to low mass resolving power in conventional continuous ion extraction MALDI TOF-MS is due to the different initial velocities of identical *m/z* ions and metastable ion formation. Improvements in mass resolution can be achieved by utilizing delayed pulsed ion extraction (see Figure 2-4), which can compensate for the difference in the initial ion velocity distribution of the MALDI generated ion packet such that same *m/z* ions arrive simultaneously at a space focal plane located at the detector.[68-70] When delayed pulsed ion extraction is applied, the acceleration voltage is switched on a few hundred nanoseconds after the laser pulse has irradiated the sample.[71] The ions at the back of the desorption plume (lower velocity) are accelerated more and the ions at the front of the plume (higher velocity) are accelerated less, and they are spatially focused at the detector when properly adjusted.

No compensation is made with continuous ion extraction linear TOF-MS for ions with the same *m/z* but different initial ion velocities. Broadening of the ion velocity distribution due to

collisional processes in the ion source can also be minimized by allowing the dense plume of MALDI generated ions packet to dissipate prior to ion acceleration from the ion source. This results in narrower ion arrival time distributions and provides better mass resolution when compared to continuous ion extraction. Utilization of the delayed pulsed ion extraction technique in conjunction with reflectron TOF-MS allows additional improvements in the obtainable mass resolution and accuracy by compensating the initial velocity distribution and the metastable ion fragmentation.[72-75] Such improvements in mass resolving power and accuracy yield better sequence specific information for unknowns.

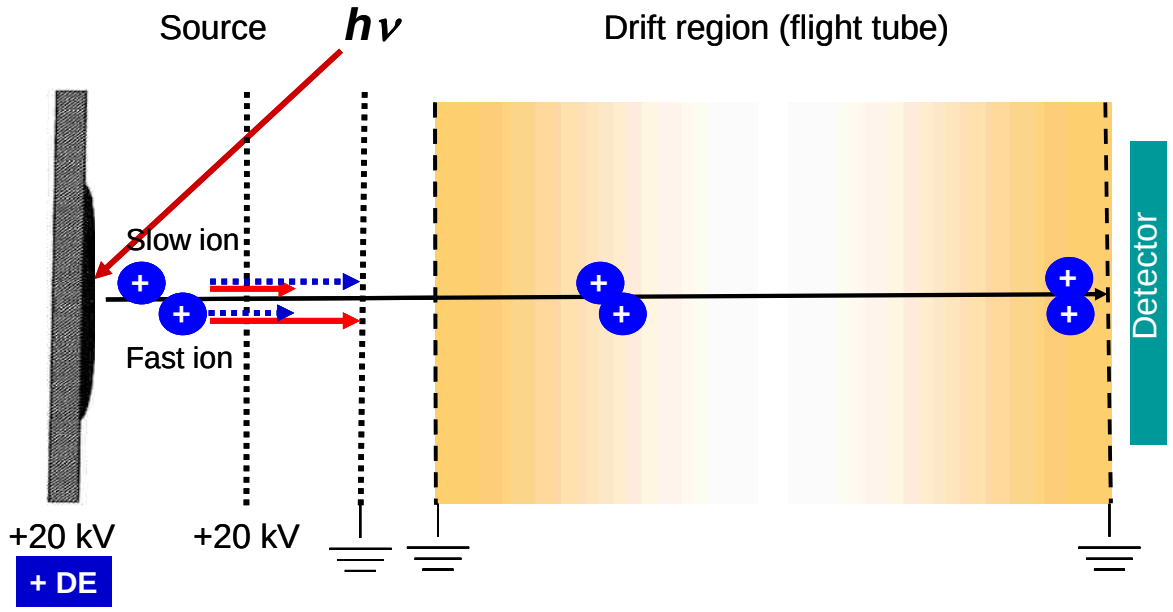


**Figure 2-4.** Diagram of a delayed and pulsed ion extraction MALDI time-of-flight mass spectrometer. The delay extraction voltage is supplied to the target a few hundreds ns time delay after irradiation. The solid (red color) arrow shows initial velocity strength, and the dotted (blue color) arrow shows delayed extraction strength.

## 2.2. MALDI Mass Spectrometry

### 2.2.1. Commercial MALDI Time-of-Flight Mass Spectrometry

A commercial MALDI time-of-flight mass spectrometer (OmniFlex, Bruker Daltonics, Billerica, MA)[57,76,77] shown in Figure 2-5 was used to evaluate MALDI substrates (Chapter 3), to

analyze pollens with a systematic approach (Chapter 4), and to analyze collected aerosol particles (Chapters 5). The mass spectrometer is equipped with a dual microchannel plate (MCP) detector for linear and reflectron mode with delayed ion extraction. A 337 nm UV nitrogen laser (pulse width: 3 ns, pulse energy: 150 μJ max.) at a repetition rate of 2 Hz was used for sample ionization. The laser pulse energy is controlled by rotating a graduated neutral density wheel in the path of the laser. An accelerating voltage of 19 kV was employed with delayed ion extraction. Focusing was accomplished using a set of three lenses configured as an adjustable 2:1 telescope with a final 25 cm focusing lens.

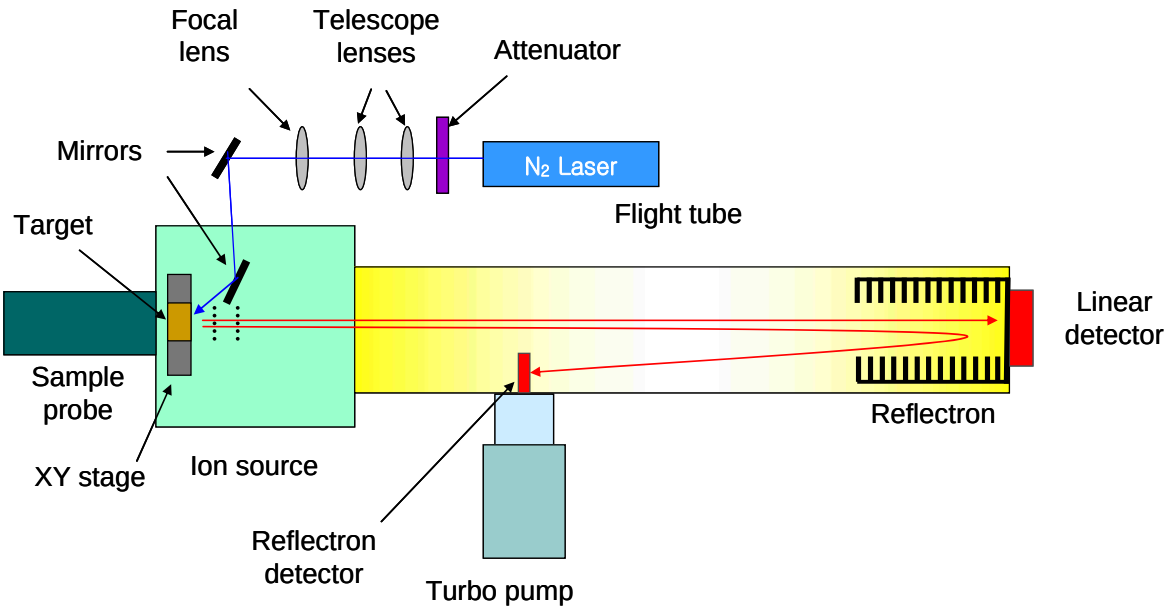


**Figure 2-5.** Diagram of a commercial MALDI time-of-flight mass spectrometer. The mass spectrometer is equipped with delayed ion extraction and linear and reflectron detectors.

The laser energy was measured with a pyroelectric joulemeter, ED-104AX (Gentec, Inc., Palo Alto, CA), and the spot size was recorded. The UV laser spot size, estimated from photographic burn paper (Pacific Coast Photo, Santa Cruz, CA) adhered to the target surface, was approximately 250 x 800 $\mu m^2$ for UV measured with a microscope. The laser energy versus

laser fluence conversion values for the stock 337 nm UV nitrogen laser used in Bruker Omniflex mass spectrometer are listed in Table 2-1. Signal suppression in a selected *m/z* range was accomplished using deflection plates. Mass spectra obtained in this research were typically summed an average of 50 laser shots to produce final spectra, otherwise, it is mentioned in the description. No baseline correction was performed on the mass spectra obtained.

**Table 2-1.** Laser energy vs. laser fluence conversion chart for a 337 nm UV nitrogen laser used in the commercial MALDI time-of-flight mass spectrometer.

| Laser energy | Laser fluence |
|---|---|
| 50% | 89.3 J/m$^2$ |
| 60% | 125.0 J/m$^2$ |
| 70% | 160.7 J/m$^2$ |
| 80% | 196.5 J/m$^2$ |
| 90% | 232.1 J/m$^2$ |
| 100% | 250.0 J/m$^2$ |

* Laser spot size was measured to 250 x 800 μm$^2$.

### 2.2.2. Transmission Geometry MALDI Mass Spectrometry

The mass spectrometer used for the biological sample analysis in this research (Chapter 6) was a home-built MALDI reflectron time-of-flight mass spectrometer shown in Figure 2-6. The mass spectrometer consists of an ion source chamber that is maintained at a pressure of 3.2 x $10^{-6}$ torr by a 2400 L/s 6-inch diffusion pump (VHS-6, Varian, Palo Alto, CA) and a 1 m linear flight tube that is maintained at a pressure of 1.2 x $10^{-7}$ torr by a 1200 L/s 4-inch diffusion pump (VHS-4, Varian). The mass spectrometer was equipped with a 18 mm dual microchannel plate detector (R.M. Jordan, Grass Valley, CA) for linear mode detection and a two-stage 40 mm dual microchannel plate detector (R.M. Jordan) for reflectron mode detection. The reflector voltage

was maintained at the range of 105 - 115% of acceleration voltage with a home-built voltage divider. The voltage divider consisted of a series of high-power rated resistors, which were divided by 2:1 resistance ratio. Therefore, the supplied reflector voltage was maintained at 66.7% to the front ring and 100% to the back ring of the two-stage reflectron ion mirror. The reflector was made of a series of metal rings, which were connected with a series of resistors to gradually decrease voltages from the back to the front rings in order to repel ions. The deflection plates were home-made to guide the ion packet to the reflectron detector and were run at voltages ranging from 350 to 550 V.

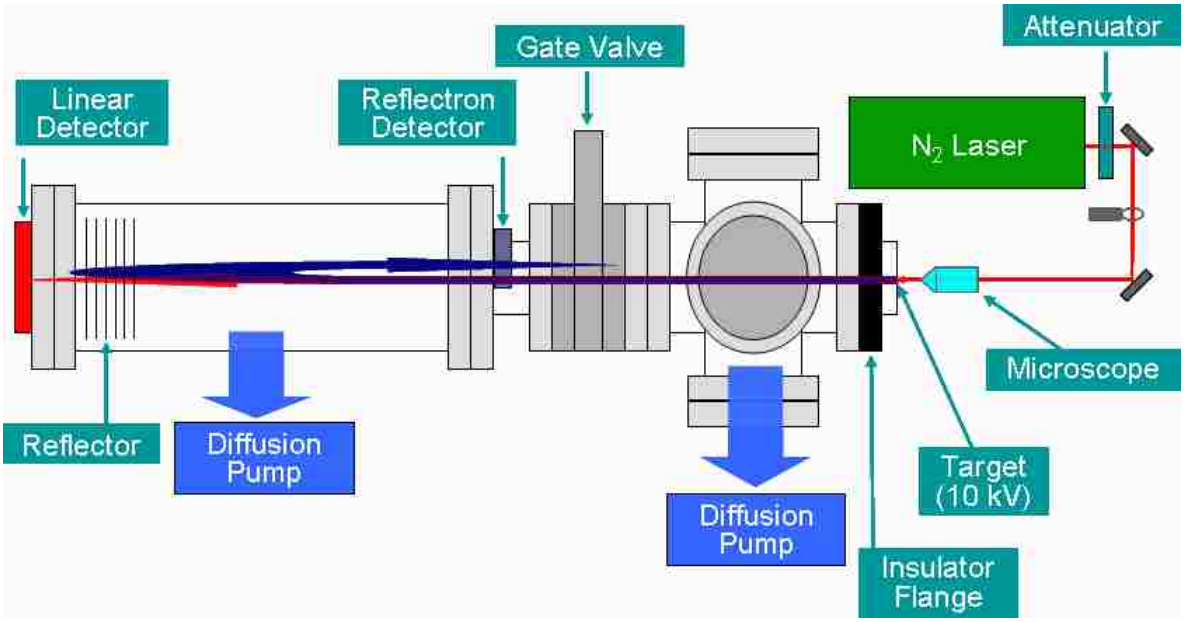


**Figure 2-6.** Diagram of a transmission geometry MALDI mass spectrometer with a microscope objective lens. The mass spectrometer is equipped with linear and reflectron detectors.

Initially, the mass spectrometer was built in a conventional front-side laser irradiation configuration for the comparison of mass spectra obtained from back-side laser irradiation configuration (Transmission geometry). The ion source was later converted to transmission geometry and a microscope objective lens was used for laser focusing as shown in Figure 2-7.

The transmission geometry ion source consists of an insulator flange made of 8-inch diameter and 1-inch thick Delrin (acetyl resin) where the center of the flange is machined to accept the 3-inch diameter stainless steel target holder flange. The target holder flange is electrically isolated by the Delrin flange and is held at high voltage during operation. The sample target is attached to the target holder flange and sealed with a thin Teflon tape as a gasket from outside of the ion chamber. The ion extraction grid is at a distance of 5 mm from the target flange and has 1 cm central hole, which is covered by 90% transmission grid (70 lpi). The ion extraction grid is held at ground potential for static acceleration. Samples are deposited on the vacuum side of a glass substrate, which is optically transparent to the laser wavelength used. The substrate can be accessed from back side at atmospheric pressure. The laser is introduced from the back side of the sample target in transmission geometry and irradiated sample through the glass slide to ionize. Microscope objective lenses were used for better spatial resolution at a different magnification: 4X, 10X, and 40X. A 254 mm focusing lens was used for transmission geometry without a microscope objective lens. A 1.0 mm thick microscope glass slide was used for UV substrate and a 0.6 mm thick silicon wafer was used for the IR substrate.

The ions were accelerated at a continuous potential of 10 kV (2000 V/mm) and were mass separated in a 1 m linear flight tube in linear mode as well as reflectron mode. The high mass detection limit for the reflectron mode was below *m/z* 3,000. Ions were post-accelerated with an additional 2 kV on both the linear and reflectron detectors. The detector signal was sent to the 50 Ω input of a 500 MHz digital oscilloscope (9350M; LeCroy, Chestnut Ridge, NY), which was triggered by a pulse delay generator (DG535; Stanford Research Systems, Sunnyvale, CA) that also synchronized the laser pulse. Mass spectra were averaged on the oscilloscope and transferred to a computer using a general purpose interface bus (GPIB) connection controlled by LabView software (National Instruments, Austin, TX).

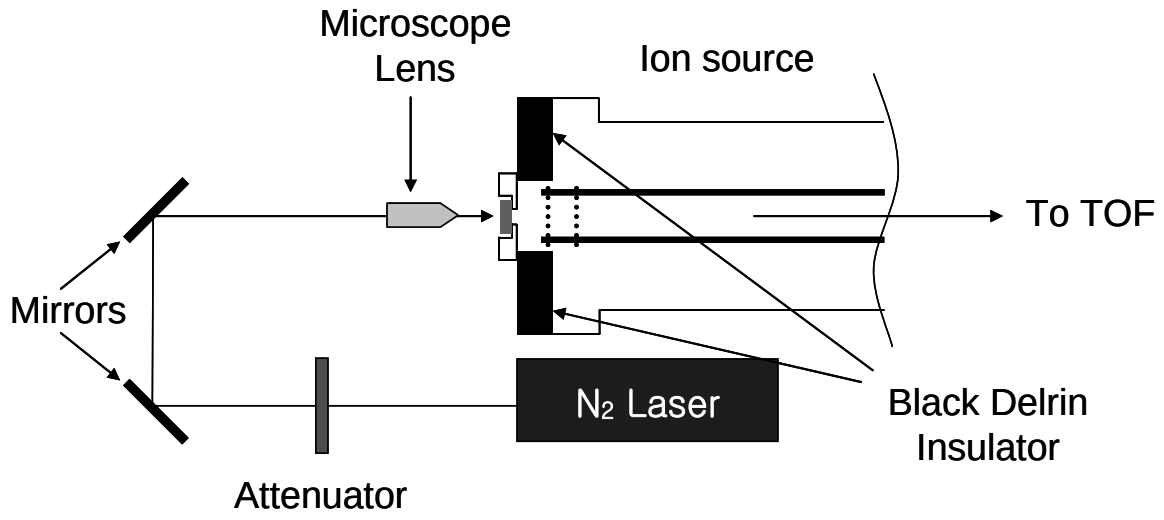


**Figure 2-7.** Diagram of the ion source of the transmission geometry instrument. The laser beam is moved to focus on other spots by moving the mirror and microscope objective lens.

UV and IR lasers were employed for sample ionization in a transmission geometry as well as a reflection geometry. First, a 337 nm nitrogen laser (VSL-337ND-S; LSI, Franklin, MA) was used as a UV laser and attenuated using a variable neutral density filter mounted on a rotating stage. The pulse temporal width of the UV laser was 4 ns and the maximum laser energy was 300 μJ. Focusing was achieved using a 254 mm focal length fused-silica lens and a spot size of 150 x 150 $\mu m^2$ was recorded using laser burn paper. A 2.94 μm Er:YAG (Bioscope, Bioptic Laser Systems, Berlin, Germany) laser was used as an IR laser source. The IR laser has a maximum pulse energy of 15 mJ and a pulse width of 100 ns. The spot size of the IR laser on a laser burn paper was 200 x 200 $\mu m^2$, measured with a microscope.

### 2.2.3. MALDI Ion Mobility Mass Spectrometry

Experiments in Chapter 7 were performed using an ion mobility orthogonal extraction time-of-flight mass spectrometer (IM-oTOF-MS) with a MALDI ion source. Figure 2-8 shows a schematic of the MALDI IM-oTOF-MS, which was developed by Ionwerks, Inc. (Houston, TX).[78] Ions were created by a UV or IR laser and injected into an ion mobility drift tube held at a

pressure of 5 Torr helium gas. A Nd:YAG laser pumped mini-optical parametric oscillator (Opolette, OPOTEK, Carlsbad, CA) was used to perform IR-LDI and IR-MALDI analyses. The laser has a 400 nm continuous tuning from 2.6 to 3.45 μm wavelength ranges, 20 Hz pulse repetition rate, a pulse energy of 1 mJ across the tuning range, and a pulse temporal width of 5 ns. A 1 kHz repetition rate Nd:YLF diode pumped Q-switched UV laser (Crystalaser, Reno, NV) was used for the UV MALDI analyses. A 349 nm Nd:YLF (fourth harmonic) pulsed laser was irradiated on the sample spots at a rate of 200 Hz. The spot size of the laser was approximately 200 μm. To prevent depletion of the sample, the plate was continuously moved to irradiate a fresh surface. Quartz and $CaF_2$ lenses with focal lengths of 15 cm were used for the UV and IR irradiation, respectively. The IR laser provides vibrational activation via the O-H bond stretch mode. The IR laser with a short focal length lens provided sufficient energy to ionize most of the samples. The sample chamber was equipped with the sapphire window, and a $CaF_2$ lens was mounted inside vacuum for IR laser focusing. The laser energy was attenuated by changing the pump laser flash lamp voltage, and beam focusing was performed.

Ion mobility resolution up to 30 was achieved with the 5-inch long ion mobility drift tube with applied voltage of 1900 V. After IM separation, the ions exit the mobility cell where they pass through a differentially pumped region and then the ions are orthogonally accelerated into a 40 cm reflectron TOF mass spectrometer, which achieves a resolution of 3,500 for ions with *m/z* 1,000. The instrument has a sensitivity of 2 fmol for peptide standards. An X-Y sample stage provides 1 μm accuracy in beam positioning and sample scanning of a standard 96-well sample plate. The sample is at ground potential to ease sample introduction, which requires the application of high voltage bias in the ion mobility cell to pull the ions through the He gas. The mass spectrometer flight tube is floated at this bias voltage. This bias voltage can be switched so that either negative or positive ions can be analyzed.

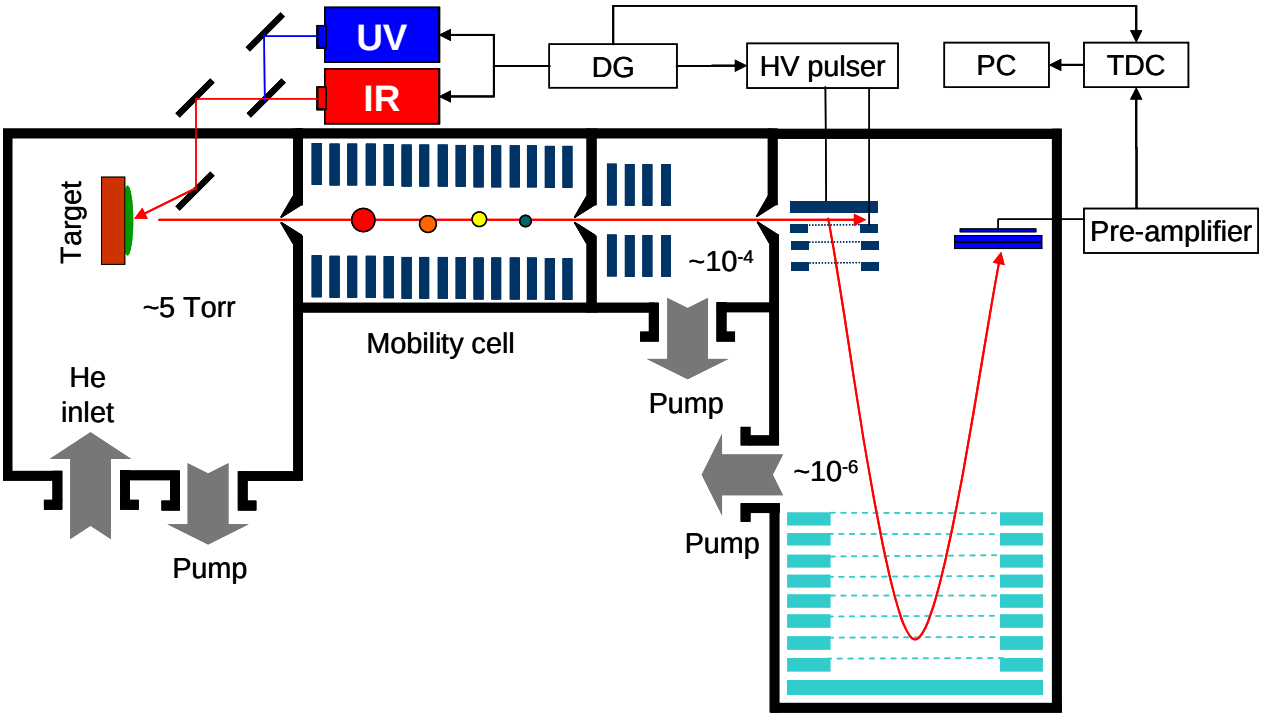


**Figure 2-8.** Diagram of the UV and IR MALDI IM-oTOF-MS. The ultraviolet (UV) and infrared (IR) lasers are triggered by the delay generator (DG) and directed at the same target spot. The delay generator (DG) also triggers high voltage (HV) pulser and time-to-digital (TDC) converter. The ion signal from the reflectron detector is pre-amplifed, and then, the signal is transferred to TDC and computer (PC).

In contrast to high vacuum MALDI, the ablation plume is collisionally cooled within microseconds by interaction with the He drift gas. After the laser pulse, the ions drift to the end of the mobility cell, which is biased by 1900 V applied to a resistive divider network connected between the sample plate and the exit of the mobility spectrometer. The mobility separated ions then pass through the skimmer into a differentially pumped orthogonal time-of-flight mass spectrometer where they are mass analyzed and the spectra recorded as a function of mobility drift time. The mobility drift times are typically several milliseconds while the flight times within the mass spectrometer are typically less than one hundred microseconds. Therefore, several hundred mass spectra are acquired after every laser pulse at intervals of every 30 to 150 μs (depending on the mass range). Spectra are stored individually along with the associated

mobility times. This process is repeated for several hundred laser shots, until each of the mass spectra contains sufficient intensity to construct plots of the molecular ion mobility as a function of *m/z*. The data are presented as 2D false color contour plots of ion intensity as a function of ion mobility drift time and *m/z*.

## 2.3. Samples and Reagents

### 2.3.1. Analytes

In Chapter 3, a wide mass range of analytes was investigated in order to compare the characteristics of different substrates from low mass region to high mass region. Riboflavin (Vitamin $B_2$, $C_{17}H_{20}N_4O_6$, 376.4 Da), bovine serum albumin (BSA, 66,430.3 Da), and phosphorylase b from rabbit muscle (97 kDa) were purchased from Sigma-Aldrich (St. Louis, MO). Lyophilized bacteria samples of *E. coli* strain W (ATCC 9637), *E. coli* B strain (ATCC 11303) *B. subtilis* (ATCC 6633), and Gramicidin D (G-5002) were also purchased from Sigma-Aldrich and used without further purification. All of the pollen analytes used in Chapter 4, giant ragweed from grass (*ambrosia trifida*), black walnut (pollen from *juglans nigra*), and corn pollen (*zea mays*) were purchased from Sigma-Aldrich and stored in the freezer prior to use. A test bioaerosol suspension of gramicidin D in Chapter 5 was prepared in methanol at a concentration of 1 mg/mL to take SEM images. The bacteria suspension was prepared by dissolving 5 mg of *E. coli* in 1 mL of 4:1 (v/v) acetonitrile (ACN) and 0.1% trifluoroacetic acid (TFA) in deionized water. It was found that the TFA reduced particle clumping in the solution and produced higher particle counts from the nebulized solution.

In Chapter 7, the standard peptides and proteins such as bradykinin at 6 mg/mL, bovine insulin at 10 mg/mL, and cytochrome c at 7 mg/mL were prepared by 1:1 (v/v) ACN/0.1% TFA. A mixture of potential bioaerosol interferants was simulated by mixing Arizona road dust (Powder Technology Inc., Burnsville, AZ) at 30 mg/mL, pollen at 15 mg/mL (5 mg each of giant

ragweed, black walnut, and corn pollen), carbon black at 10 mg/mL, and 60 mg/mL of salts (35 mg/mL of ammonium sulfate and 25 mg/mL of sodium chloride).

### 2.3.2. Calibration Standards

External mass calibration was achieved with Bruker calibration standard kits: Peptide Standard Kit, Protein Standard Kit I and Protein Standard Kit II, purchased from Bruker Daltonics (Billerica, MA) for mass spectra obtained in Chapters 3, 4, and 5. The constituent information of the calibration standard kits is shown in Appendix A. The calibration standard kit containing dry peptides or proteins was dissolved in 125 µL of 0.1% TFA in deionized water, vortex mixed for 30 seconds, and then stored in a freezer prior to use. An aliquot of peptide and protein calibration standards was mixed with a saturated CHCA or SA matrix, which was dissolved in 1:1 (v/v) ACN:$H_2O$. A 0.5 µL of the mixture was deposited on a target and allowed to air dry for mass analysis. The dried droplet method was used for calibration standard analysis.

### 2.3.3. Matrices

The MALDI matrices -cyano-4-hydroxy-cinnamic acid (CHCA, Sigma), 3,5-dimethoxy-4-hydroxycinnamic acid (sinapinic acid, SA, Sigma), trans-hydroxy-3-methoxycinnamic acid (ferulic acid, FA, Aldrich), 1,2-ethanedicarboxylic acid (succinic acid, Sigma), 3,4-dihydroxy-cinnamic acid (caffeic acid, CA, Sigma), and dihydroxybenzoic acid (DHB, Sigma) were used without further purification. Saturated matrix solutions were prepared by dissolving 20 mg of the matrix in 1 mL of 1:1 (v/v) acetonitrile and deionized water. Three MALDI matrices were chosen for the systematic sample preparation in Chapter 4 and were sinapinic acid, CHCA, and ferulic acid. The CHCA matrix was stored in the freezer prior to use.

A number of UV and IR matrices (Chapter 7) were prepared by dissolving them in 1:1 (v/v) ACN/ $H_2O$. Most of the matrices were saturated: succinic acid at 70mg/mL, DHB at 100 mg/mL, CHCA at 30 mg/mL, sinapinic acid at 30 mg/mL, and caffeic acid at 20 mg/mL.

Samples and matrices were deposited on 16-spot ion mobility targets using the dried droplet method with 1:2 (v/v) analyte/matrix ratio.

### 2.3.4. Solvents

Methanol, ethanol, acetonitrile (ACN), acetone, chloroform and dichloromethane (DCM) were purchased from Sigma-Aldrich (St. Louis, MO), and trifluoroacetic acid (TFA) was purchased from Fisher Scientific International (04902-100, Pittsburgh, PA). The solvent composition in Chapter 4 was acetonitrile with TFA in deionized water, and the TFA concentration was varied to 0.1%, 0.5% and 2.0%.

a) b)

**Figure 2-9.** Photographs of 7x7 Omniflex MALDI targets; a) a stainless steel and b) a target modified to accommodate a silicon wafer. A 0.5 µL quantity of analyte mixed with 1 µL of matrix was deposited on both target substrates and allowed to air dry. First row: CHCA and SA; Second row: peptide calibration standard with CHCA; Third row: BSA with SA.

## 2.4. Fabrication of Silicon Wafer Targets

Commercially available 49-well (7x7) stainless steel targets (Bruker Daltonics, Billerica, MA) were used for MALDI substrates in Chapter 3. A piece of silicon wafer was placed directly onto a stainless steel target, which was milled to accommodate the thickness of the silicon wafer.

A target was milled out at approximately 1.6 mm on the center. A 0.6 mm thick antimony doped single crystal silicon (100) wafer[77,79] purchased from Silicon Quest International (Santa Clara, CA) was attached on the center of the target with 1 mm thick carbon conductive double-sided tape (Electron Microscopy Sciences, Ft. Washington, PA) to make the surface height of the silicon the same as the stainless steel surface. Figure 2-9 shows photographs of a stainless steel target a) and a modified silicon wafer target b) with sample deposits.

**Table 2-2.** $L_9$ ($3^3$) orthogonal array of Taguchi experimental design (a set of nine experiments). The number of run is a combination of different levels of three factors.

| # of Run | Matrix | Solvent | Deposition |
|---|---|---|---|
| 1 | M1 | S1 | D1 |
| 2 | M1 | S2 | D2 |
| 3 | M1 | S3 | D3 |
| 4 | M2 | S1 | D2 |
| 5 | M2 | S2 | D3 |
| 6 | M2 | S3 | D1 |
| 7 | M3 | S1 | D3 |
| 8 | M3 | S2 | D1 |
| 9 | M3 | S3 | D2 |

## 2.5. Taguchi Experimental Design

Taguchi experimental designs are based on orthogonal arrays, which are identified with a name such as $L_8$ indicating an array with 8 runs. Classical experimental designs are also based on orthogonal arrays but are identified with a superscript to indicate the number of variables. Thus, a $2^3$ classical experimental design also has 8 runs. In this research, A $L_9$ ($3^3$) orthogonal array[80,81] Taguchi experimental design was carried out to evaluate the effects of the MALDI sample

preparation parameters because it was the most suitable for the conditions being investigated (three factors by three levels). The array is shown in Table 2-2. The three parameters (factors) were matrix, solvent composition, and deposition method. The subsidiary three levels for each factor are listed in Table 2-3. The $L_9$ ($3^3$) orthogonal array of Taguchi experimental design requires only 9 experiments to obtain the same accuracy and to minimize the association of errors compared to the classical design that needs 27 experiments to represent the same information. A set of 9 experiments were carried out for each pollen analyte and the subsequent mass spectra were recorded for data analysis.

**Table 2-3.** $L_9$ ($3^3$) orthogonal array of Taguchi experimental design and the description of three different factors and their subsidiary levels.

| Factors / Levels | Matrix (M) | Solvent (S) | Deposition (D) |
|---|---|---|---|
| 1 | FA | 1:1 ACN/$H_2O$ (0.1% TFA) | Dried droplet |
| 2 | CHCA | 1:1 ACN/$H_2O$ (0.5% TFA) | Seed layer |
| 3 | SA | 1:1 ACN/$H_2O$ (2.0% TFA) | Bottom layer |

### 2.6. Test Bioaerosol Generation

A schematic of the particle collection system is shown in Figure 2-10. Test bioaerosol particles were generated using 10 mL of bacteria suspension that was placed in a Collison nebulizer (BGI, Waltham, MA) and nebulized using filtered house air at 30 psi pressure as the carrier gas. Particle size distributions for particles generated in this manner have been published previously and are approximately 1.5 μm in diameter at a concentration of 0.5 to 1 x $10^4$ /$cm^3$ exiting the nebulizer.[56,82] The bioaerosol particles were then directed through a 10 mm i.d. by 30 cm length Tygon tube into an Andersen N6 single-stage bioaerosol impactor (Thermo Andersen, Smyrna, GA). Air is drawn into the impactor at a flow rate of 5 L/min with a vacuum pump. A

gap of approximately 2 mm between the Tygon tube and the impactor inlet compensates for a pressure difference between outgoing flow from the nebulizer and incoming flow to the impactor. The impactor was modified to accept the mass spectrometer sample target, which can be rotated with a clock motor during particle collection to disperse the sample on the target. In this work, the target was held stationary to produce a single "spot" for each of the 400 inlet holes in the impactor. The target protrudes approximately 3 mm above the floor of the impactor so that the MALDI target has the appropriate distance from the impactor nozzles.

Bioaerosol particles were collected on bare or matrix pre-coated targets. Matrix coated targets were prepared by depositing 400 μL of saturated matrix solution over the entire surface of the target and allowing it to dry. After particle deposition, the target was removed from the impactor and inserted into the mass spectrometer for off-line analysis. In some cases, the matrix or solvent was added to the target prior to analysis. Aerosol particle collection time was approximately four and half minutes. For the dried droplet method, the bacteria solution and matrix solution were pre-mixed to 1:1 (v/v). A 1 μL of the mixture was deposited on the target and allowed to air dry.

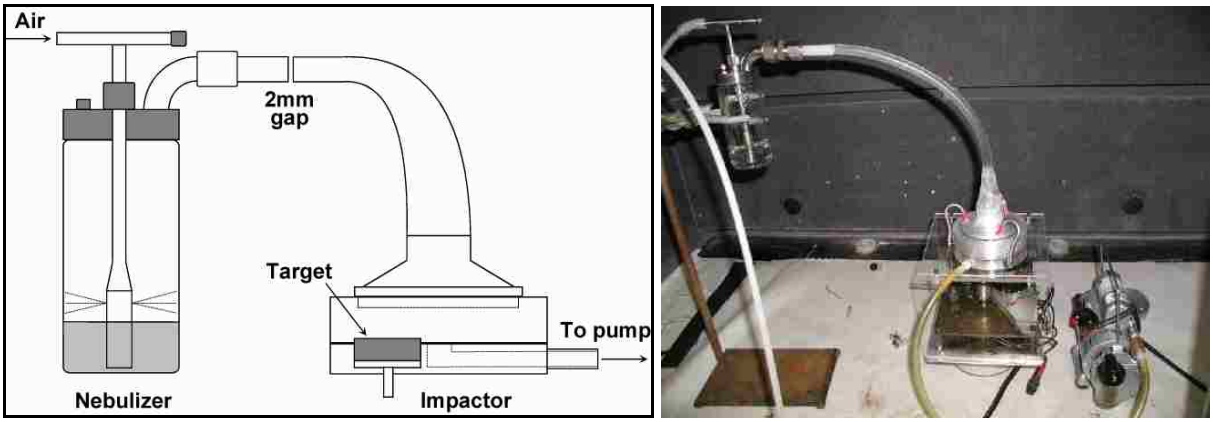


a) b)

**Figure 2-10.** Diagram a) and a photograph b) of the test particle generator (Collison nebulizer) and modified Andersen N6 impactor particle collection devices. The bacteria suspension is nebulized, drawn to the impactor by a pump, and impacted on the target surface seated in the impactor.

## 2.7. Scanning Electron Microscopy

Scanning electron microscopy (SEM) images of samples were investigated in Chapters 3 and 5. To further evaluate analyte/matrix co-crystallization characteristics of both targets in Chapter 3, SEM images were investigated with the samples spots shown in Figure 2-9. In Chapter 5, SEM was used to examine the surface of matrix precoated targets with impacted particles. Gramicidin D particles impacted on a sample target precoated with DHB matrix were investigated by SEM. Prior to SEM, targets were pre-coated with approximately 20 nm of gold/palladium (60/40) for 2 minutes in a sputter coater (S-150, Edwards, Fairfield, CA) at an argon gas pressure of 0.1 torr and an applied current of 10 mA. The samples deposited on both stainless steel and silicon wafer targets were investigated at 4 kV with a SEM (Stereoscan 260, Cambridge Instruments, Cambridge, UK) located in the Louisiana State University Socolofsky Microscopy Center.

# CHAPTER 3. MALDI MASS SPECTROMETRY ON SILICON

## 3.1. Introduction

A number of MALDI substrates have been studied with the goal of improving sensitivity, enhancing ionization efficiency, concentrating samples, and increasing reproducibility. These approaches include porous silicon,[83-85] graphite,[86,87] silicon/graphite,[88] gold,[89,90] carbon nanotube,[91-93] and teflon,[94] surfaces. The hydrophobic MALDI substrates were used to concentrate samples resulting in improved sensitivity and enhanced detection limit.[90,94-96] A hydrophobic target (with the commercial name Anchorchip) has been investigated with large volume dilute samples evaporated to a small spot on a MALDI target.[94,95] The target consists of a hydrophobic polymeric surface around a perimeter of small hydrophilic spots, which are about 200 to 800 μm in diameter. This allows the deposition of large volume solvent droplets that evaporate to the minimal surface area of the hydrophilic spots, resulting in concentrated analyte and matrix crystals. Due to higher concentration of the analyte in the small spot, the sensitivity can be increased up to ten times if the sample is sufficiently desalted. Gundry *et al*.[96] have used a disposable hydrophobic surface, SILCLEAN 3700 (1-methoxy-2-propyl acetate), for the analysis of peptides. This process involves masking the hydrophilic sample spot prior to spraying SILCLEAN 3700 around the perimeter of the liquid masking agent. Hydrophobic targets are limited to the concentration of relatively low μL volumes of solvent.[94-96]

Porous silicon substrates have been used in the past for small molecule analysis with a matrix-free soft ionization technique known as desorption/ionization on silicon (DIOS).[97,98] It has been shown that peptides and small proteins can be ionized using a UV laser without matrix if the sample is deposited on a porous silicon surface. The DIOS approach has the advantages of high sensitivity, tolerance for impurities such as salts and detergents, and particularly lack of low

mass interference from matrix ions.[98] DIOS has been demonstrated in proteomics[83] and forensics[84] applications and has been used for the direct detection of peptides from cells cultured on the silicon surface.[99] Detailed studies suggest that residual solvent adsorbed on the porous silicon surface may be integral to the DIOS process.[100] Efficient ion formation in DIOS is generally attributed to the special properties of porous silicon, including its high surface area, thermal conductivity, UV absorptivity, and its ability to trap solvent or residual gas molecules.[101]

However, the DIOS approach is disadvantageous in that it requires an additional step for the photoelectrochemical etching of silicon wafer, involves the complex cleaning procedure with a possible residual signal effect, and degrades over time on the porous surface owing to exposure to air.[76,100] Although it has been reported that proteins up to *m/z* 18,000 can be analyzed by DIOS with a UV laser,[83] the matrix-free DIOS is typically used with small molecules such as pharmaceuticals, peptides, small proteins, synthetic polymers, and enzymes in the mass range up to *m/z* 700 that are difficult to observe with MALDI due to low mass interferences by matrix ions.[76]

Non-porous silicon targets have been used for matrix-free analysis with infrared lasers for peptide and protein ionization (mass range up to *m/z* 17,000).[76,77] The heterogeneous MALDI sample deposits on typical stainless steel targets require searching for "sweet spots" where the analytes of interest are locally dispersed on matrix crystals, producing widely varying ion signals.[102,103] One of the greatest advantages of the untreated silicon substrate is that it leads to a homogeneous sample spot so that a search for a sweet spot is not necessary. Thus, it increases spot-to-spot and shot-to-shot reproducibility, which is useful for high-throughput and automated sample analysis. The untreated silicon wafer surface is hydrophobic, which allows large volume sample to be concentrated on a small spot after solvent evaporation.

In this research, we demonstrated the benefits of using untreated silicon wafers compared

to conventional stainless steel targets for MALDI analysis of large as well as small molecules. Samples and matrices were deposited on silicon wafers and commercial stainless targets and irradiated with a 337 nm $N_2$ laser. The resulting ions were accelerated and mass separated in a time-of-flight mass spectrometer.

### 3.2. Experimental

In this research, a commercial stainless target was modified to accommodate a silicon substrate, which is shown in Figure 2-9b. The performance of both targets was evaluated through a wide mass range by the analysis of proteins, bacteria, and calibration standard kits detailed in Appendix A. Laser energies were recorded for each mass spectrum to measure laser fluences. The laser spot size was measured at 250 x 800 $\mu m^2$ using photographic burn paper. To investigate background signals in the low mass region (up to *m/z* 1,000) the stainless steel target was carefully cleaned to avoid a memory effect caused by the sample and matrix residues from previous use. The stainless steel target was first cleaned in an ultrasonic bath for 30 minutes in a biological grade detergent (Alconox, VWR International, West Chester, PA) dissolved in hot water. The target was washed then sonicated for an additional 30 minutes in dichloromethane. Finally, the target was washed and cleaned in an ultrasonic bath for 5 minutes in ethanol. The silicon wafer target was prepared as a new substrate for the low mass background signal analysis.

### 3.3. Results and Discussion

Photographs of the stainless steel and modified silicon target with sample deposits are shown in Figure 2-9 a and b, respectively. Dried droplet deposits of 1.5 µL of 1:2 (v/v) analyte and matrix were deposited on each spot for both target substrates and allowed to dry in air. The first row of both targets in Figure 2-9 is 1.5 µL of CHCA (left) and SA (right) matrices. Both spots in the second row are peptide standards mixed with CHCA matrix, and both spots in the

third row are BSA mixed with SA matrix. The sample spot sizes are somewhat smaller on the silicon surface compared to the stainless steel surface.

### 3.3.1. SEM Images of MALDI Samples

To further evaluate analyte and matrix co-crystallization characteristics for both substrates, scanning electron microscopy images were investigated for both target samples shown in Figure 2-9. The SEM images of samples deposited on stainless steel and silicon are shown in Figure 3-1 and Figure 3-2, respectively. From the first to last row of SEM images in Figure 3-1 and Figure 3-2 are CHCA (a and b), SA (c and d), peptide standard mixtures with CHCA (e and f), and BSA mixed with SA (g and h), respectively. The first column of both SEM images shows a full sample spot, and the second column shows a 400 times magnified image of the sample spot. The sample spot on silicon were generally 20% to 40% smaller in area compared to stainless steel. This suggests that the silicon surface is more hydrophobic than that of stainless steel. The CHCA matrix formed an approximately 30 μm flower shaped crystals, and the SA matrix formed approximately 40 μm parallelogram shaped crystals after drying. The peptide and protein analytes were embedded in the matrix crystals at approximately 1:1,000 to 1:10,000 molar ratios so that they would not be expected to perturb the crystal structure.

### 3.3.2. Background Signal Comparison in the Low Mass Region

To investigate background signals in the low mass region up to *m/z* 1,000, freshly cleaned silicon and stainless steel targets were prepared and irradiated with the UV laser at different laser fluences. Figure 3-3 shows mass spectra obtained in this experiment with both MALDI substrates, a) silicon and b) stainless steel, up to *m/z* 1,000. The mass spectra shown are a summation of 50 laser shots in reflectron mode. The laser irradiation of the blank silicon substrate in Figure 3-3a produced no background signal through an entire mass region, even at maximum laser fluence.

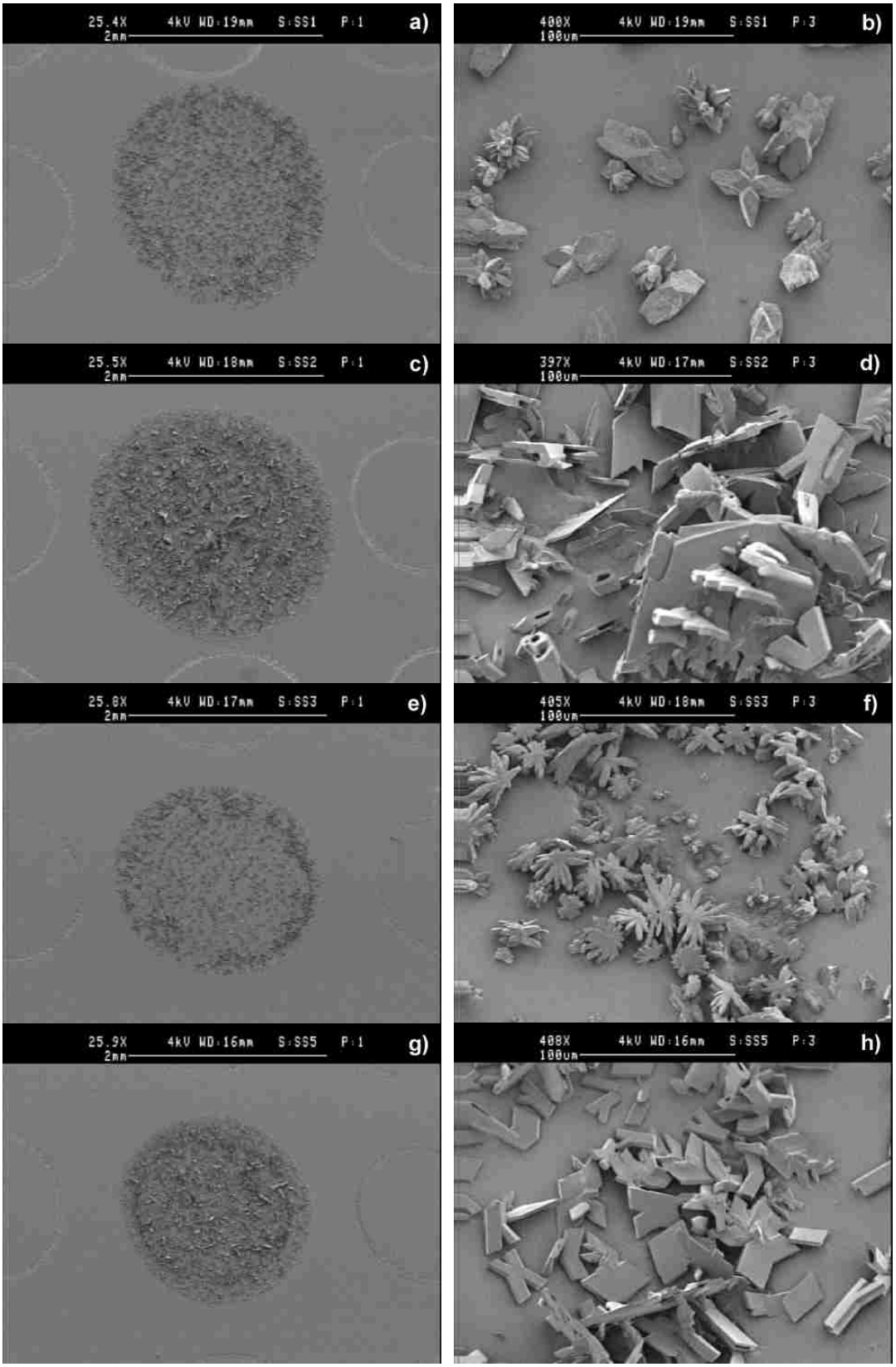


**Figure 3-1.** SEM images of MALDI sample spots on a stainless steel target.

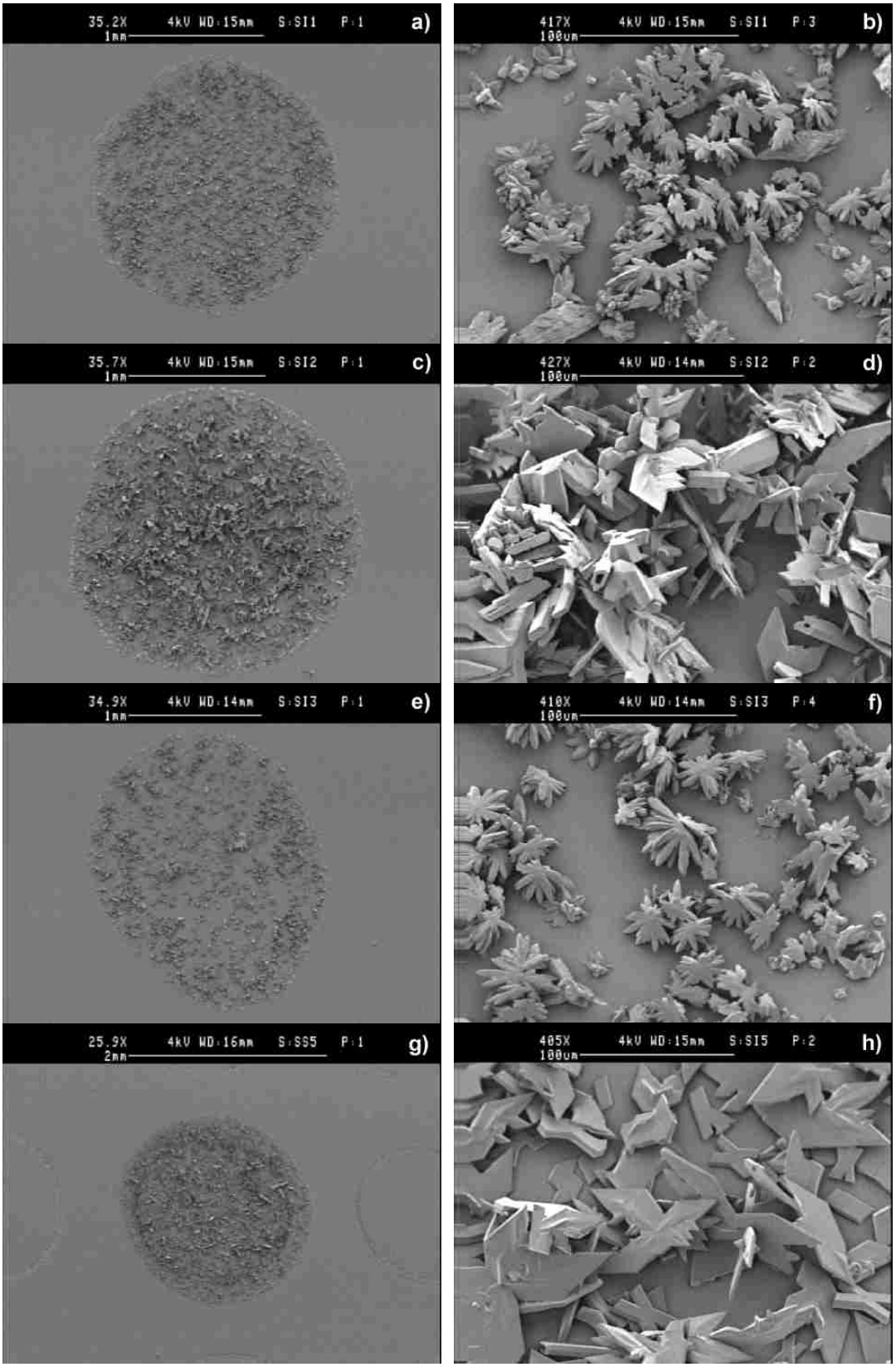


**Figure 3-2.** SEM images of MALDI sample spots on a silicon target.

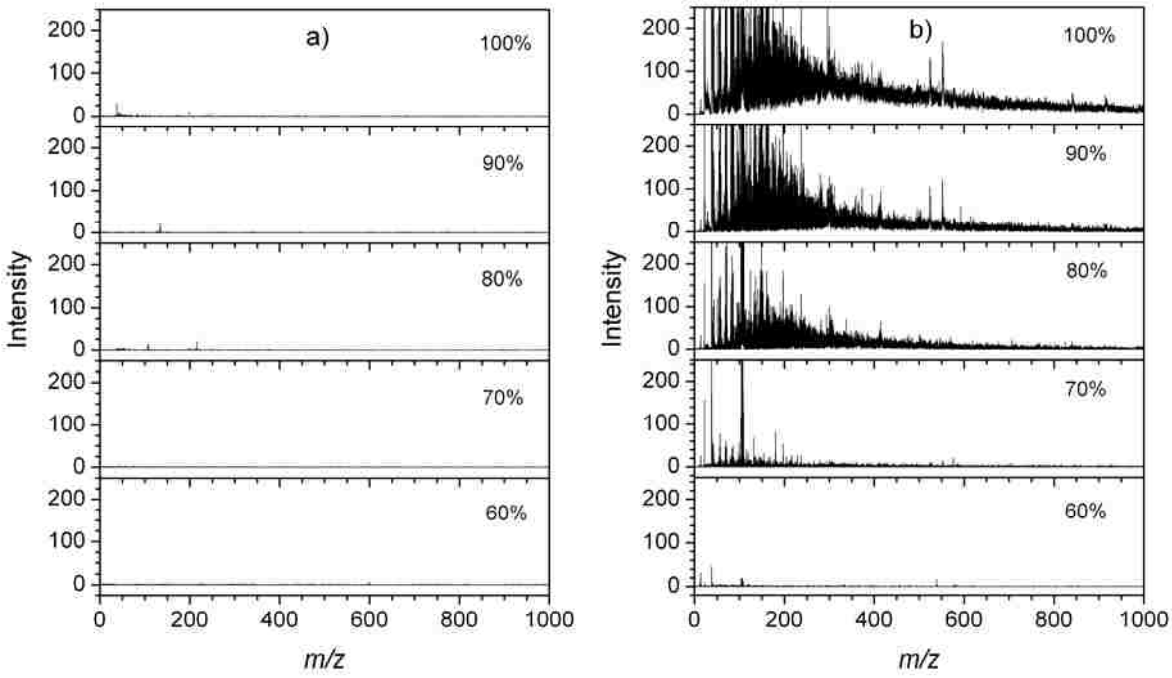


**Figure 3-3.** Mass spectra obtained from blank target irradiation of a) silicon wafer and b) stainless steel target. The mass range up to *m/z* 1,000 was investigated. Each mass spectrum is a sum of 50 laser shots. See the Table 2-1 for laser energy to fluence conversion.

On the other hand, the laser irradiation of the blank stainless steel substrate in Figure 3-3b produced significant background signals from the stainless steel surface, increasing with laser fluence above 160 J/m$^2$ in the mass region up to *m/z* 600. This shows that the stainless steel target is less suitable for the analysis of small molecules if the laser energy penetrates the sample layer and ablates target materials.

### 3.3.3. Small Molecule Analysis

To investigate MALDI target substrate characteristics for small molecule analysis in the mass region up to *m/z* 1,000, riboflavin was used as a test analyte. The matrix-free laser desorption/ionization (LDI) mass spectra of riboflavin with silicon and stainless steel target are shown in Figure 3-4. The concentration of riboflavin was 3.1 pmol/μL dissolved in 1:1 (v/v)

ACN/deionized water. A 1 μL volume of analyte solution was loaded onto both substrates then allowed to dry at room temperature. The laser energy used to obtain each mass spectrum was 65% for both substrates while the threshold laser energy was 55% for silicon and 62% for stainless steel. Both mass spectra were a summed average of 30 laser shots in reflectron mode. Peaks at 243.1 Da and 257.2 Da were assigned as fragment peaks labeled with asterisks (∗) in Figure 3-4 a and b. Peak resolution (3100 for Si and 2900 for SS) and signal-to-noise ratio (240 for Si and 75 for SS) were not significantly affected by the substrates but were slightly better with the silicon wafer while the signal intensity (730 for Si and 180 for SS) of the peaks in the two mass spectra were comparable.

An interesting result is that the stainless steel target produced some background signal from the ablation of substrate materials in the mass range from 0 to 100 Da and from 490 to 560 Da, labeled with diamonds (♦) in Figure 3-4b. The stainless steel target produced weak analyte peaks even at higher laser energies where high background signals from substrate ablation were also observed. In contrast, the silicon substrate produced intense analyte peaks without background signal even at full laser energy.

A notable observation in this research is that the peak intensity increased after several of laser shots for the silicon substrate, and thereafter, was steady. It has been reported that an abundant signal for intact noncovalent protein complexes (e.g., multiply charged ions, multimers, etc.) could be obtained for the first laser shot on a not-yet-irradiated sample spot exclusively.[105-110] Subsequent laser exposure of the same sample spot has predominately yielded signals of monomeric protein ions. This effect has been named to "first-shot phenomenon." [105-110] Rosinke *et al.*,[105] first reported this effect and assumed that the noncovalent complex can only be observed for the first shot at a given sample position.

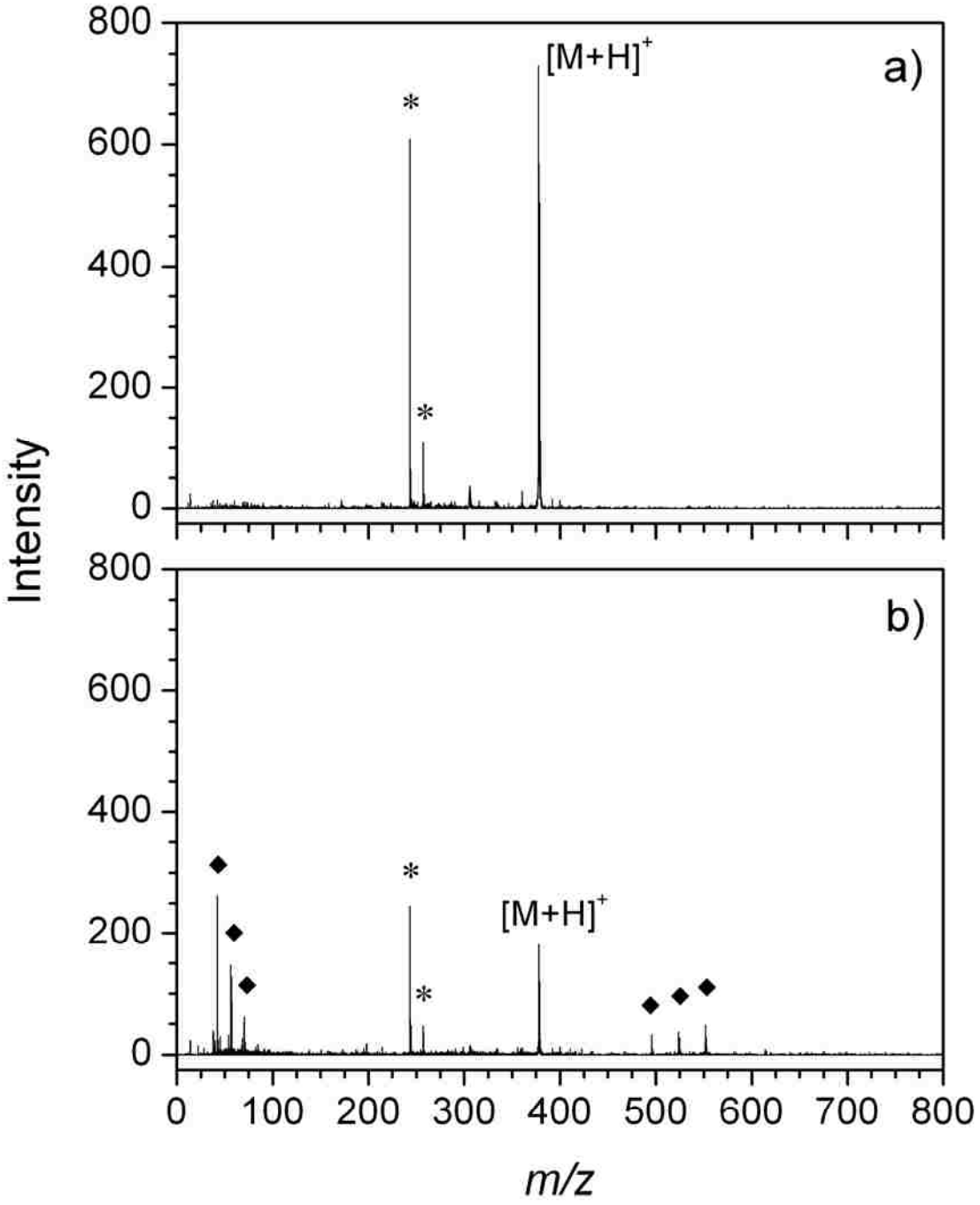


**Figure 3-4.** Matrix-free LDI mass spectra of riboflavin (376.4 Da, $C_{17}H_{20}N_4O_6$) on a) a silicon wafer and b) a stainless steel substrate. Peaks labeled with asterisks (∗) at 243.1 Da and 257.2 Da are assigned as fragments of riboflavin. Peaks labeled with diamonds (♦) at 42.1, 56.2, 70.3, 495.6, 524.6 and 551.8 Da are assigned as backgrounds from the ablation of the stainless steel substrate.

Successive laser shots at the same position primarily produced monomer ions. In contrast to the first-shot phenomenon, no ion peak was generated during the first few laser shots on a fresh sample spot from the silicon substrate.

### 3.3.4. Large Molecule Analysis

Silicon can be used for large molecule analysis by MALDI mass spectrometry. BSA (66.5 kDa) and phosphorylase b (97 kDa) from rabbit muscle could be analyzed with the silicon substrate as well as the stainless steel substrate, and their mass spectra are shown in Figure 3-5. The concentration of BSA and phosphorylase b was 10 pmol/μL and 2.4 pmol/μL, respectively, dissolved in 1:1 (v/v) ACN/0.1% TFA in deionized water. A 1 μL of each analyte was mixed with 2 μL of SA matrix and deposited onto both substrates. The analyte to matrix molar ratio was approximately 1: 8,900 for BSA and 1: 32,600 for phosphorylase b. The laser energy used to obtain mass spectra for BSA and phosphorylase b was 90% and 95% for silicon and 70% and 70% for stainless steel substrate while the threshold laser energy was 58% and 63% for silicon and 54% and 61% for stainless steel. The silicon required somewhat higher laser fluence than stainless steel substrate for large molecule analysis. Mass spectra shown in Figure 3-5 are a summed average of 100 laser shots in linear mode. Peak resolution (93 for Si and 87 for SS for BSA, 88 for Si and 92 for SS for phosphorylase b) and S/N (590 for Si and 390 for SS for BSA, 130 for Si and 105 for SS for phosphorylase b) were not significantly affected by the substrate but were slightly better with the silicon. Monomer, dimmer, trimer, as well as multiply charged peaks were observed in the BSA and phosphorylase b mass spectra for both substrates, but the silicon substrate produced greater peak intensities.

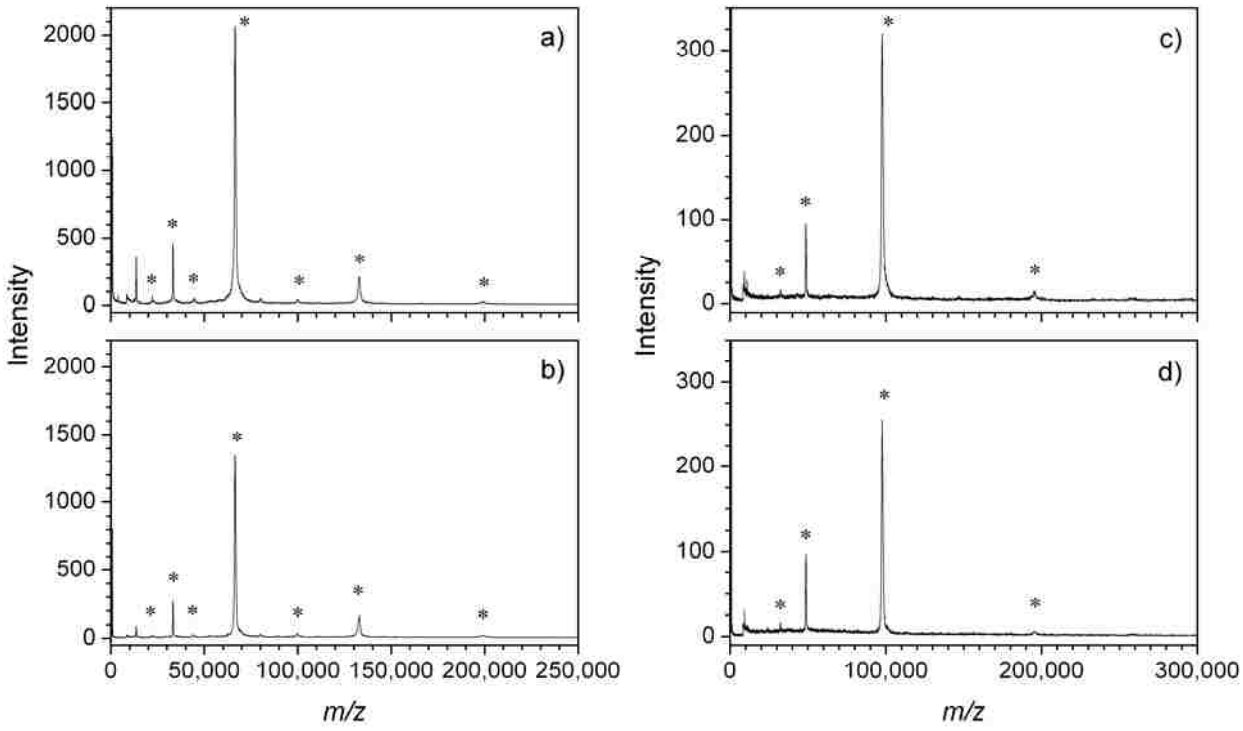


**Figure 3-5.** Large molecule mass spectra for BSA on a) Si and b) SS, and phosphorylase b on c) Si and d) SS with SA matrix. Ion suppression was used below *m/z* 10,000. Peaks labeled with asterisks (∗) in BSA mass spectra from left to right are assigned as $[M+3H]^{3+}$, $[M+2H]^{2+}$, $[2M+3H]^{3+}$, $[M+H]^{+}$, $[3M+2H]^{2+}$, $[2M+H]^{+}$ and $[3M+H]^{+}$. Peaks labeled with asterisks (∗) in phosphorylase b mass spectra from left to right are assigned as $[M+3H]^{3+}$, $[M+2H]^{2+}$, $[M+H]^{+}$ and $[2M+H]^{+}$.

### 3.3.5. Bacteria Analysis

Figure 3-6 shows mass spectra of a gram-negative bacterium, *Escherichia coli*, a lyophilized cell of strain W. A 5 µg/µL concentration of *E. coli* W strain in 1:1 (v/v) ACN/0.1% TFA was mixed with SA matrix at 1:2 (v/v) ratio. A 1 µL volume of the mixture was deposited onto both substrates. The laser energy was 65% for silicon and 60% for stainless steel, and the threshold laser energy was 55% for silicon and 50% for stainless steel. Mass spectra were a summed average of 50 laser shots in linear mode. Ion suppression was used below *m/z* 3,000. Some unique biomarker peaks at 15,602 Da and 35,128 Da could be obtained with both silicon and stainless steel substrates but could not be identified with database searching. Mass

fingerprinting can be used to find a unique pattern of peaks for bacteria that can be used for the identification of strain level of species.[54,111] Overall the bacteria analysis for the silicon substrate gave similar performance to the stainless steel substrate.

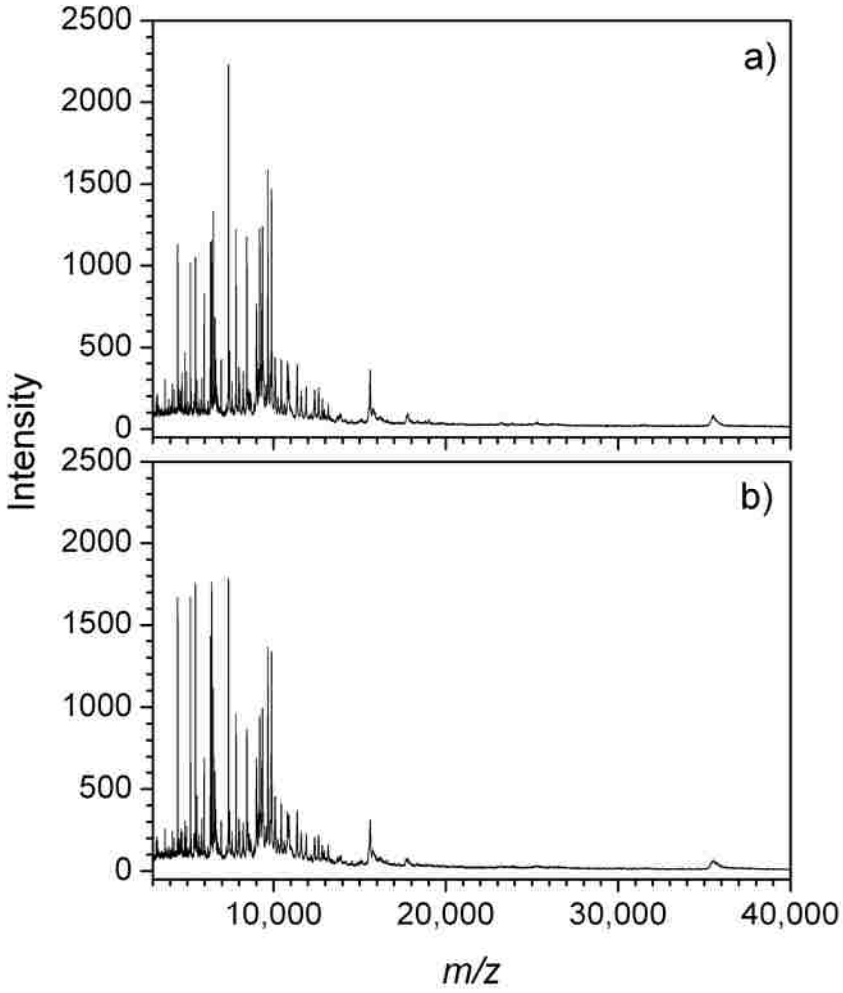


**Figure 3-6.** *E. coli* W strain mass spectra with SA matrix on a) silicon wafer and b) stainless steel target. Ion suppression was used below *m/z* 3,000, and the mass spectra were cut off below *m/z* 3,000. Mass peaks at 15,602 Da and 35,128 Da could be obtained with both substrates but could not be identified with database searching.

### 3.3.6. Shot-to-Shot and Spot-to-Spot Reproducibility

A remarkable difference between two substrates was the shot-to-shot and spot-to-spot reproducibility of the silicon target. The peptide standards, angiotensin II and ansgiotensin I,

were mixed with the saturated CHCA matrix and deposited onto both targets with the dried droplet method. To quantify these characteristics for both substrates, thirty mass spectra were recorded by irradiating a single spot for shot-to-shot reproducibility and by irradiating multiple spots for spot-to-spot reproducibility measurements. The average and the relative standard deviation (RSD) of peak height and area for the molecular ion peaks of the peptide standards, angiotensin II and ansgiotensin I are shown in Table 3-1. The shot-to-shot reproducibility of the silicon substrate is about one and a half times better than the stainless steel substrate while the spot-to-spot reproducibility is three to ten times better for the silicon substrate. The shot-to-shot reproducibility is worse than the spot-to-spot reproducibility for silicon substrate because the signal intensity decreased gradually with the laser shot increment due to the faster sample depletion on a single spot. On the other hand, the spot-to-spot reproducibility is worse than the shot-to-shot reproducibility for stainless steel substrate because the inhomogeneous matrix crystals produced sweet spots. It is reported that the relative standard deviation of the shot-to-shot and spot-to-spot reproducibility for dried droplet sample preparation on stainless steel substrates is 20-90%.[104]

**Table 3-1.** The shot-to-shot and spot-to-spot reproducibility measurements of peptide standards deposited on stainless steel (SS) and silicon (Si) substrates expressed as an average with relative standard deviation. Data were calculated from 30 mass spectra of a single laser shot.

| Analytes \ Substrates | | Shot-to-Shot | | Spot-to-Spot | |
|---|---|---|---|---|---|
| | | SS | Si | SS | Si |
| Angiotensin II | Height | 144 ± 17% | 166 ± 10% | 112 ± 33% | 234 ± 6% |
| | Area | 587 ± 23% | 677 ± 17% | 508 ± 39% | 755 ± 14% |
| Angiotensin I | Height | 163 ± 14% | 215 ± 9% | 97 ± 33% | 239 ± 3% |
| | Area | 951 ± 15% | 815 ± 10% | 538 ± 38% | 1052 ± 7% |

### 3.4. Summary

In this chapter, silicon wafer targets were demonstrated for the analysis of riboflavin, BSA, phosphorylase b, and *E. coli* and compared to stainless steel targets. The surface characteristic of non-porous silicon substrate is hydrophobic, and thus it produces 20% to 40% more concentrated sample spots after solvent evaporation resulting in better ion signal. Silicon substrates produced less background signal in the low mass region even at maximum laser fluence. On the other hand, stainless steel substrates produced significant background signals in the mass region below *m/z* 600 due to surface ablation, which increases with laser fluence above 160 J/m$^2$. This implies that the stainless steel target is less suitable for small molecule analysis due to surface ablation.

The silicon substrate required somewhat lower laser fluence for riboflavin analysis but required somewhat higher laser fluence for high mass molecule analyses than did stainless steel. The silicon produced intense and reproducible signals. Peak resolution and S/N were not significantly affected by the substrate, but detection limit was approximately ten times better with silicon substrate. A notable observation for the silicon substrate is that the ion signals increased after several laser shots, and thereafter were stable in contrast to some previous reports reporting a first-shot phenomenon.[105-110]

The most notable observations on silicon substrate were shot-to-shot and spot-to-spot reproducibility. The RSD of peak height and area of angiotensin II and angiotensin I for the silicon substrate is approximately 1.5 times better for shot-to-shot and 3 to 10 times better for spot-to-spot reproducibility compared to the stainless steel substrate. The spot-to-spot and shot-to-shot reproducibility for MALDI sample preparation are important figures of merit for applications needing quantification, high-throughput, and automated sample analysis. Overall the

silicon substrate showed excellent performance for the analysis of low mass molecules as well as high mass molecules.

The off-line bioaerosol collection on MALDI substrates requires highly reproducible signals. Thus, the silicon substrate is a great substitute for the conventional stainless steel MALDI substrate. Little or no low mass background signals on the silicon substrate help bioaerosol identification by mass fingerprinting to find a unique pattern of bioaerosol peaks.

# CHAPTER 4. TAGUCHI OPTIMIZATION OF MALDI

## 4.1. Introduction

Although MALDI-MS has been extensively studied, the technique suffers from some disadvantages, such as poor shot-to-shot reproducibility, matrix crystal inhomogeneity, short sample life time, and strong dependence on the sample preparation method.[112,113] Analytes embedded in a matrix crystal are typically inhomogeneous and often gives irreproducible ion signals.[96,102,103] Thus, it is often necessary to search for sweet spots to obtain adequate performance.[114-116] It is important to obtain homogeneous MALDI spots that yield signals from the entire spot reproducibly for mass spectrometric analysis. A number of research groups have devoted significant effort to find best MALDI sample preparation methods related to matrix,[57,117-120] solvent composition,[121-123] and deposition method,[120,124,125] but finding the best sample preparation for a variety of analytes is still empirical.[126-132] To find the best combination of parameters is difficult not only because of the number of tests required but also because of the inter-parameter interaction effects. McComb *et al*.[133] have investigated several parameters that influence MALDI sample preparation: choice of matrix, solution volume, solvent composition, solvent drying rates and matrix/analyte co-crystallization methods. Their results were notable, but the interaction effects among sample preparation parameters were ignored since they changed one parameter at a time while the other parameters were fixed.

In the 1940's Genichi Taguchi developed a technique, called "Taguchi's statistical approach" or "Taguchi experimental design."[134] Taguchi experimental design provides a systematic and efficient method for determining optimum parameters and getting maximum information with minimal experiments. In addition, it enables the determination of the complex interaction effects associated with parameters involved. Interactions are often important and may

be missed when investigations are carried out by changing one variable at a time. The objective is to select the best combination of controlled parameters so as to achieve the most robust process with respect to the signal-to-noise ratio. Taguchi experimental design has a number of advantages over conventional classical and factorial designs such as an efficient data analysis with a minimal number of experiments, the ability to study interaction effects between parameters, low source of errors, easy prediction of optimization results, step by step statistical controlling the conditions, low cost, and less time.[135]

There are a number of sample preparation methods developed for MALDI applications. These include dried droplet,[37,120,136, 137] vacuum drying,[138] crushed crystals,[136,139] slow crystal growing,[137,140] active thin film,[141-143] pneumatic spray,[144,145] electrospray,[26,146] fast solvent evaporation,[136,147,148] sandwich,[149,150] seed-layer (two-layer), [120,123,136] and bottom-layer.[124] In this research, three of the most widely used sample deposition methods were used and are described in the experimental section. The Taguchi experimental design was used to optimize MALDI sample preparation for the analysis of three pollens: giant ragweed from grass (*ambrosia trifida*), black walnut (pollen from *juglans nigra*), and corn pollen (*zea mays*) since they are potential background for biological aerosol particle analysis.[151] Interaction effects between parameters were also investigated.

**4.2. Experimental**

Pollen analytes were prepared by dissolving 1 mg of each pollen in 100 µL of solvent. Small amounts of pollen could be suspended in the 1:1 (v/v) acetonitrile and TFA in deionized water. A number of MALDI solvents were tested to suspend pollens such as acetonitrile, water, ethanol, methanol, acetone, dichloromethane and chloroform but none of them showed good results. Matrices were prepared in the same combination of solvents as analytes. Three sample deposition methods were chosen since they play an important role in a successful MALDI

analysis. A brief description of the sample preparation procedure is follows. 1) Dried droplet: A 1 μL of analyte was mixed with a 2 μL of matrix and spotted on a target and allowed to air dry. 2) Seed-layer: A 1 μL of matrix solution was spotted on a target and allowed to dry. Then, A 2 μL of 1:1 (v/v) analyte/matrix mixture was spiked on top of the first matrix layer and allowed to air dry. 3) Bottom-layer: A 1 μL of analyte was spotted on a target and allowed to air dry. A 2 μL of matrix solution was then deposited on top of the analyte layer and allowed to air dry. All mass spectra were acquired using a commercial MALDI time-of-flight mass spectrometer.

**4.3. Results and Discussion**

Mass spectra were obtained by conducting the experiments shown in Table 2-2. It is impossible to directly compare the individual mass spectra because only one level of parameter in a mass spectrum is the same as another, while the other levels are different. A series of nine mass spectra were obtained for each pollen, and the results were compared by grouping three combinations of mass spectra, which have the same level of each factor. The criteria of the comparison are based on the figures of merit such as the number of peaks, signal-to-noise ratio, and mass resolving power.

Three sets of nine mass spectra of black walnut (Figure 4-1), giant ragweed (Figure 4-2), and corn pollen (Figure 4-3) were obtained. External calibration was performed for all of mass spectra with calibration standard kits. The mass spectra in Figures 4-1, 4-2, and 4-3 were sorted in the order of experiment number from top to bottom. Pollen mass spectra were obtained in linear mode and were summed at an average of 50 laser shots to produce a final spectrum. No baseline correction was performed on the mass spectra shown in the figures. All of the mass spectra were obtained at the minimum laser fluence necessary to retrieve peaks equivalent to full laser fluence.

**Table 4-1.** Comparison of the average number of peaks in pollen mass spectra (corn pollen, giant ragweed, and black walnut) in the effect of different levels of matrix, solvent and deposition.

| Factors | Levels | Corn pollen | Giant ragweed | Black walnut |
|---|---|---|---|---|
| Matrix | FA | **31.3** | 28.0 | 14.0 |
| | CHCA | 26.3 | **47.0** | **23.0** |
| | SA | 24.7 | **47.0** | **23.0** |
| Solvent | ACN/$H_2O$ (0.1% TFA) | **28.7** | 36.3 | 20.0 |
| | ACN/$H_2O$ (0.5% TFA) | 26.7 | 42.0 | 17.7 |
| | ACN/$H_2O$ (2.0% TFA) | 27.0 | **43.7** | **22.3** |
| Deposition | Dried Droplet | **31.3** | 44.3 | **28.0** |
| | Seed Layer | 23.7 | 33.0 | 22.7 |
| | Bottom layer | 27.3 | **44.7** | 9.3 |

* Bold numbers are the highest number of peaks for each factor in each pollen.

Sample preparation parameters were found to significantly influence the mass spectra obtained. Some sample preparations showed mass spectra with abundant peaks and good resolution while some others showed no peak in the entire mass region. The number of peaks was determined on the basis of signal-to-noise ratio greater than 10 in the mass region over 1,000 Da. Table 4-1 shows a comparison of the average number of peaks in the mass spectra of the three pollens with different parameter levels (matrix, solvent, and deposition). The main effects of sample preparation parameters for black walnut (a, b, and c), giant ragweed (d, e, and f), and corn pollen (g, h, and i) by figures of merit, the number of peaks, S/N, and resolution are shown in Figure 4-4. The magnitude of the significance among factors affecting the quality of mass spectra can be determined by measuring the range of data of the levels of factors in Figure 4-4. The wider range of data between the levels of a factor, the more significant the factor is.

### 4.3.1. Matrix Effect

Three cinnamic acid derivatives of CHCA, SA, and FA were chosen for MALDI matrices since they were reported to be good matrices, especially in the detection of high mass proteins or peptides.[152,153] CHCA and SA matrices produced more peaks than FA matrix for giant ragweed and black walnut pollens while FA matrix produced more peaks than CHCA and SA matrices for corn pollen. Generally, MALDI matrices are classified as hot, intermediate, and cold matrices on the basis of their internal energy, threshold laser fluence, and fragmentation pattern.[117,118,154,155] The hot matrices produce lower internal energy and require lower threshold laser fluence, thus, generate more fragmentation at the same laser fluence than the cold matrices do.[118] It is reported that the CHCA and SA matrices are hot and the FA matrix is intermediate.[154] CHCA matrix generally produces more peaks in the low mass region up to *m/z* 5,000 while SA matrix produces more peaks in the high mass region over *m/z* 5,000.[156] Overall, the S/N and resolving power increased in the order of FA < CHCA < SA as shown in Figure 4-4 (◆, solid line) for black walnut and giant ragweed pollens, but CHCA was slightly better than SA for corn pollen. Among these three factors, the choice of matrix was the most important factor influencing the quality of mass spectra.

### 4.3.2. Solvent Effect

It is reported that the pH of the solvent affects mass spectra by extracting peptides and proteins more efficiently from bacteria and cells.[157] A 1:1 ACN/water solution containing 0.1%, 0.5%, and 2.0% of TFA was chosen to evaluate the effects on the pollen mass spectra. The pH of these solvents was measured with a pH meter: 1:1 (v/v) acetonitrile with 0.1%, 0.5% and 2.0% TFA produced 1.84, 1.26 and 0.82 pH value, respectively. The number of peaks and the spectral signal intensity increased as the concentration of TFA increased up to 3%, suggesting its ability to solubilize peptides and proteins from cells.[157]

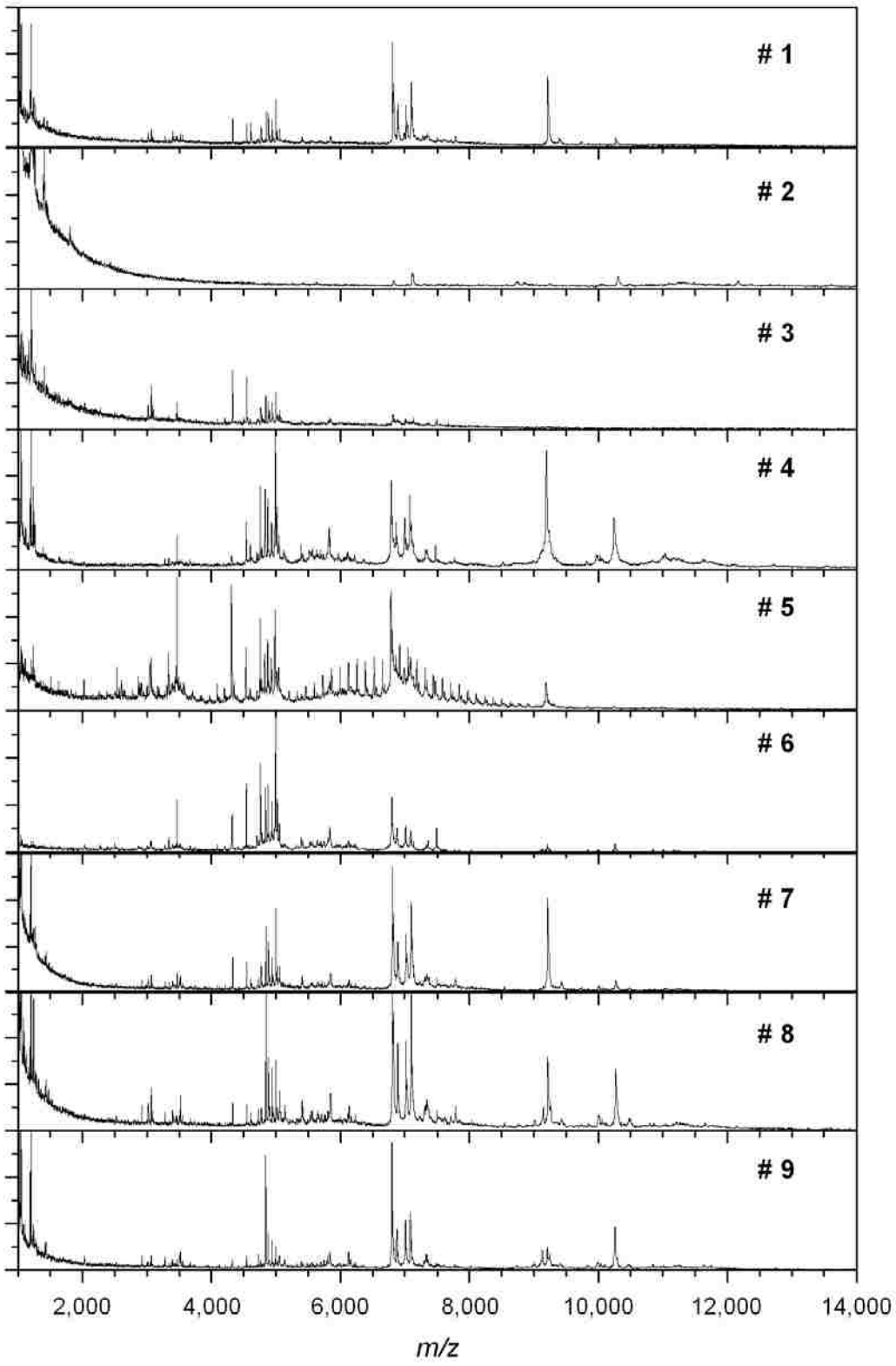


**Figure 4-1.** A set of nine mass spectra of black walnut pollen. Mass spectra were sorted by the experiment number from top to bottom. Mass spectra were obtained at the minimum laser fluence. Mass spectra were obtained in linear mode and were summed at an average of 50 laser shots. External calibration was performed, and no baseline correction was used.

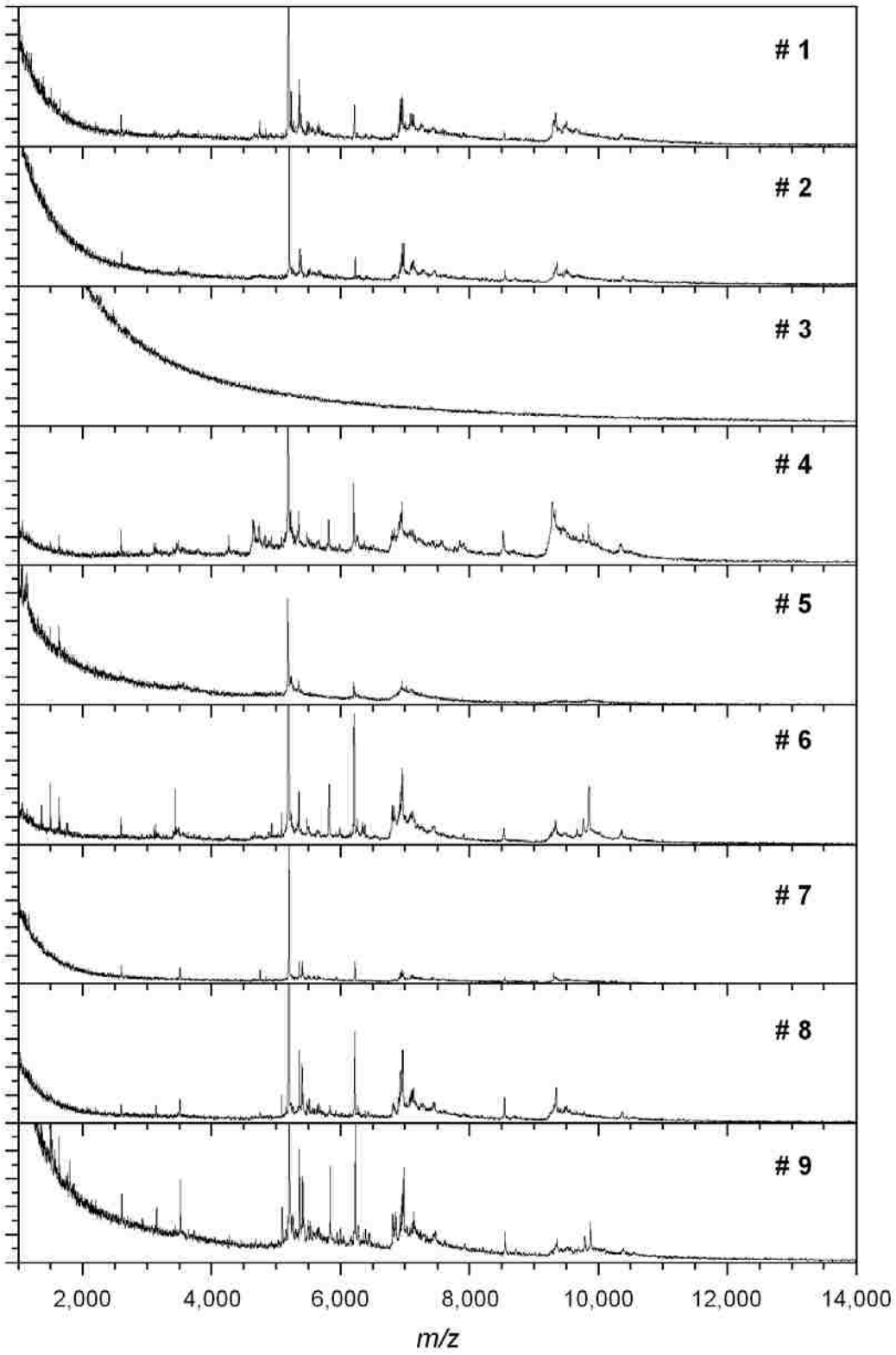


**Figure 4-2.** A set of nine mass spectra of giant ragweed pollen. Mass spectra were sorted by the experiment number from top to bottom. Mass spectra were obtained at the minimum laser fluence. Mass spectra were obtained in linear mode and were summed at an average of 50 laser shots. External calibration was performed, and no baseline correction was used.

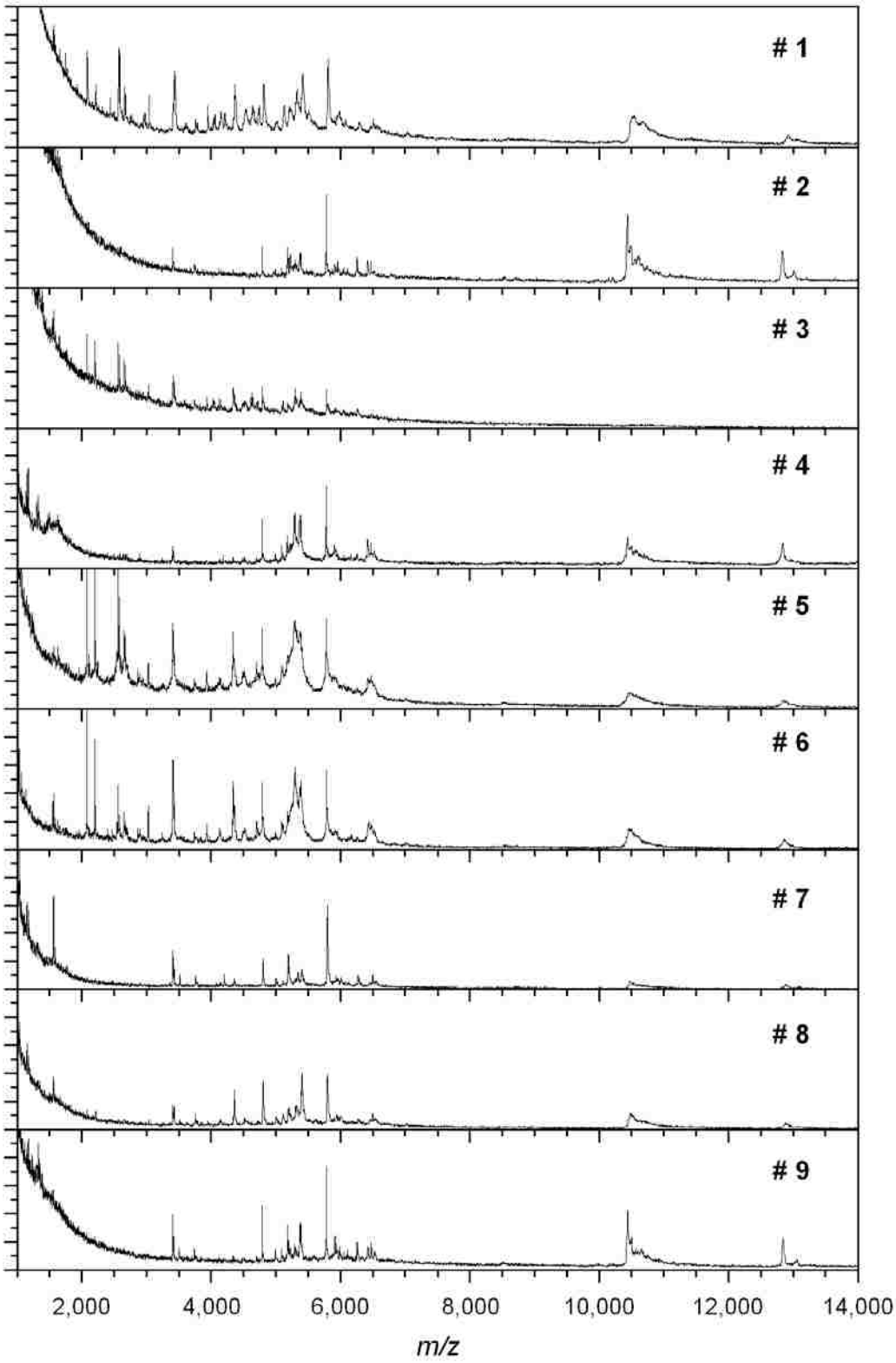


**Figure 4-3.** A set of nine mass spectra of corn pollen. Mass spectra are sorted by the experiment number from top to bottom. Mass spectra were obtained at the minimum laser fluence. Mass spectra were obtained in linear mode and were summed at an average of 50 laser shots. External calibration was performed, and no baseline correction was used.

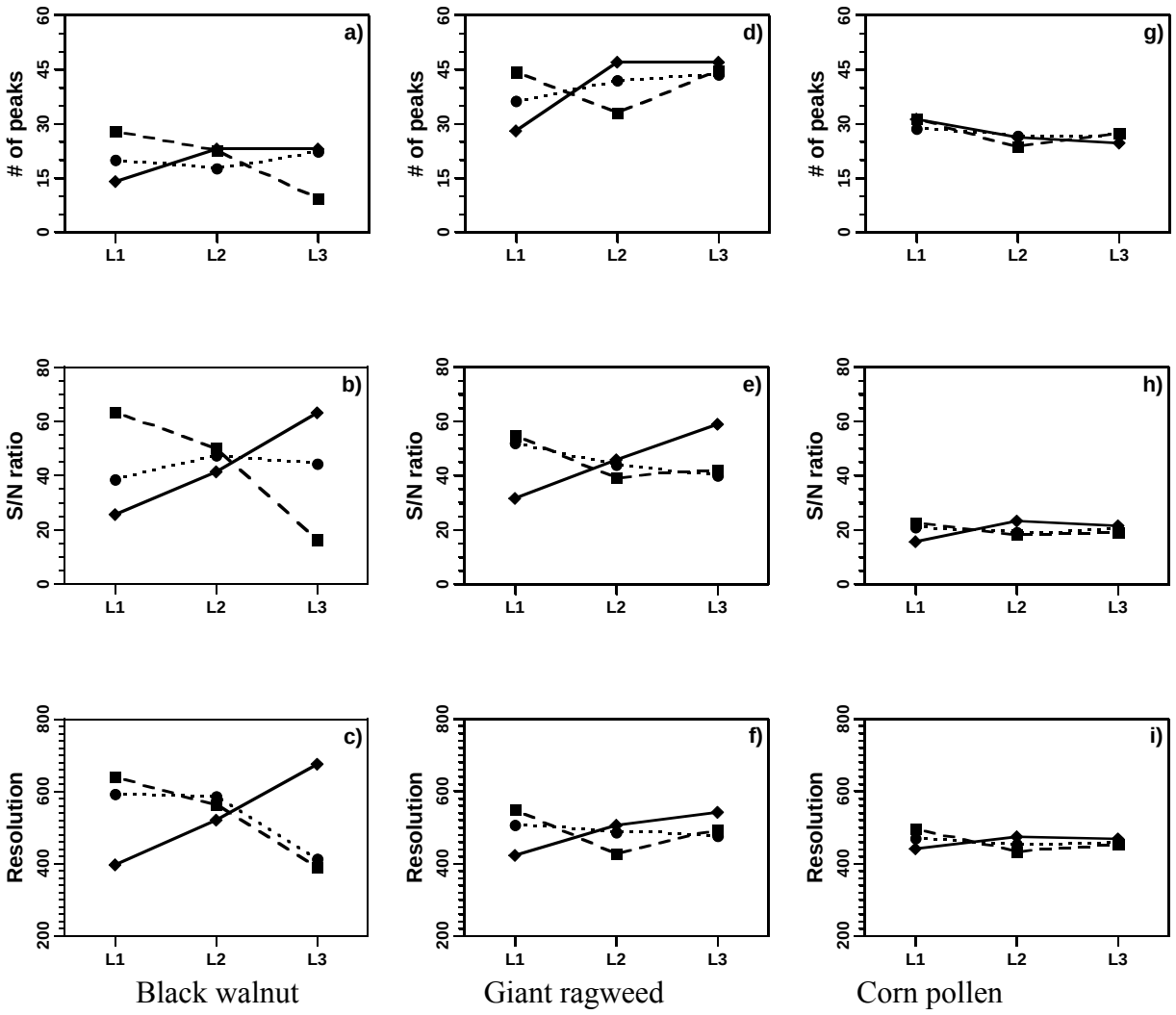


**Figure 4-4.** The effects of sample preparation parameters, matrix (◆, solid line), solvent (●, dotted line), and deposition (■, dashed line) on MALDI mass spectra for black walnut (a, b, and c), giant ragweed (d, e, and f), and corn pollen (g, h, and i) compared by figure of merit, number of peaks, S/N, and resolution.

But the number of peaks and intensity dropped as the concentration greater than 3% TFA. In this experiment, the highest concentration of 2.0% TFA produced more peaks for black walnut and giant ragweed as shown in Figure 4-4 (●, dotted line). But the 0.1% TFA produced slightly more peaks than the 2.0% TFA in corn pollen (see Table 4-1). The S/N and mass resolving power were inversely proportional to the concentration of TFA. Of the three sample preparation

parameters, the solvent composition appeared to have the least effect on mass spectra in terms of number of peaks, S/N, and resolution.

### 4.3.3. Deposition Effect

The MALDI sample deposition method is also known to significantly affect mass spectral signal.[120,124,125] Of the three deposition methods, the dried droplet method produced the best mass spectra for the three pollen analytes in terms of number of peaks, S/N, and resolution. With the exception of giant ragweed, the bottom-layer method produced slightly more peaks than the dried droplet method. The seed-layer and bottom-layer methods were the worst for corn pollen and back walnut, respectively, in terms of number of peaks, S/N, and mass resolving power. The giant ragweed pollen generated a unique polymeric peak pattern with a combination of CHCA and 0.5% TFA, and bottom-layer method. The mass spectrum of giant ragweed pollen is expanded in Figure 4-5. The unique polymeric peaks were generated in the mass region between 5,000 Da and 9,000 Da, and were spaced by 132.1 Da from each other. The mass difference of two adjacent peaks in each series might correspond to the loss of xylose ($C_5H_{10}O_5$, 132.1 Da),[158-160] which is an essential sugar saccharide of the pentose class and is vital to cellular communication. Xylose can be found in the embryos of most edible plants. Leonard *et al.*[161] also found a similar mass spectrum from Art v 1, the major allergen of mugwort (*Artemisia vulgaris*) pollen, which contains galactose (Gal) and arabinose (Ara). There were a series of 132 Da different mass peaks in the mass region from 6,000 Da to 9,000 Da. They interpreted the set of mass with spacing of 132 Da as dansyl-(Ara-)Hyp-(Ara-)Hyp, which indicates the presence of contiguous β-Ara-Hyp pairs in Art v 1.

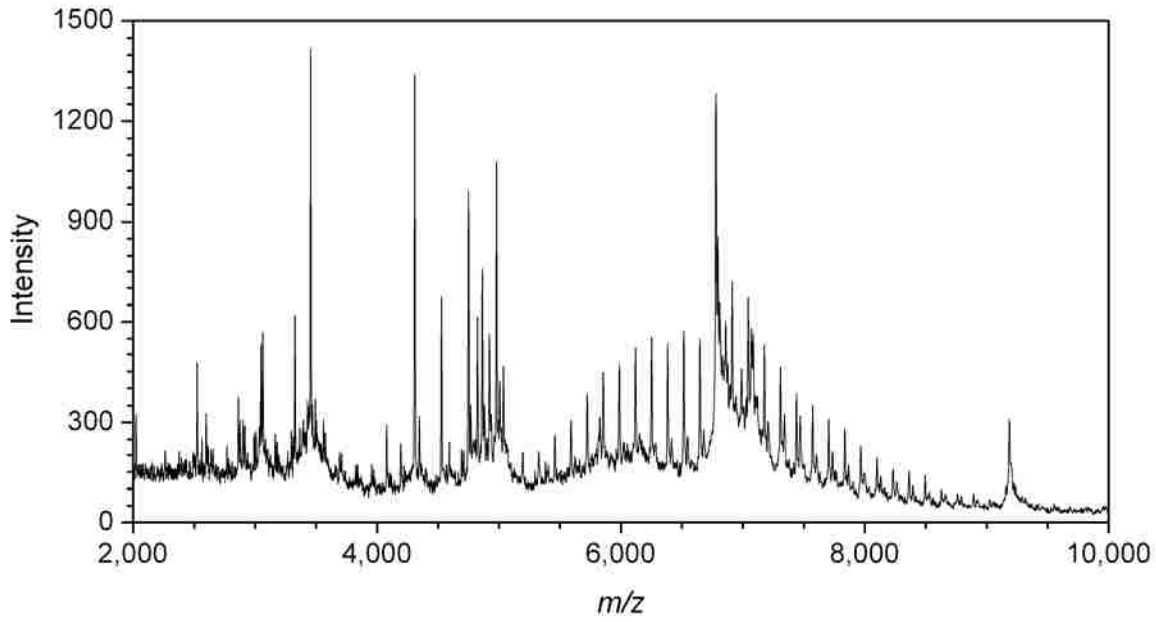


**Figure 4-5.** An expanded mass spectrum of giant ragweed pollen obtained from the combination of CHCA, 2.0% TFA, and bottom-layer. The mass spectrum corresponds to Taguchi experiment number 5 (M2S2D3) in Table 2-2.

### 4.4. Summary

A $L_9$ ($3^3$) orthogonal array of Taguchi experimental design was used to optimize the MALDI sample preparation parameters: matrix, solvent composition, and deposition method. Experiments were carried out in a random sequence of the Taguchi experimental plan. The resulting three sets of nine mass spectra were compared by grouping three combinations of mass spectra, which have the same level of each parameter with the criteria of number of peaks, S/N, and mass resolving power. Sample preparation parameters were shown to significantly influence the mass spectra obtained. CHCA and SA matrices produced more peaks than FA matrix in giant ragweed and black walnut pollens, while FA matrix produced more peaks than CHCA and SA matrices in corn pollen. Overall, the average of S/N and resolving power increased in the order

of FA < CHCA < SA. The pH of solvents was varied from 0.1%, 0.5%, and 2.0% TFA in 1:1 (v/v) acetonitrile/water solution to evaluate the effects on the mass spectra of pollens. Generally, the number of peaks in the mass spectra increased with TFA concentration, but S/N and mass resolving power decreased with TFA concentration. The dried droplet sample deposition method produced the best mass spectra for the three pollen analytes.

With giant ragweed, a unique polymeric peak pattern was produced with a combination of CHCA and 0.5% TFA, and bottom-layer method in the mass region between 5,000 Da and 9,000 Da. The peaks were spaced by 132.1 Da in the mass region and might be caused by the loss of xylose units ($C_5H_{10}O_5$, 130.1 Da).[158-160] Of the three sample preparation parameters, choice of matrix was the most important factor and solvent composition was the least important factor.

Taguchi experimental design is also useful to optimize parameters associated with the bioaerosol collection procedure. These parameters include flow rate, collection time, MALDI matrix, solvent addition, etc. The interaction effects between parameters of off-line bioaerosol collection can also be easily determined by Taguchi experimental design with minimum number of experiment.

# CHAPTER 5. BACTERIA DEPOSITION

## 5.1. Introduction

One of the chief issues in MALDI analysis of bioaerosols is the mixing of the matrix and the analyte.[12,56,162,163] This can be done in several ways: collected particles (or extracted material) can be mixed with matrix and deposited on the target,[52,164] particles can be collected on a matrix-coated target,[56] or matrix can be added to the particles by condensation.[12,162,163] Analysis of collected particulate affords the most freedom in sample treatment prior to analysis but is complicated and requires multiple sample preparation steps. Addition of matrix by condensation has been demonstrated previously both with off line[12] and on-line particle ionization.[56,162,163] The condensation matrix addition approach allows the ionization of particulates without deposition but as currently implemented, is not sufficiently sensitive for practical applications. Deposition on a matrix-coated target is attractive because it has the potential for rapid analysis and the process requires few preparatory steps. Initial results indicate that the mixing of matrix and analyte after deposition on the target is critical to obtaining good signal and suppressing background interferences.[165,166]

Recently, several research groups have demonstrated results showing that bacteria can be identified through their characteristic mass spectra using MALDI mass spectrometry with minimal fragmentation.[52,162,164] MALDI mass spectrometry has also been used to identify capsid proteins of intact virus particles.[167] For MALDI analysis of bacteria, lysed or whole bacteria are deposited on a metal surface along with matrix. These mass spectra are typically free of interferences from growth medium constituents or contaminants.[168] One approach to this analysis is based on proteomic bacterial identification. Identification of microbes based on protein

database searching[53] and MALDI spectrum fingerprinting[54,111] has been actively developed for homeland and national security applications.

In this study, collected bacteria-containing aerosol particles were analyzed by an off-line method using MALDI mass spectrometry. SEM images of collected gramicidin D particles were investigated to better understand the interaction between the matrix and the impacted bioaerosol particles. A variety of methods were explored to enhance the mass spectral signals of the collected bioaerosol particles comparable to a dried droplet of the bacteria suspension.

## 5.2. Experimental

Test bioaerosols containing bacteria were generated using a Collison nebulizer and collected on a MALDI target mounted in a modified Andersen N6 bioaerosol impactor.[57] The target was removed from the impactor and analyzed using MALDI time-of-flight mass spectrometry. Three different configurations were used: 1) particles collected on a bare target with matrix added later by a pipette, 2) particles collected on a matrix pre-coated target with post-collection pipette addition of solvent and 3) particles collected on a pre-coated target with post-collection spray deposition of solvent. The bioaerosol deposition methods were compared to the standard dried droplet MALDI sample preparation. The relative merits of the different deposition methods are discussed in terms of bioaerosol detection with minimal sample treatment and manipulation for use in remote and unattended MALDI mass spectrometry based bioaerosol detection instruments.

## 5.3. Results and Discussion

### 5.3.1. SEM Images

In order to better understand the interaction between the matrix and the impacted analyte, SEM images were taken of impacted particles produced by the Collison nebulizer on matrix precoated targets while the impaction stage was in static (non-rotating) mode. Figure 5-1 shows

SEM images of gramicidin D particles impacted on a sample target coated with 2,5-dihydroxybenzoic acid (DHB, Sigma) matrix. In this sample, the target was coated with 400 μL of DHB, and the aerosol particles were generated by the Collison nebulizer and collected on the target for one minute in the Andersen impactor. Figure 5-1a is an SEM image of a single impaction area. This image shows that a less dense peripheral region surrounds a dense center, which is roughly 250 μm in diameter. The total impaction area including the center and perimeter region is approximately 750 μm in diameter. A close-up of the peripheral region is displayed in Figure 5-1b, in which gramicidin D particles are deposited on the DHB crystals. The perimeter of the impaction area is the region where the matrix and analyte are the most thoroughly mixed together. This would explain the results in which analyte signal was improved when the laser irradiated the perimeter of the impaction spot, but no analyte signal was observed when the laser irradiated the center of the impaction spot since the analyte and matrix were not mixed in a proper ratio for MALDI analysis.

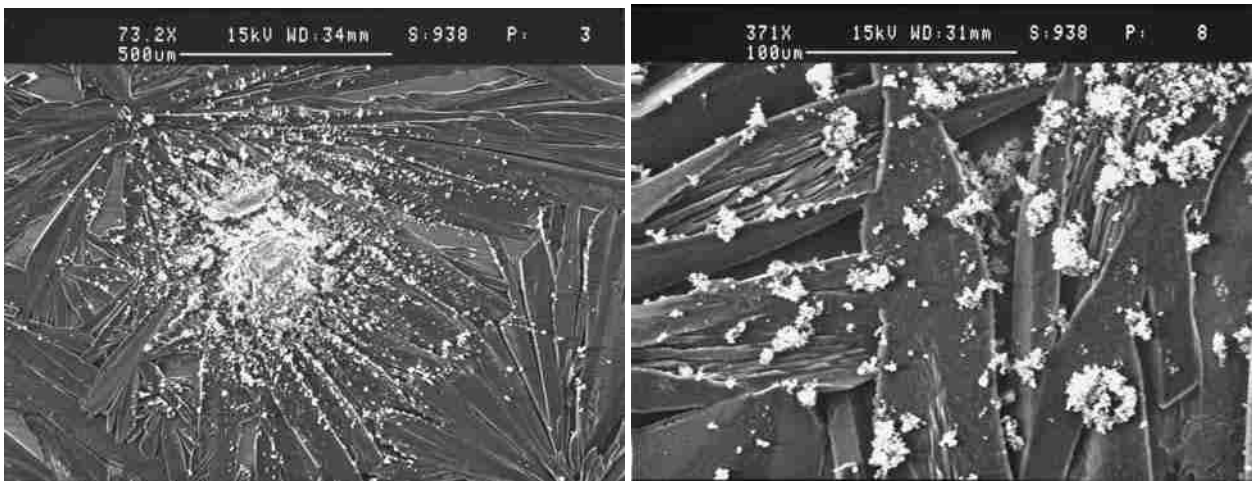


a) b)

**Figure 5-1.** SEM images of gramicidin D particles impacted on a sample target pre-coated with DHB matrix. a) 73X scale image of an impacted sample spot and b) 371X scale image of the perimeter of the impacted sample spot.

### 5.3.2. Collected Particle Concentration

In this experiment, the Collison nebulizer was used to generate aerosol particles from a bacteria suspension. The nebulizer was operated at a flow rate of 5 L/min with filtered house air. At this flow rate, approximately 5,000 to 10,000 particles/$cm^3$ with a mean diameter of 2 μm were generated.[12] The aerosol particle impaction time was four and half minutes for this experiment. The number of particles collected on the target by the aerosol impactor can be estimated from the total concentration, volume, collection time, and flow rate, and was 100 to 200 million particles. The Andersen N6 aerosol impactor has 400 holes. Thus, the number of particles on a single target spot is 300 to 600 thousand. The number of particles collected on a single spot is most likely overestimated because several sources of aerosol particle losses were not considered. For example, the bacteria suspension was extremely concentrated in the approximately 3 mL suspension remaining in the Collison nebulizer after four and half minutes of nebulization. There is also particle loss between the Collison nebulizer outlet and the Andersen impactor inlet tube where there is a gap of approximately 2 mm to compensate a pressure difference between outgoing flow from the nebulizer and incoming flow to the impactor. In addition, the loss of particles from condensation in the impactor nozzles was not considered. Finally, aerosol particles that did not stick to the target were not considered. We can estimate the number of particles collected on a single spot if it is assumed that: 1) 70% of the bacteria suspension remained in the 3 mL of residual suspension, 2) 10% of the nebulized aerosol particles were lost at the 2 mm gap because of the slight overflow from the nebulizer, 3) 20% of nebulized suspension condensed in the impactor nozzles, and 4) 50% of aerosol particles did not stick and were drawn into the pump. In this case the total number of particles deposited on each spot will be approximately one tenth of the above calculated value: 30,000 to 60,000 particles.

The volume of bacteria suspension deposited on a single spot can also be calculated from the volume of the nebulized bacteria suspension and the number of impactor holes and is 17.5 µL/hole. If we consider the losses of the nebulized bacteria suspension estimated above, the actual volume of bacteria suspension deposited onto a single spot is 2 µL. This volume is close to the volume of bacteria solution deposited by the dried droplet method, which is 1 µL of bacteria solution. If so, the volume of deposited bacteria solution on a single spot is about similar to that of dried droplet, but the analytes were not mixed with the matrix well, resulting in lower ion signals.

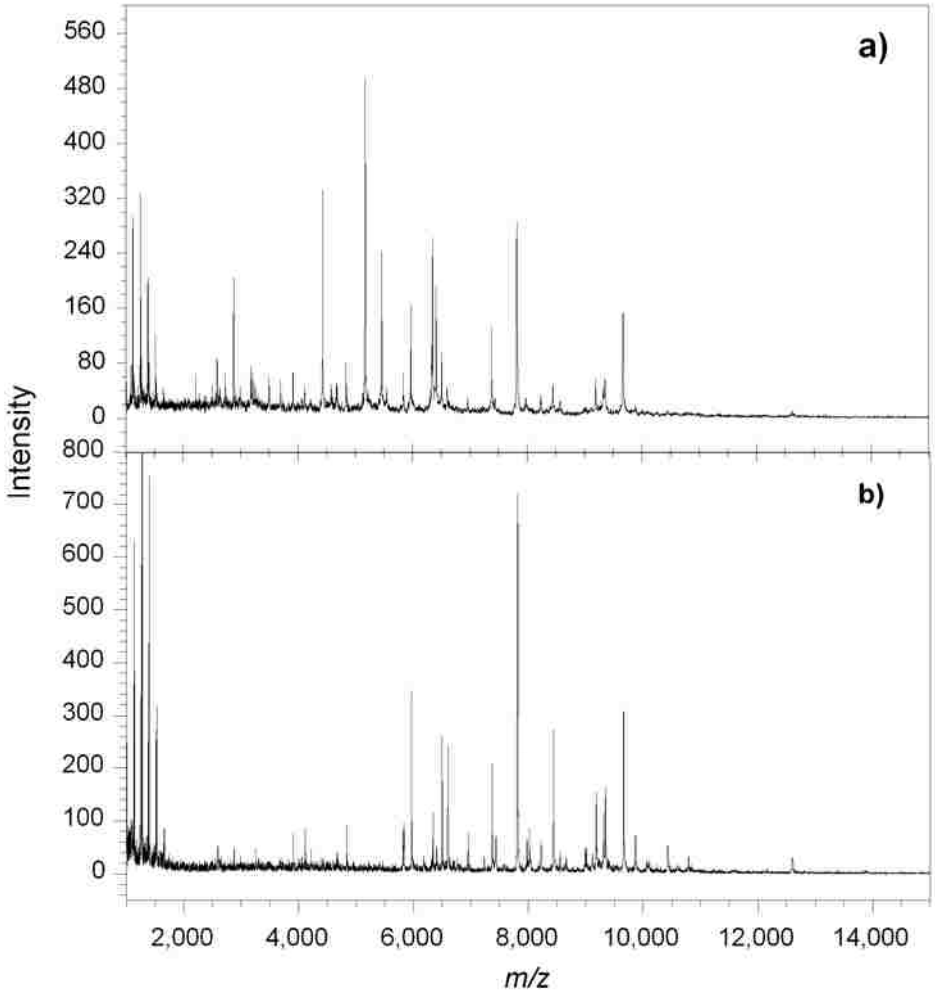


**Figure 5-2.** MALDI mass spectra of *E. coli* bacteria using a) CHCA and b) SA matrices.

### 5.3.3. Dried Droplet Deposition of Bacteria

MALDI mass spectra of *E. coli* deposited using the dried droplet method are shown in Figure 5-2 and will be used for comparison with those obtained from the collected bacteria aerosol particles shown below. These mass spectra are similar to those reported previously that several dozen peaks are resolved in the *m/z* range above 1,000.[169] The locations and relative intensities of the peaks depend on a number of factors including bacterial strain,[170] growth stage,[53,171] and the matrix used.[53,111,170-172] In Figure 5-2, between 30 and 40 peaks were observed in the mass range between 1,000 and 13,000 with a signal-to-noise ratio up to 100 and an average mass resolving power of 600 and 1,100 for CHCA and SA, respectively. The CHCA matrix generally produced more peaks in the *m/z* range below 6,000 as compared to SA.[156] Over 95% of the peaks that have a signal-to-noise ratio higher than 3 were reproducibly obtained in mass spectra observed in this region.

### 5.3.4. Rotating and Static Target

The Andersen impactor was modified to accept a MALDI target that can be rotated by a clock motor, while the aerosol particles were impacted on the target in order to disperse particles over the surface of the target so that the particles and matrix can be mixed well for better MALDI performance. The target was seated approximately 3 mm higher than the surface of the base plate to achieve the proper distance between the impactor nozzle and the surface of target. The target was connected to the axle of an AC motor by a shaft extending through a hole in the base plate underneath the target. There was no distinctive difference in mass spectra between a rotating target and a static target (data not shown) as long as the spot near the perimeter of the impaction area was irradiated on the rotating or the static target. Thus the targets were used in static mode for further analysis.

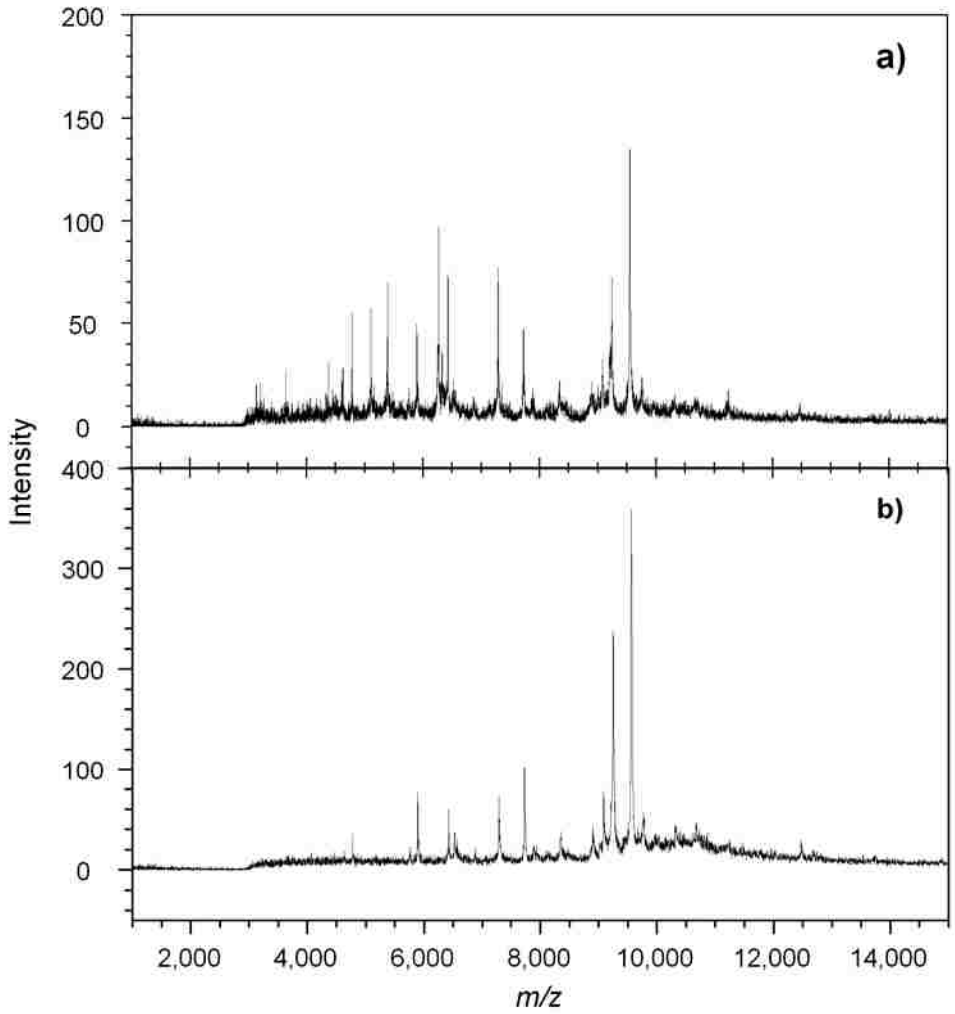


**Figure 5-3.** Mass spectra of *E. coli* bacteria obtained by depositing 1µL of a) CHCA and b) SA matrix on the collected test bioaerosol particles. Ion suppression was used below *m/z* 3,000, resulting in some baseline discontinuity.

### 5.3.5. Choice of Matrices

In the initial bioaerosol MALDI experiment, test bioaerosols were generated from a solution of lyophilized *E. coli* and collected on a MALDI target for four and a half minutes in the modified Andersen impactor. After particle collection, the target was removed from the impactor, and 1 µL of saturated matrix solution was added to each collected spot on the target. Figure 5-3a shows the mass spectrum resulting from the addition of CHCA, and Figure 5-3b shows the mass spectrum obtained from SA addition. For MALDI analysis of collected bioaerosol particles,

approximately one-third higher laser fluence was required to obtain adequate signal in the higher *m/z* region (above 6,000) compared to the dried droplet sample preparation. Ion suppression was employed below *m/z* 3,000 to reduce the background signal and the baseline from fragment peaks, matrix peaks and other interferences caused by the increased laser fluence. The S/N is comparable between Figure 5-2 and Figure 5-3, but in Figure 5-3, there are approximately half as many resolved peaks, and there are few appearing above *m/z* 10,000. The observed mass resolving power is a factor of two lower for the particles collected on SA matrix in Figure 5-3b compared to those collected on CHCA matrix in Figure 5-3a. The mass resolving power in Figure 5-3a is approximately 800 for CHCA, which is slightly higher than that observed with the dried droplet method (Figure 5-2a). Overall, there are fewer peaks in Figure 5-3 as compared to Figure 5-2; however, all of peaks observed in Figure 5-3a and Figure5-3b match with corresponding peaks in Figure 5-2a and Figure 5-2b, respectively.

### 5.3.6. Effects of Solvent Addition

Mass spectra obtained by depositing bioaerosols on matrix-coated targets are shown in Figure 5-4. The matrix-coated target was prepared by depositing 400 μL of matrix solution on the target to cover the entire surface and allowed to dry before the target was placed in the impactor. The target was removed from the impactor after bioaerosol deposition and inserted directly into the mass spectrometer for analysis without further treatment; the mass spectrum Figure 5-4a was obtained as a result. The jump in signal at *m/z* 3,000 reflects the ion suppression pulse and resulting shift in baseline. No signal was observed above 3,000, and only unresolved low *m/z* signal was recorded. However, signal could be recovered if solvent was added to the target after the bioaerosol was collected on the matrix pre-coated target. Figure 5-4b and 5-4c show the result of adding 200 μL of a 1:1 (v/v) mixture of acetonitrile and water on the spot of collected particulate deposited on CHCA and SA matrix-coated targets, respectively. The SA

target mass spectrum in Figure 5-4c is similar in terms of number of peaks, S/N and mass resolving power (greater than 800) compared with Figure 5-2b, the SA dried droplet mass spectrum. The CHCA target mass spectrum in Figure 5-4b is somewhat lower in quality with fewer peaks and poor mass resolving power (approximately 200) at one-third higher laser fluence compared to the dried droplet mass spectrum in Figure 5-2a.

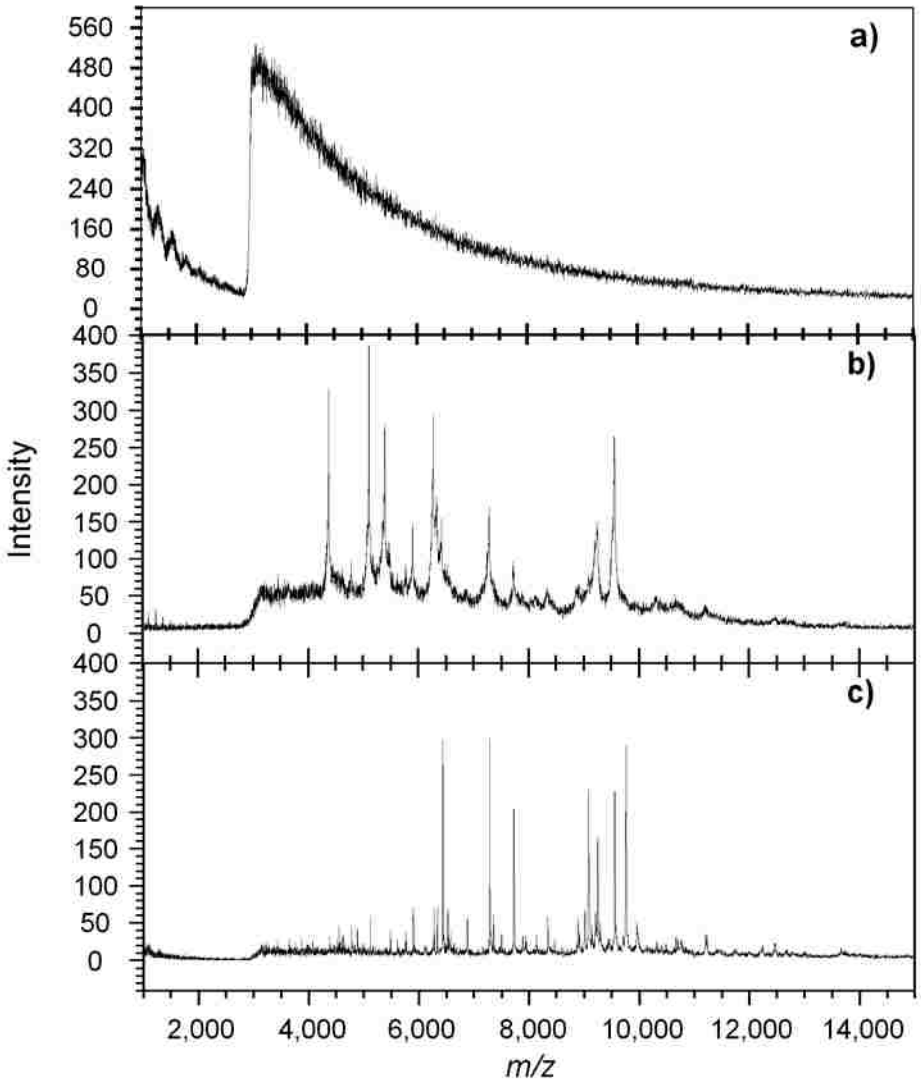


**Figure 5-4**. MALDI mass spectra of test bioaerosols deposited on a target pre-coated with a) SA matrix and no additional treatment, b) CHCA plus 200 µL of solvent, and c) SA plus 200 µL of 1:1 (v/v) acetonitrile/water solvent. Ion suppression was used below *m/z* 3,000, resulting in some baseline discontinuity.

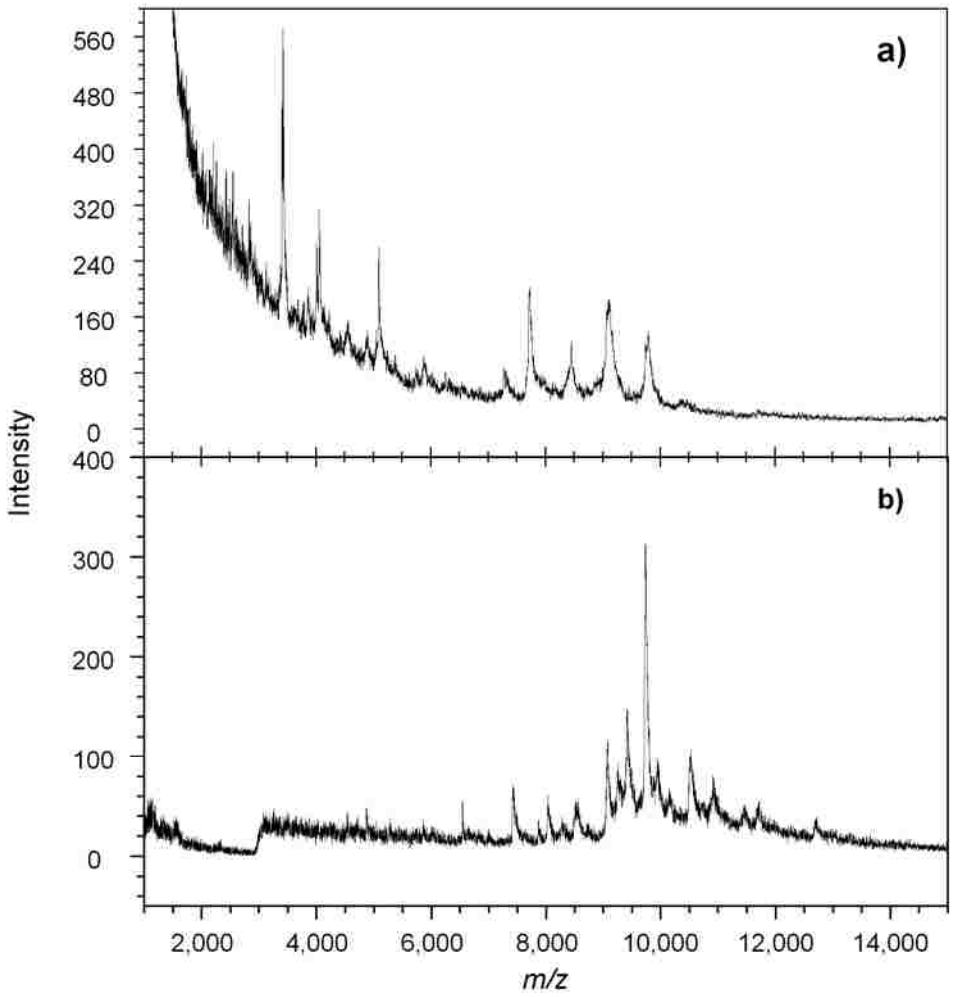


**Figure 5-5.** MALDI mass spectra of test bioaerosols deposited on a target pre-coated with a) CHCA and b) SA matrix with 1:1 (v/v) acetonitrile/water solvent added afterward by spray deposition.

### 5.3.7. Solvent Addition Methods

As a final test of the impaction on the matrix approach, test bioaerosols were deposited on matrix-coated targets followed by spray deposition of solvent. These results are shown in Figure 5-5. Matrix-coated targets were inserted into the impactor and test bioaerosol particles were deposited on the target. Solvent was deposited on the target in the form of aerosol particles delivered to the throat of the impactor. The solution of 1:1 (v/v) acetonitrile/water was nebulized using the Collison nebulizer and collected on the target for four and a half minutes. It is possible

that some of the solvent was deposited by vapor condensation due to evaporation from the particles; however, sufficient solvent was added to the sample deposit to partially recover the high-mass signal. Several peaks are observed in the mass spectra, but they are relatively few in number and broad with a mass resolving power of 75 and 100 for CHCA and SA respectively. A possible method for field applications to recover the signal efficiently is that a matrix can be mixed with analyte by continuous spraying of matrix solutions during and following the bioaerosol deposition through the impactor.

### 5.4. Summary

Test bioaerosol particles formed by nebulizing a solution of lyophilized *E. coli* bacteria and impacted on a target by a modified impactor were tested with several methods of particle collection and subsequent matrix or solvent addition for off-line analysis. The number of particles collected on the target by the aerosol impactor was estimated from the total concentration, volume, impaction time, and flow rate. The number of particles calculated theoretically was most likely overestimated because several sources of aerosol particle losses were not considered. Considering the aerosol particle losses, it was estimated that 30,000 to 60,000 particles were deposited per spot. The volume of bacteria solution deposited on a spot was estimated at approximately 2 μL and was close to the volume of bacteria solution deposited with the dried droplet method (1 μL). The test bioaerosol particles collected on a spot was double of dried droplet deposition, but the collected particles were not mixed with matrix well, resulting in lower ion signals.

Of these methods, particles collected on a matrix pre-coated target with post-collection solvent addition gave the best results, which were nearly identical to those obtained using the standard dried droplet approach. The number of peaks and the mass resolution, however, were lower. Deposition on a matrix pre-coated target without later solvent addition did not result in

mass spectra: some types of post-collection reagent addition (either solvent or matrix solution) was necessary to obtain mass spectra. The fact that solvent or matrix addition is necessary to obtain MALDI mass spectra of collected bioaerosol particles has important implications for portable and transportable instrumentation for bioaerosol detection. A remote automated data collection system based on a MALDI MS approach must have a solvent reservoir and a mechanism for the addition of the solvent to the matrix target prior to analysis. Simple deposition onto matrix pre-coated targets will most likely not be sufficient. This will add to the size and complexity of such an instrument and require periodic reagent replenishment. The mechanical complexity of such a system might be reduced if the liquid reagents are sprayed into the impactor after (or potentially during) particle deposition, but operation in this mode will result in lower performance.

# CHAPTER 6. TRANSMISSION GEOMETRY MALDI

## 6.1. Introduction

Matrix-assisted laser desorption/ionization is one of the most versatile techniques for the ionization of large and nonvolatile biologically relevant molecules such as peptides, proteins, and nucleotides. However, nearly all MALDI analyses use a front-side laser irradiation for desorption and ionization where the laser irradiation and the ion extraction take place on the same side of the sample. Due to the laser focusing limitations, front-side geometry MALDI is limited to a spatial resolution of typically greater than 30 μm.[173-175] While this is insufficient to obtain the spatial distribution of the molecules within a cell since the diameter of an average cell is much smaller, it has allowed the spatial distribution of relatively large structures such as proteins in a tissue to be recorded.[176] Several approaches have been taken to achieve improved spatial resolution. A Schwarzschild microscope objective mounted outside of the vacuum chamber was used for focusing the laser beam to achieve 1 μm resolution with LDI for the analysis of Rhodamine 6G.[177] A spatial resolution of 4 μm was achieved for UV MALDI with an ultrahigh vacuum (UHV) compatible microscope objective with a focal length of 40 mm.[178] This was mounted on a telescopic and a maneuverable UHV flange for use with a nitrogen laser. A modified objective lens in front-side geometry was used to obtain a spatial resolution of 1 μm for laterally resolved mass spectrometric surface analysis.[179]

An alternative method of laser irradiation for MALDI analysis is irradiating the sample from the back-side of a transparent substrate in transmission geometry, with a directly focused laser beam,[180-182] a laser beam focused through an optical fiber,[183-185] or a microscope objective lens, which allows for a tight laser focusing without compromising either the laser or ion optics. Vertes *et al*.[181] were the first to demonstrate MALDI of neuropeptides (substance P and

bombesin) in transmission geometry using a LAMMA 500 instrument at 266 nm wavelength with nicotinic acid as a matrix. Ehring *et al*.[182] introduced transmission geometry to identify the contribution of photochemical and thermal effects in the formation and ejection of biomolecule ions in the MALDI process. Samples were irradiated from the back side as well as the front side through specially fabricated quartz holders with a 200 nm gold layer, which is optically non-transparent, resulting in that only thermal effects can contribute to the back side irradiation. Schűrenberg *et al*.[183] compared UV-MALDI of peptides and proteins in transmission geometry and reflection geometry and found that there were distinct differences in the respective plume dynamics. The mean velocity of the ions in the plume becomes zero in transmission geometry, while the jet-like plume expansion was generated in conventional reflection geometry. Lennon and Glish[184] introduced a 335 nm Nd:YAG laser from a fiber optic to irradiate the back side of a sample through a small piece of quartz in a quadrupole ion trap mass spectrometer. In their study, the sample lifetime over 2500 laser shots could be achieved in transmission geometry. Perez *et al*.[185] first introduced laser desorption in transmission geometry in a Fourier-transform ion cyclotron resonance mass spectrometer (FT-ICR). They found that ions desorbed in transmission geometry have less translational energy than those desorbed in reflection geometry, and therefore, the transmission mode irradiation improves the trapping efficiency of ions desorbed by MALDI in FT-ICR. Galicia *et al*.[180] used transmission geometry laser illumination with atmospheric pressure matrix-assisted laser desorption/ionization (AP MALDI) to eliminate the need for a metallic sample holder. The transmission geometry allows the analysis of samples on their native transparent surfaces, such as cells or tissue sections on slides. Due to the coincidence of the sampling orifice axis with the direction of the plume expansion in transmission geometry, there is also a potential benefit in terms of improved ion collection efficiency and sensitivity.

To achieve ion generation from the back side of a sample target in transmission geometry, several laser ionization techniques can be used. Figure 6-1 shows a diagram of possible approaches of UV and IR laser irradiation in transmission geometry MALDI mass spectrometry: 1) UV MALDI ionization, 2) IR matrix-free LDI ionization, and 3) IR LDI with UV laser post-ablation ionization. Figure 6-1a shows a commonly used method in transmission geometry MALDI analysis.[181,182] Analyte and matrix are deposited on the front side of a quartz substrate (a UV wavelength transparent target) where the sample side is exposed to a vacuum. A UV laser irradiates the sample from the back side of the substrate to ionize. A microscope objective lens is positioned between the laser and sample substrate to achieve a tight lateral focusing. Second, Figure 6-1b shows that an IR laser is used instead of a UV laser to achieve matrix-free ionization of the analyte since IR lasers have some advantages compared to UV lasers, which include a soft ionization, large amount of material ablation (in-depth ablation), liquid matrix availability (such as glycerol), and less fragmentation.[76,82,186] It is reported that the ionization efficiency of an IR laser ($\lambda$ = 2.94 μm) is 10 times less than that of a UV laser ($\lambda$ = 337 nm).[187-189] Third, Figure 6-1c shows a combination of IR and UV laser ionization. IR LDI with UV laser post-ablation ionization approach has a great potential of better sample desorption by IR laser and ionization with a UV laser.[186] In this setup, the sample is irradiated with the minimal IR laser fluence to desorb analyte particles into the gas phase and then those particles are ionized by post-ablation with a UV laser perpendicular to the IR laser. This has the potential to not only improve the ionization efficiency but also enable matrix-free soft ionization.

In this research, we have constructed a MALDI mass spectrometer that uses a microscope objective to focus the laser onto a sample that is supported on a transparent target from the back side in transmission geometry.

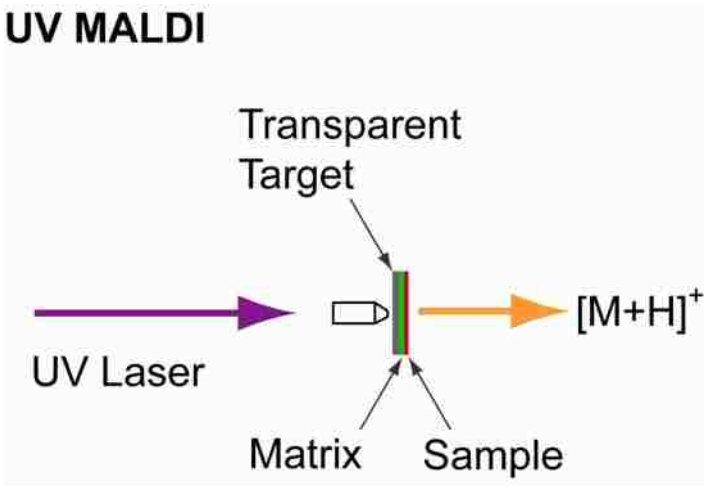


**a)**

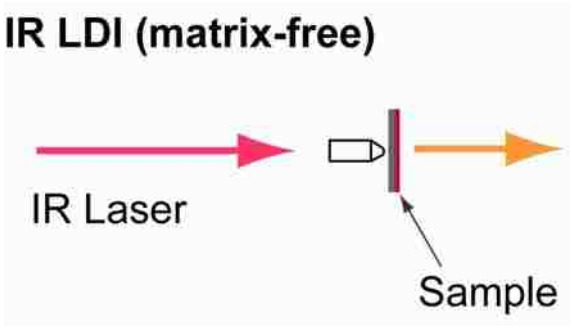


**b)**

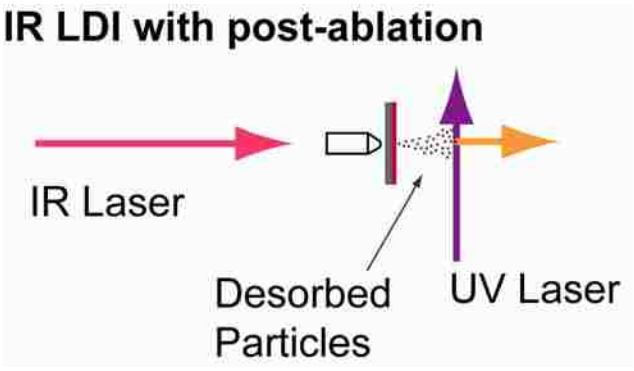


**c)**

**Figure 6-1**. Diagram showing possible approaches of UV and IR laser introduction in transmission geometry MALDI mass microscope: a) UV MALDI ionization, b) IR matrix-free LDI ionization, and c) IR LDI with UV laser post-ablation ionization.

In this mode, the spatial resolution of the image is limited by the microscope magnifying optics with an ultimate goal of a single cell analysis and precise MALDI imaging. In transmission geometry, the restrictions for guiding the laser beam through the ion optics can be overcome, eliminating problems associated with complex optical systems. Our ultimate application for this instrument is the analysis of single deposited bioaerosol particles, but the system is equally applicable for the analysis of single cell or a micrometer resolution imaging of thin tissue sections.

**6.2. Experimental**

In this work, the UV MALDI ionization approach shown in Figure 6-1a was employed in transmission geometry. An aliquot of peptide and matrix was deposited on a thin glass substrate and allowed to air dry. The sample target was then mounted on the vacuum flange so that the sample side was exposed to vacuum while the back of the substrate could be accessed at atmospheric pressure. A 337 nm nitrogen laser was used for UV MALDI analysis. The laser beam was moved across the sample in the x and y dimensions by adjusting a mirror and objective lens while mass spectra were acquired in a linear or a reflectron time-of-flight mass spectrometer. Figure 6-2 shows a photograph of the transmission geometry MALDI mass spectrometer.

For the initial studies, matrix and peptide standards such as angiotensin II, bradykinin, angiotensin I, substance P, bombesin, ACTH (1-17), and ACTH (18-39), were prepared in sub-picomole concentration for both reflection geometry and transmission geometry MALDI analysis. Saturated matrix solutions of CHCA, sinapinic acid, and DHB were prepared in 1:1 (v/v) acetonitrile/$H_2O$. A 1 μL of analyte mixed with 2 μL matrix solutions were spotted on a target with the dried droplet method and allowed to air dry at room temperature.

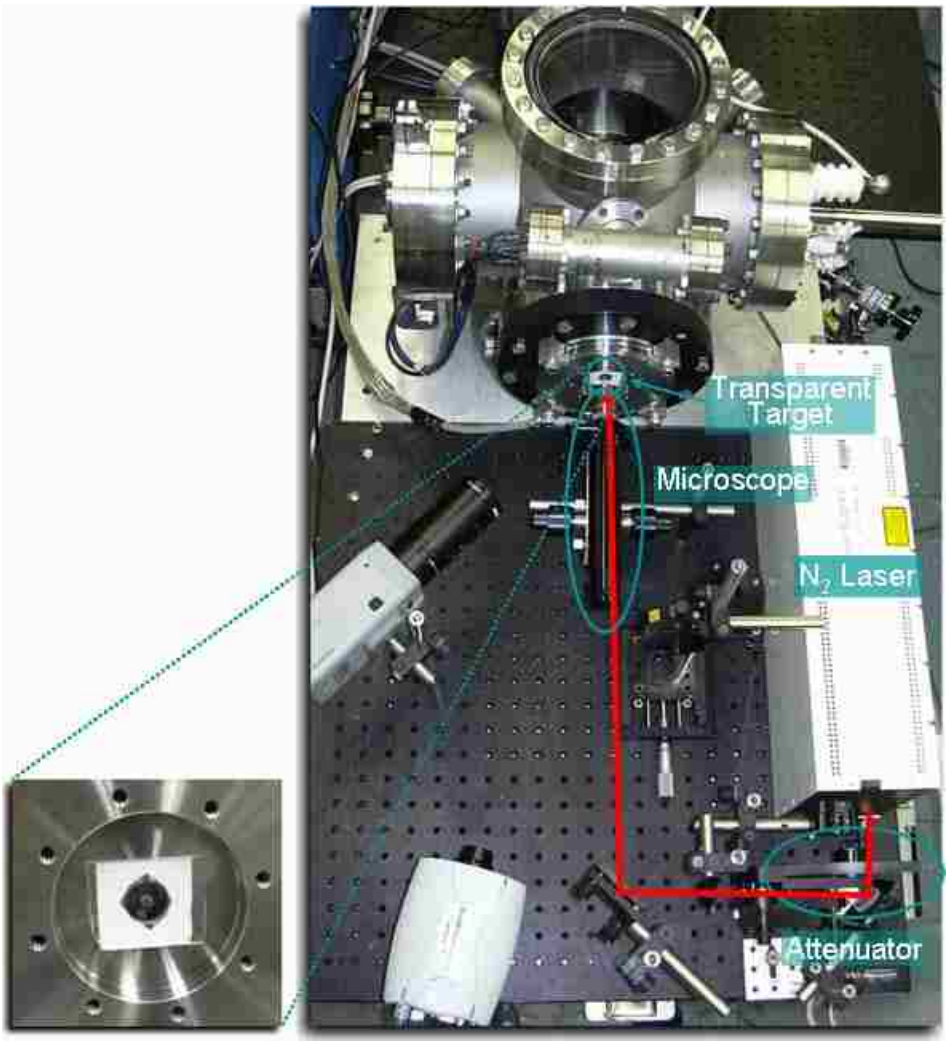


**Figure 6-2.** Photograph of a transmission geometry MALDI mass spectrometer with microscope objective lens. The inset image shows a magnified area of the stainless steel target holder and glass target substrate with sample deposits. The white thin film behind the glass substrate is a teflon tape gasket.

### 6.3. Results and Discussion

A conventional front side irradiation (reflection geometry) MALDI mass spectrometer was constructed and tested for performance with common MALDI matrices and peptides for the comparison with data obtained from transmission geometry. Figure 6-3 shows a MALDI mass spectrum of CHCA matrix obtained from the reflection geometry in the reflectron mode of operation. Isotopic resolution for the molecular ion peak of CHCA matrix could be obtained with

the reflection geometry; mass resolving power of 800 could be achieved for the molecular ion peaks. After the successful demonstration of front side geometry, the ion source was converted to the transmission geometry in which a laser irradiates samples from the back side of the target.

Transmission geometry MALDI mass spectra were obtained using the peptide mass standards, bradykinin and angiotensin I, mixed with CHCA matrix on a glass microscope slide target. A 337 nm nitrogen laser was focused on the back side of the sample through a 25 cm $CaF_2$ focusing lens. First, the same focusing lens and optics used for the front side configuration were used to compare the performance of the two geometry configurations. The experiments with both geometry configurations were carried out in a static acceleration mode with a linear or reflectron TOF mass spectrometer.

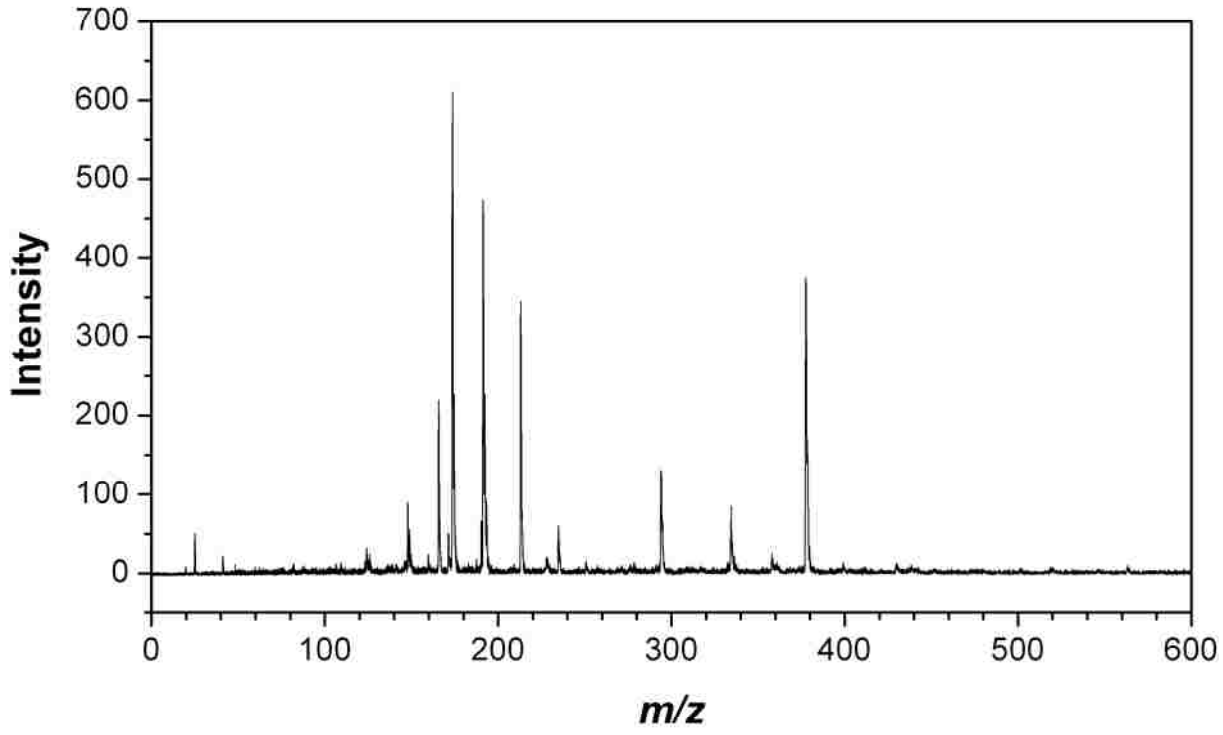


**Figure 6-3.** MALDI mass spectrum of CHCA matrix obtained from reflectron mode in reflection geometry.

The effects of instrumental parameters such as substrate material, laser power, acceleration voltage, ion mirror voltage, and deflector voltage were investigated to find optimal conditions for the detection of the analyte ions. In transmission geometry, approximately ten times the laser energy was required to obtain mass spectra compared to the reflection geometry.[180] In this study, a 1.0 mm thick microscope glass slide, which has a transmittance of approximately 95% at 337 nm,[190] was used for UV irradiation. It is reported that the substrate conductivity, substrate surface, and composition do not affect the ion yield generated in transmission geometry.[180] Therefore, no significant difference was expected in the mass spectra from the various surfaces and substrate materials. But laser transmission efficiency is affected by the absorption coefficient of the substrate used.[180] Therefore, a higher laser fluence is required for a lower transparent substrate of the laser wavelength used in transmission geometry.

### 6.3.1. Transmission Geometry vs. Reflection Geometry

The following two figures show the comparison of MALDI mass spectra of bradykinin (Figure 6-4) and angiotensin I (Figure 6-5) with a) 4X microscope objective lens in transmission geometry, b) transmission geometry, and c) reflection geometry. Mass spectra obtained by reflection geometry and transmission geometry are 10 shot and 5 shot averages, respectively. Samples were completely depleted within tens of laser shots in the transmission geometry. Thus, the laser beam was shifted to irradiate a fresh sample spot during the mass spectra acquisition by adjusting the reflecting mirror and the objective lens. The transmission geometry configuration yielded a ten times lower intensity signal[180] and required a higher laser fluence[182,183] compared to reflection geometry. The mass resolving power of both peptides was significantly decreased with the transmission geometry not only because the mass spectra of a) and b) were obtained in linear mode while c) was obtained in reflectron but also because the transmission geometry was not fully optimized at the time. The mass resolving power of mass spectra a), b), and c) in both

Figure 6-4 and 6-5 was approximately 40, 150, and 350, respectively.

A dried droplet sample preparation with 1:1 ACN/$H_2O$ solvents typically produces large matrix crystals in nonuniform distributions on a glass microscope slide and generated a thick layer of sample spot, which is approximately 10 μm thick.[183] Since the ion emission in transmission geometry occurs from the bottom of the sample by the back side laser irradiation, a thin sample layer is required for efficient ion plume generation.[183] The sample thickness along with the absorption length calculated by the absorption coefficient of the matrix, greatly affects the plume distribution in transmission geometry. If the sample thickness is less than the absorption length, the laser is able to penetrate the entire sample layer and allows the plume to expand. On the other hand, if the sample thickness is greater than the absorption length, the plume is formed but its expansion is inhibited by a barrier of solid sample, decreasing the ion transport efficiency.

In the case of the CHCA matrix, the absorption coefficient of solid samples at 337 nm of the nitrogen laser wavelength is ~2.2 x $10^5$ $cm^{-1}$.[191] Thus, the corresponding sample layers must be less than 45 nm for CHCA for the undisturbed ion plume to occur. Since the thickness of the dried droplet deposited layer is much greater than the absorption length for CHCA, it is probable that the plume expansion for the CHCA samples was hindered by the thick layer of matrix. In this case, the laser introduction approach described in Figure 6-1c may avoid the problem of a thick layer of sample by combining the efficient sample removal of the IR laser and the efficient ionization of the UV laser.[186] It has been reported that the threshold for particle formation is approximately ten times larger for IR than UV.[14,82] An additional analytical application of IR LDI with UV post-ablation ionization in transmission geometry includes systems in which analytes are deeply embedded in a supporting material such as proteins separated in one- and two-dimensional gels, whole cells, and tissues.

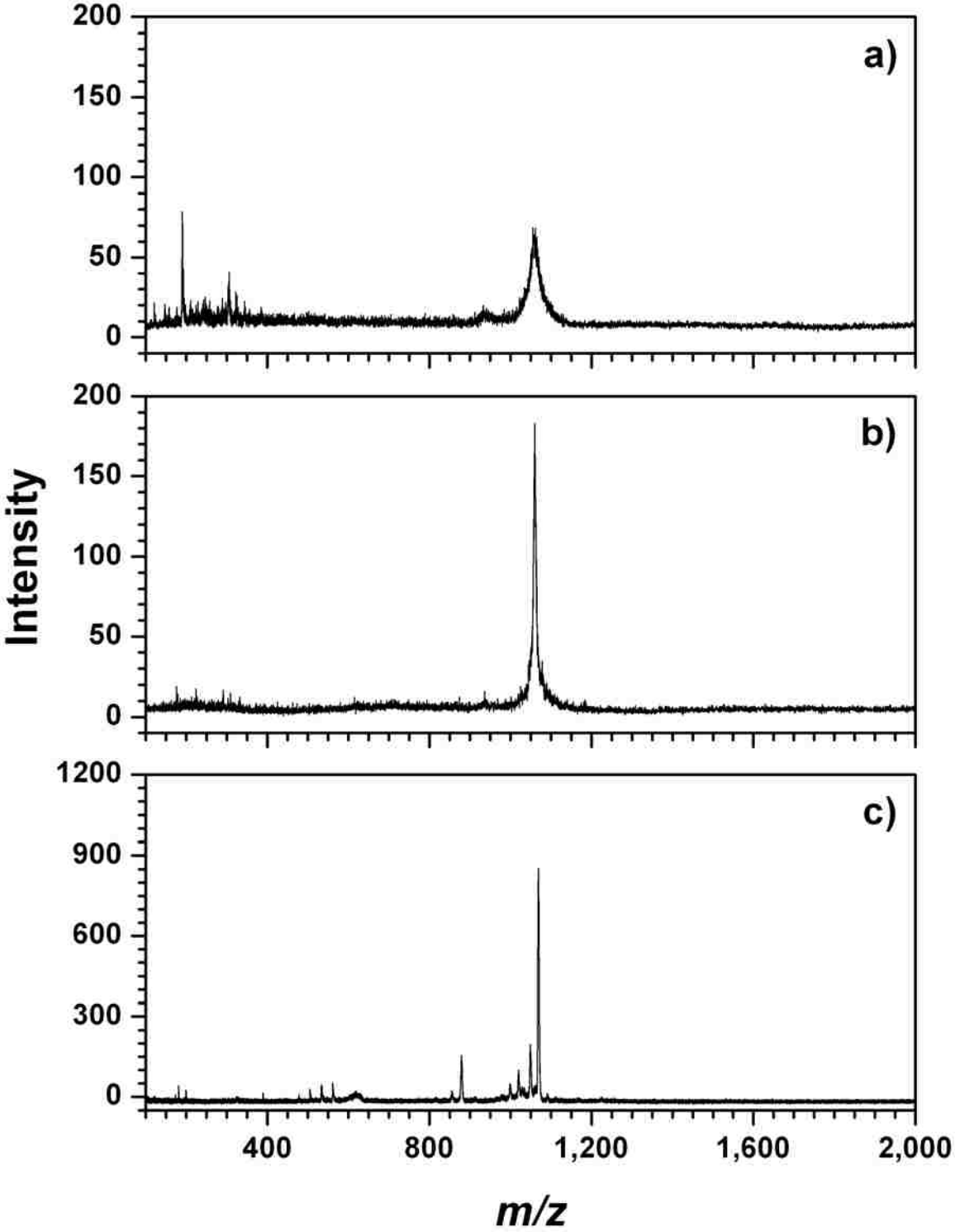


**Figure 6-4.** MALDI mass spectra of bradykinin in a) transmission geometry with 4X microscope objective lens, b) transmission geometry, and c) reflection geometry. Note that a) and b) were obtained in linear mode of detection, while c) was obtained in reflectron mode of detection.

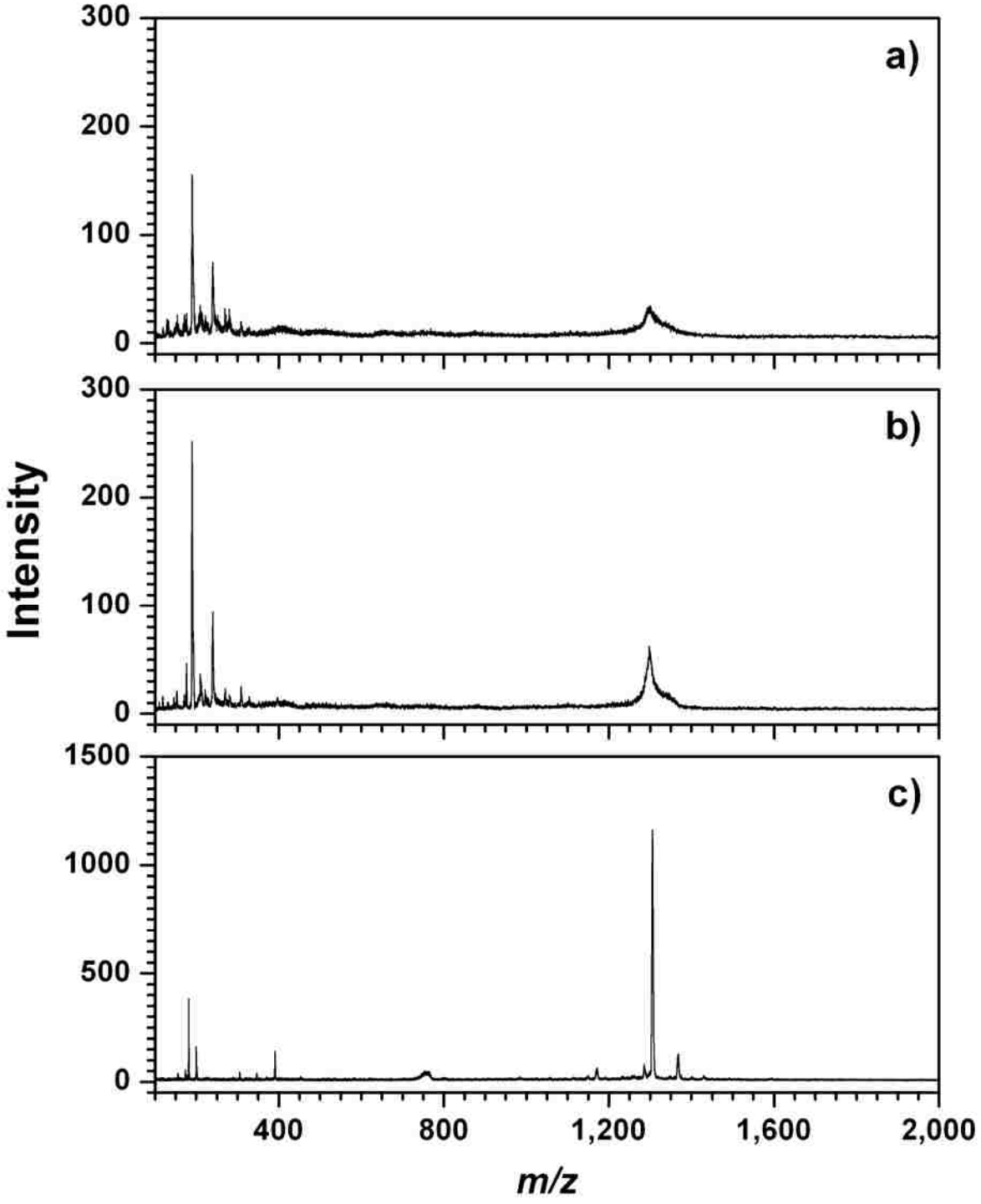


**Figure 6-5.** MALDI mass spectra of angiotensin I in a) transmission geometry with 4X microscope objective lens, b) transmission geometry, and c) reflection geometry. Note that a) and b) were obtained in linear mode of detection, while c) was obtained in reflectron mode of detection.

## 6.4. Summary

In this research, a transmission geometry MALDI mass spectrometer was coupled with a microscope objective lens to focus the laser onto a sample from the back side of a microscope glass slide for UV ionization. In this geometry, the spatial resolution of the image is limited by the microscope objective lens, resulting in a potential possibility of a single cell analysis and precise MALDI imagings without compromising either the laser or ion optics. In this experiment, the laser beam was moved across the sample spot in the x and y dimensions while mass spectra were acquired in linear or reflectron mode of operation. The instrument was demonstrated for bradykinin and angiotensin I prepared in sub-picomole concentrations for both reflection geometry and transmission geometry with or without a microscope objective lens.

In this study, the UV MALDI ionization was explored. The transmission geometry configuration yielded one order of magnitude lower intensity signal[180] and required ten times higher laser fluence[182,183] than the reflection geometry. The mass resolving power of both peptides was significantly decreased in transmission geometry because the mass spectra were obtained in the linear mode and the transmission geometry was not fully optimized at the time. Samples were completely depleted within tens laser shots in transmission geometry. Samples must be thin in transmission geometry to generate an ion plume efficiently toward ion source.

The IR LDI or IR MALDI transmission geometry on a silicon wafer target configuration maybe useful for spatially-resolved analysis of deposited bioaerosol particles or imaging of tissues since the silicon wafer is transparent to IR wavelengths. An atmospheric pressure (AP) transmission geometry MALDI may be useful to analyze the bioaerosol particles deposited on a target placed outside of vacuum for easier sample introduction.[180]

# CHAPTER 7. MALDI ION MOBILITY MASS SPECTROMETRY

## 7.1. Introduction

The principal challenge to mass spectrometry development for biological agent detection is in making the instrument small while maintaining requisite speed, sensitivity, selectivity and specificity. One approach to solve the problem is coupling ion mobility separation to a miniature matrix-assisted laser desorption/ionization time-of-flight mass spectrometer.[192-194] MALDI coupled with ion mobility mass spectrometry (IM-MS) provides a rapid means for the two-dimensional separation and identification of complex biological samples that are found in bioaerosols.

Recent developments in instrumentation for ion mobility spectrometry (IMS), a gas-phase separation method coupled with mass spectrometry, reveals potential applications of this relatively new technique for rapid, high resolution separations of analytes based on structure (ion conformation) and mass-to-charge (*m/z*) ratio. Ion mobility has been applied to the analysis of biomolecules using electrospray ionization (ESI)[195-198] and matrix-assisted laser desorption/ionization (MALDI) sources.[199,200] These techniques, combined with mass spectrometry, create a powerful tool in the analysis of proteins and peptides.

Ion mobility is a method for gas phase separation of ions based on their collision cross section.[201] In an ion mobility experiment, ions are brought into a drift tube that is held at a few torr pressure. In the drift tube, the ions move under the influence of a constant electric field while they experience collisions with the buffer gas. At the end of the drift cell, the ions can be detected, or sent into a mass spectrometer.[202] Ion mobility adds a dimension of orthogonal separation to mass spectrometry due to the ion's interaction with a neutral buffer gas. Ions having similar conformational forms display a "trend line" with respect to mass-to-charge ratio,

making it easy to isolate peptides and proteins on these trend lines. Although IM-MS separations can be achieved at resolutions comparable to high performance liquid chromatography (HPLC) and capillary electrophoresis (CE), most IM-MS instruments are operated at relatively low IM resolution (up to 200) to reduce analysis time, maximize sample throughput, and reduce the complexity of interfacing IM with MS.[203-205] Ion mobility coupled with orthogonal TOF-MS can increase throughput even further with a 1 to 10 ms gas phase separation and reduce the need for sample cleanup by more traditional time consuming separation methods such as HPLC coupled with MS.[206,207]

While ion mobility mass spectrometry has been demonstrated with a number of ionization methods, MALDI combined with ion mobility-orthogonal time-of-flight mass spectrometry (IM-oTOF MS) has been a viable technique for fast separation and analysis of biomolecules in complex mixtures.[207] MALDI IM-oTOF MS provides an advantage by initially separating different classes of biomolecules such as lipids, peptides, and nucleotides by their IM drift times prior to mass analysis.[208,209] It allows fast two-dimensional separation of ions according to their shapes and masses, minimizes mass spectral congestion, requires a minimum sample pre-treatment, and thus, has a great potential for complex mixture analysis. MALDI IM-oTOF-MS has great advantages over conventional MALDI for bacteria identification for both fingerprinting and proteomic approaches by separating the different components of the cell prior to separation by *m/z* in the mass spectrometer.[195,207-211] This IM pre-separation is particularly useful in the congested mass range below 2,000 Da. The addition of ion mobility information to bioaerosol analysis by MALDI mass spectrometry has the potential to significantly improve the selectivity and specificity while maintaining the inherent speed and sensitivity of MALDI.[208,211] This can lead to a more efficient technique for bacteria detection and recognition for military homeland security and other applications.

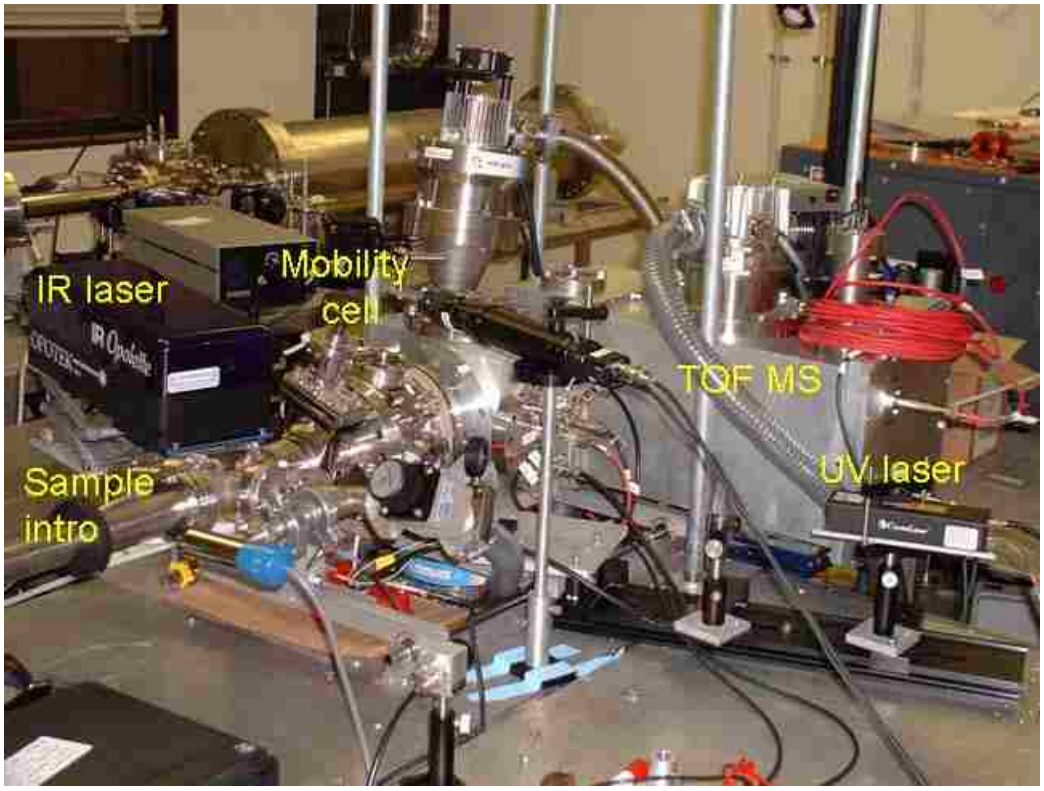


**Figure 7-1.** A photograph of UV and IR MALDI ion mobility orthogonal time-of-flight mass spectrometer constructed by Ionwerks. Copyright in Ionwerks, Inc. (Houston, TX).

### 7.2. Experimental

A photograph of the UV and IR MALDI ion mobility orthogonal time-of-flight mass spectrometry[78] (Ionwerks Inc. Houston, TX) is shown in Figure 7-1. Samples were analyzed by MALDI IM o-TOF MS in Houston. Bacteria samples of *B. subtilis* at 30 mg/mL, *E. coli* B strain at 40 mg/mL, and *E. coli* W strain at 40 mg/mL were dissolved in 1:1 (v/v) ACN/0.1% TFA, respectively and prepared by the dried droplet method. The samples of bradykinin at 6 mg/mL, bovine Insulin at 10 mg/mL, and cytochrome c at 7 mg/mL were prepared by 1:1 (v/v) ACN/0.1% TFA. A mixture of potential bioaerosol interferants was simulated by mixing Arizona road dust at 30 mg/mL, pollens at 15 mg/mL (5 mg each of giant ragweed, black walnut, and corn pollen), carbon black at 10 mg/mL, and 60 mg/mL of salts (35 mg/mL of ammonium sulfate and 25 mg/mL of sodium chloride).

UV and IR matrices were prepared by dissolving them in 1:1 (v/v) ACN/ $H_2O$. In most cases, the matrices were saturated and consisted of succinic acid at 70 mg/mL, DHB at 100 mg/mL, CHCA at 30 mg/mL, sinapinic acid at 30 mg/mL, and caffeic acid at 20 mg/mL. The samples and matrices were deposited on 16-spot ion mobility targets using the dried droplet method at a 1:2 (v/v) analyte/matrix volume ratio.

## 7.3. Results and Discussion

### 7.3.1. UV MALDI Ion Mobility of Bacteria

Ion mobility mass spectra were obtained using a MALDI ion source coupled to an ion mobility orthogonal extraction time-of-flight mass spectrometer at Ionwerks. MALDI ion mobility analysis of lyophilized bacteria was performed in order to determine whether the spectra with unique biomarkers could be produced. Figure 7-2 shows UV MALDI ion mobility mass spectra of *bacillus subtilis* obtained from a dried droplet sample preparation with CHCA (top) and SA (bottom) matrix. The y-axis of the plots represents the drift time of ions in the mobility cell in microseconds. The x-axis is the mass-to-charge ratio (*m/z*) of ions. The *m/z* range below 3,000 is particularly important since this is where the interferences between different types of molecular components are maximized. The *m/z* range greater than 3,000 was dominated by protein peaks. A 349 nm (third harmonic) Nd:YLF diode pumped Q-switched UV laser at 200 Hz repetition rate was used for the bacteria analysis. The ion mobility mass spectra in Figure 7-2 were expanded to zoom in on the region up to *m/z* 3,500 and shown in Figure 7-3. The mass spectra at the top of ion mobility spectra in Figure 7-3 were obtained by integrating the IM-MS data, which are resulted in good MALDI mass spectra with a mass range up to 3,500 Da. A distinct double trend lines could be observed up to *m/z* 3,000. The top trend line is due to bacterial lipids and the bottom trend line is peptides and proteins in both ion mobility mass spectra with CHCA and SA matrix.

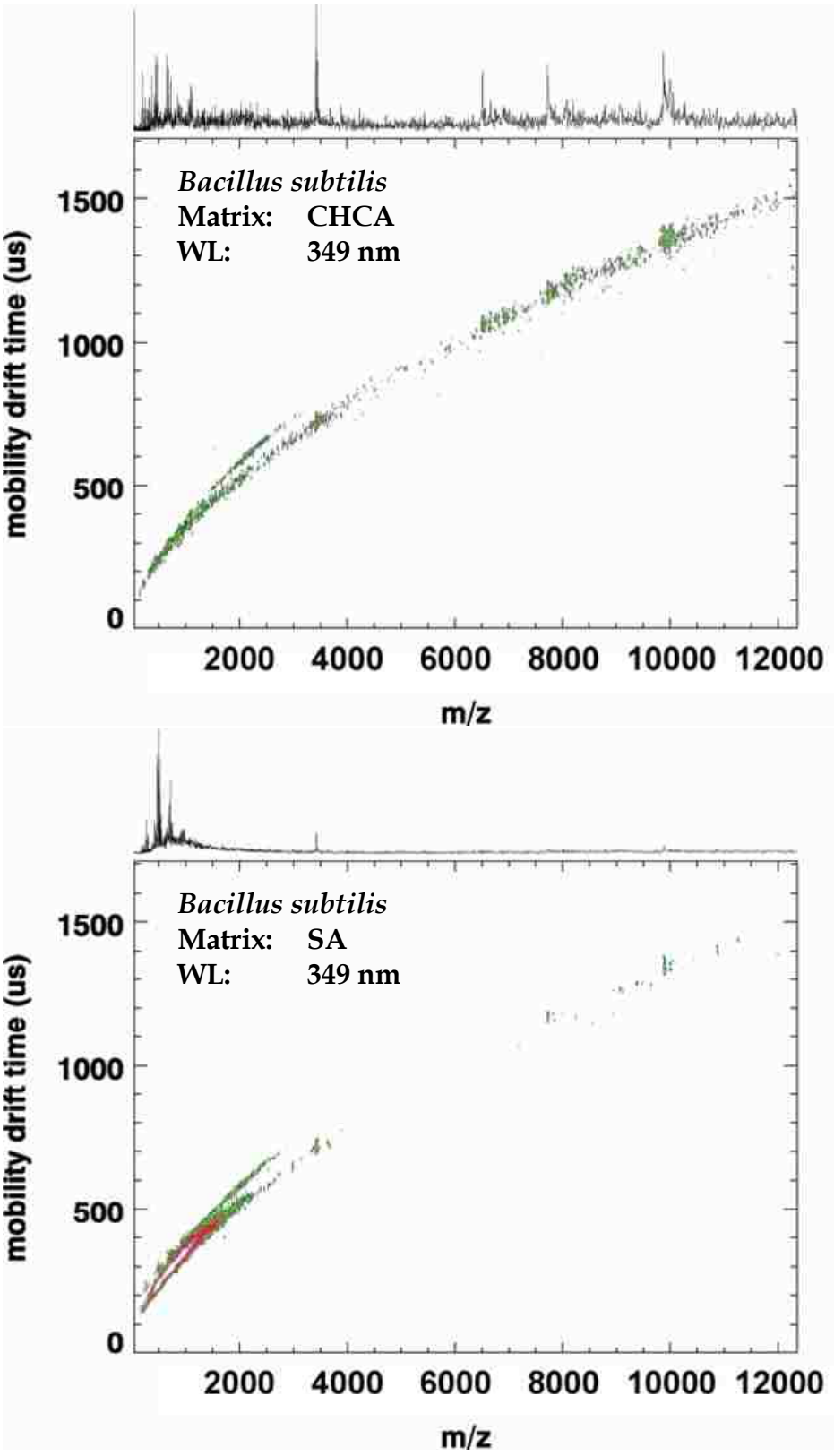


**Figure 7-2.** UV MALDI ion mobility mass spectra of *Bacillus subtilis* with CHCA (top) and SA (bottom) matrix.

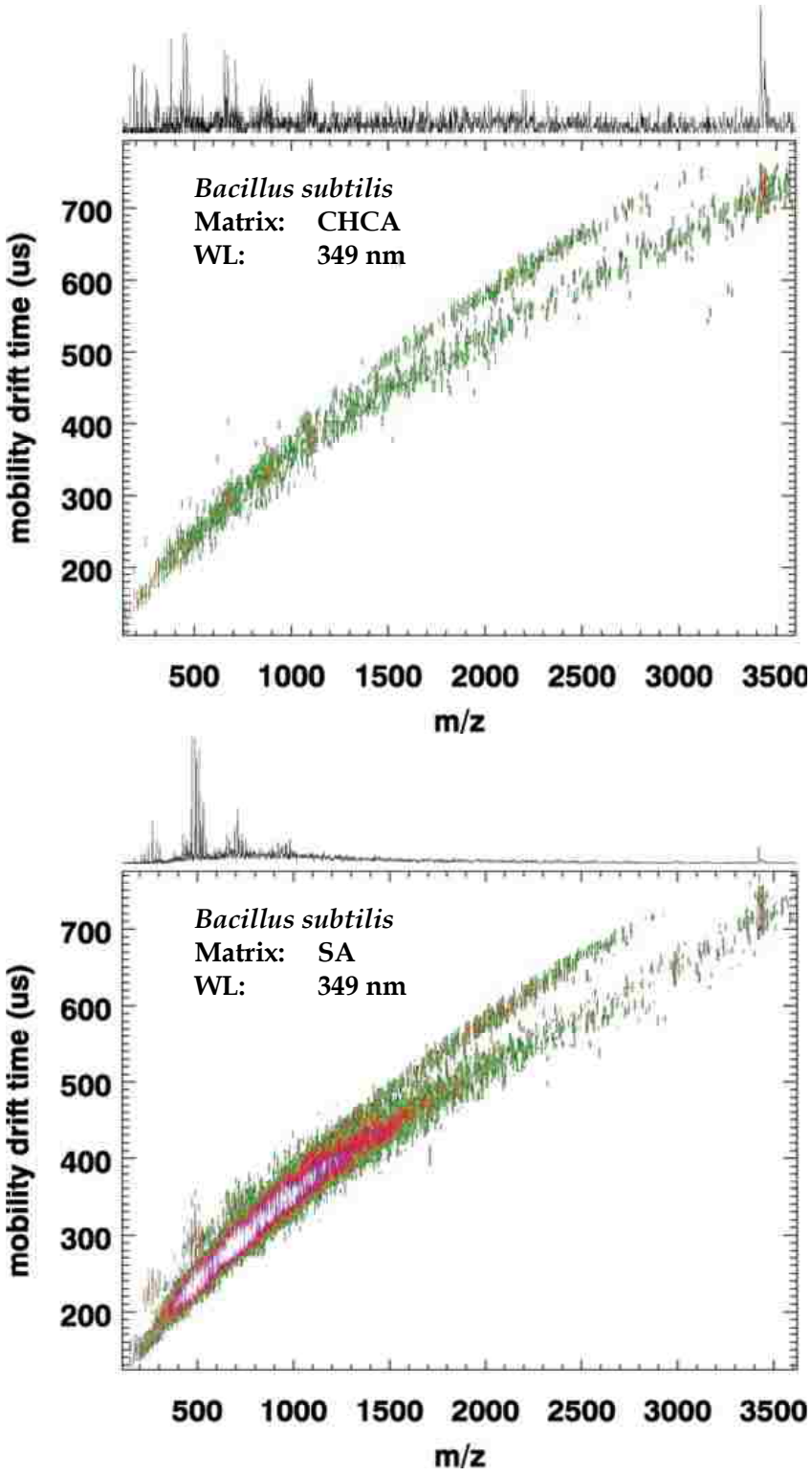


**Figure 7-3.** UV MALDI ion mobility mass spectra of *Bacillus subtilis* with CHCA (top) and SA (bottom) matrix. Ion mobility mass spectra in Figure 7-2 were expanded in the mass region up to *m/z* 3,500. The top trend line is bacterial lipids, and the bottom trend line is peptides and proteins.

### 7.3.2. IR MALDI Ion Mobility of Bacteria

Samples of *E. coli* strain B and *bacillus subtilis* were prepared with the dried droplet sample preparation method using DHB matrix. The IR laser energy was maintained slightly higher than the ionization threshold. At this level, the sample was consumed after a few laser shots, therefore, the laser beam was continuously scanned across the spot. Only a few seconds was necessary to obtain mass spectra. Figure 7-4 demonstrates IR MALDI ion mobility of different bacterial species, *E. coli* B strain and *bacillus subtilis* with DHB as a matrix. The MALDI ion mobility mass spectra for both bacteria fall into three trend lines with a roughly constant ratio of mass to drift time. This behavior suggests that three different classes of compounds are desorbed and ionized from the bacteria. The top trend line, which has the steepest slope, is thought to be lipids.[208] There are a few distinct peaks in this line in both mass spectra. An expanded view of the characteristic mass region is shown in Figure 7-5.

The computer processing of the spectra allowed re-ploting of mass spectra for the ions that belong to the lipid trend line. The differences between two bacterial species were obvious. While there were a few peaks in the 700-1,000 Da range in the *E. coli* spectrum, they were absent in that of *bacillus subtilis*. Instead, there were a few prominent peaks between 1,050 Da and 1,080 Da, which could be assigned to $C_{15}$-surfactin[212,213] (MW: 1,036.34 Da), a lipopeptide that can be extracted from *bacillus subtilis*, shown in Figure 7-6. In fact, the two most intense peaks corresponded to the attachments of $Na^+$ (1,058.8 Da) and $K^+$ (1,074.8 Da) to the parent molecular ion, although the $[M+H^+]$ ion peak could not be seen. These peaks were previously reported by Madonna *et al*.,[212] and Koumoutsi *et al*.[213] and were identified as alkali metal adducts of surfactin. Although the peptide component of the surfactin (see Figure 7-6) is much larger than the lipid chain, its mobility drift time is significantly longer than the average peptide drift time.

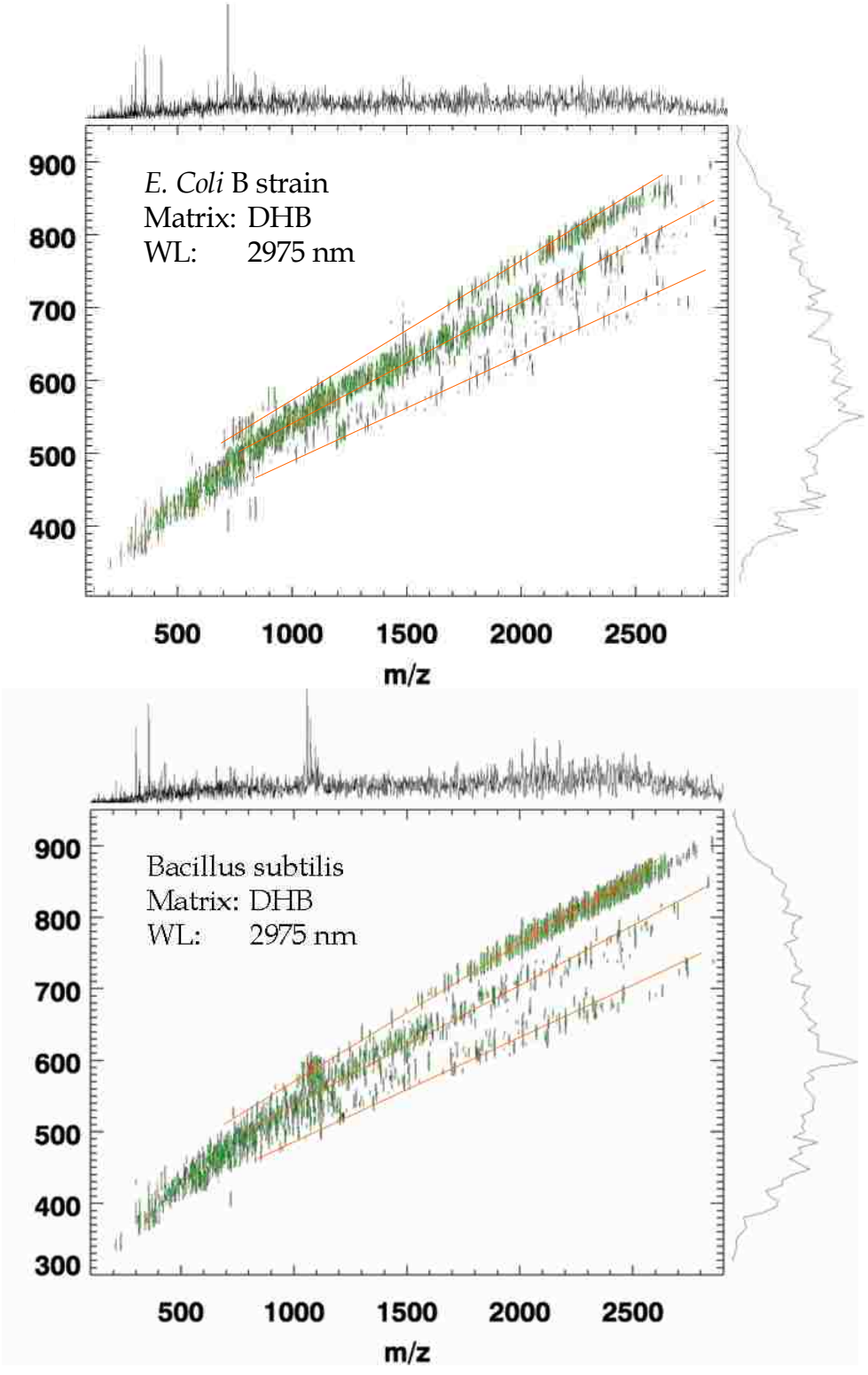


**Figure 7-4.** IR MALDI ion mobility mass spectra of *E. coli* B strain (top) and *bacillus subtilis* (bottom). The top trend line is lipids, the middle trend line is peptides/proteins, and the bottom trend line is oligonucleotides from bacteria.

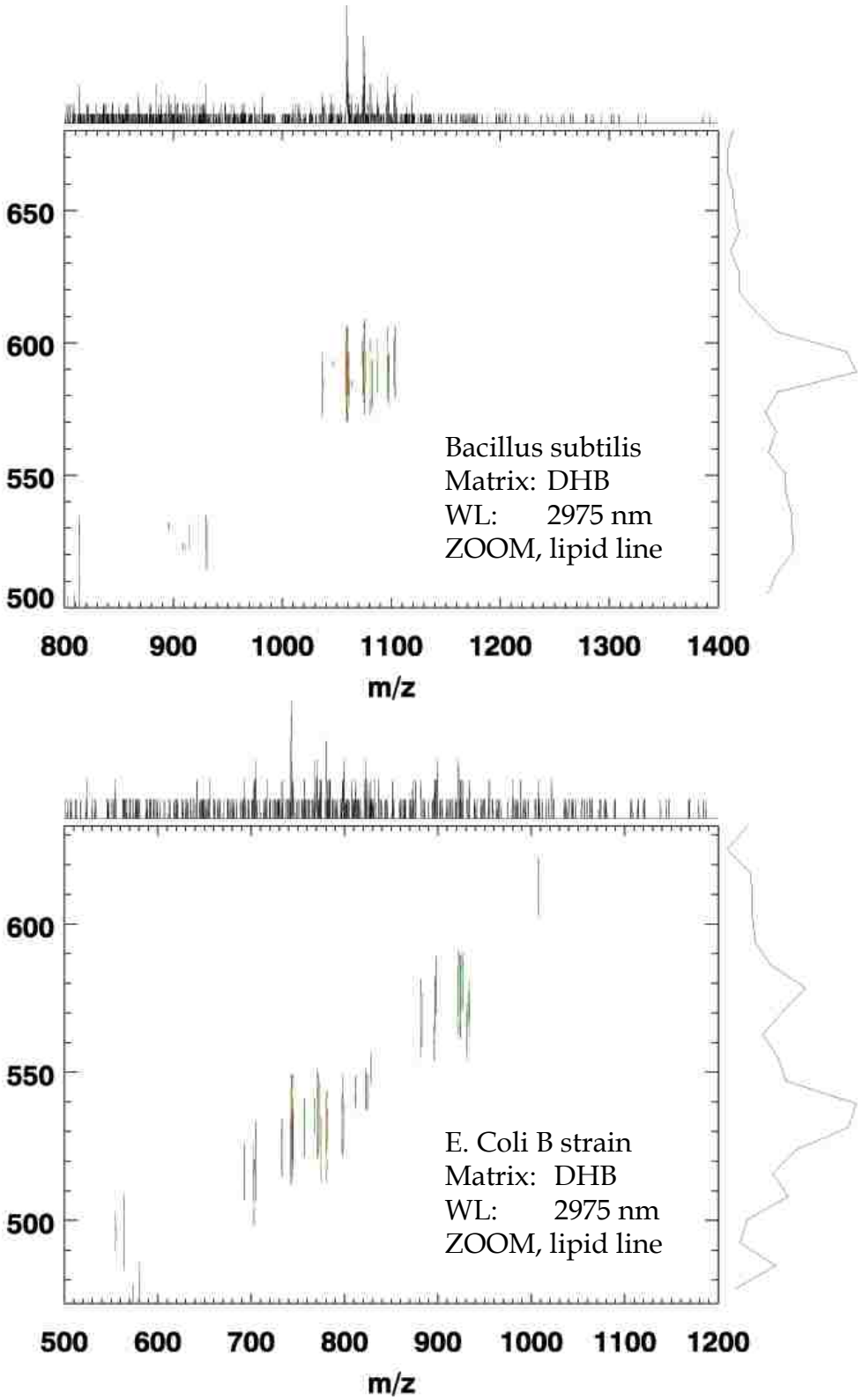


**Figure 7-5.** Expanded 2D spectra of *bacillus subtilis* (top) and *E. coli* strain B (bottom). Only the lipid trend line is shown. The 1D mass spectra also represent the fraction of ions aligned with the lipid trend line.

This fact allows easy identification in the 2D mass-mobility spectrum. There is another interesting obervation in the mass region between 2,000 and 2,500 Da belonging to the slow mobility trend line that could be attributed to larger molecular ions with fatty acid chains. The peaks were separated by 14 Da, which corresponds to carbons in alkane chains (see Figure 7-4, *bacillus subtilis* mass spectrum).

The ions in the mass region above 5,000 *m/z* (data not shown) fall on the intermediate trend line. The ions giving rise to this trend line are most likely peptides and proteins. There was also a weak trend line below the peptide trend line that could not be observed with UV MALDI. The trend line of lowest slope corresponds to ions with faster drift velocity than the peptide/protein trend line and with masses below 2,500 Da. The ions giving rise to the lowest slope line are possibly oligonucleotides.

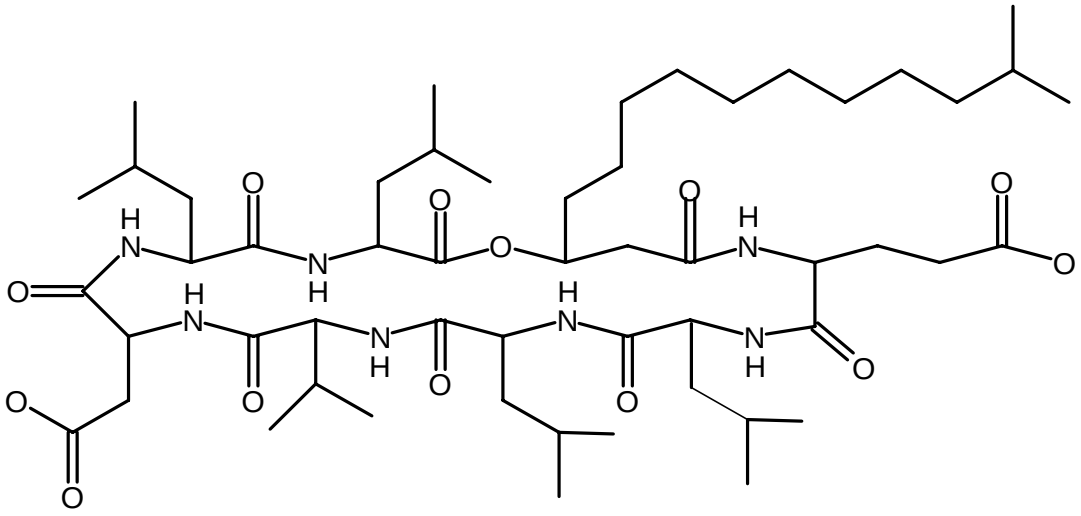

**Figure 7-6.** Structure of surfactin - a lipopeptide from *bacillus subtilis.*

### 7.3.3 Comparison of UV and IR MALDI Ion Mobility MS

Comparative tests of the system operation were performed using both UV and IR lasers. A direct ion mobility mass spectra comparison was possible since some of the matrices such as DHB work at both wavelengths. Both lasers irradiated the same spot of the sample. The MALDI

ion mobility mass spectra of a standard peptide mixture using both lasers are shown in Figure 7-7. The mobility resolution on the 2D plot corresponding to the IR MALDI is slightly lower than the UV MALDI. This degradation of the ion mobility resolution is due to jitter in the electronic triggering specific to the IR laser. The mass spectra of peptides were similar for both UV and IR wavelengths; however, much fewer laser shots were required for the IR MALDI to achieve SN ratios similar to the UV MALDI. In addition, there were a few peaks that were only present in the IR MALDI spectrum. They were revealed as a certain degree of contamination from $C_{60}$ and $C_{70}$ ions from previous sample residue at *m/z* 720 and 840, respectively. There were also a few other unidentified peaks off the peptide trend line in the IR MALDI spectrum. The observed differences revealed apparent higher sensitivity of the IR MALDI in these particular conditions. Only a few laser shots were necessary to produce complete mass spectra by IR MALDI. This is due to the large rate of material removal by an IR laser compared to a UV laser at the laser fluences just above the ionization threshold.[14,82] This particular characteristic of the process requires detection of multiple ions of the same *m/z* in one TOF extraction as opposed to the standard operation of the UV MALDI ion mobility TOF-MS where lower number of ions per pulse can be easily handled by the pulse counting techniques.

A well known feature of the IR laser ionization of analytes as opposed to the UV consists in the fact that often no matrix is necessary. In fact, even if no external matrix is added during the sample preparation, its role is taken by the trace water present in the analyte. Even though an analyte itself acts as its own matrix, intact analyte signals can be obtained due to the lower photon energy of the infrared radiation. Matrix-free operation or at least some kind of simplified matrix preparation technique would be useful for such applications as tissue imaging and bioaerosol detection.

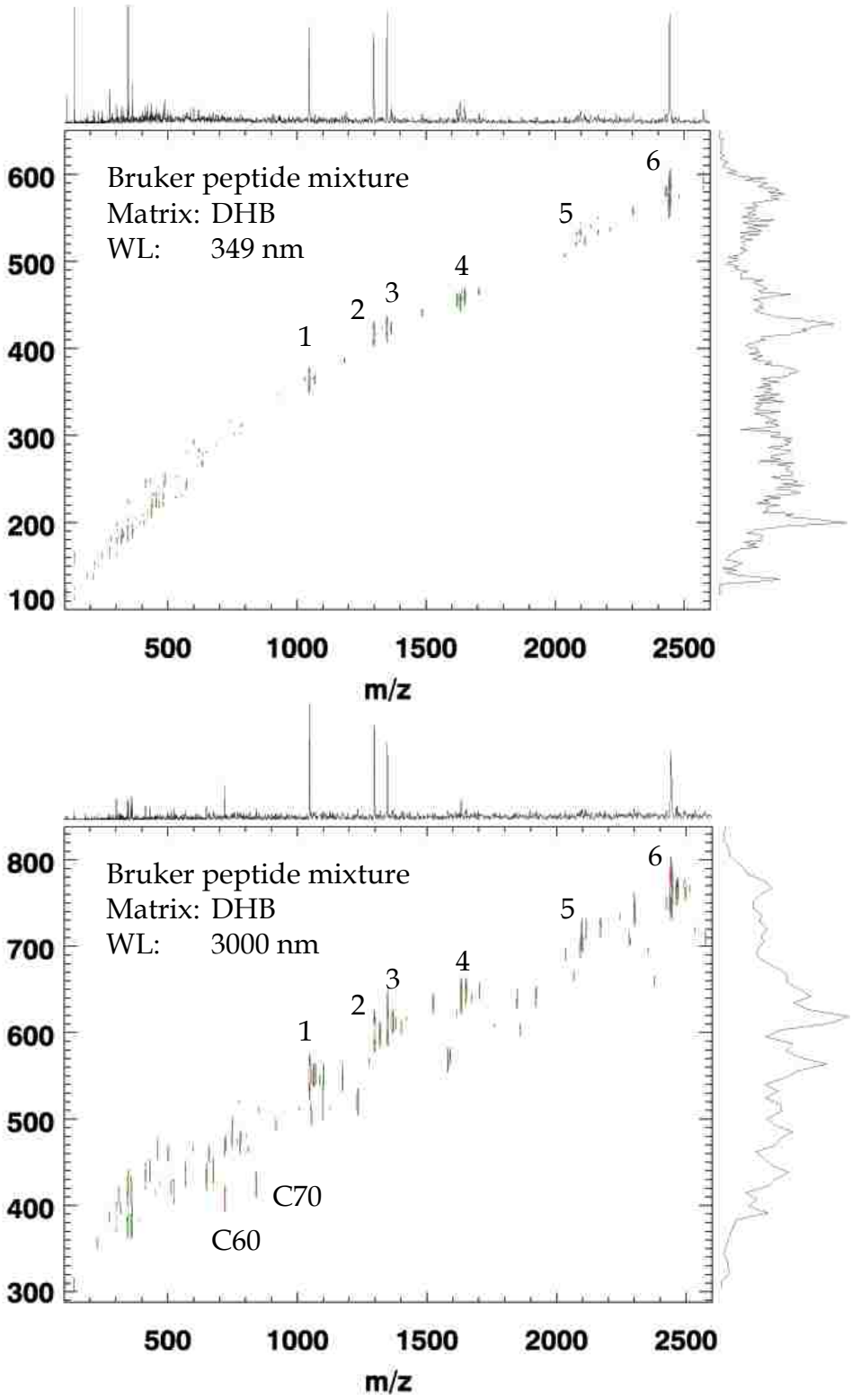


**Figure 7-7.** UV (top) and IR (bottom) MALDI ion mobility mass spectra of a peptide mixture: 1) angiotensin II, 2) angiotensin I, 3) substance P, 4) bombesin, 5) ACTH clip 1-17, 6) ACTH clip 18-39 with 100 µg/µL DHB matrix in 1:1 (v/v) acetonitrile/water. $C_{60}$ and $C_{70}$ ions at *m/z* 720 and 840 are contaminants from previous sample residue.

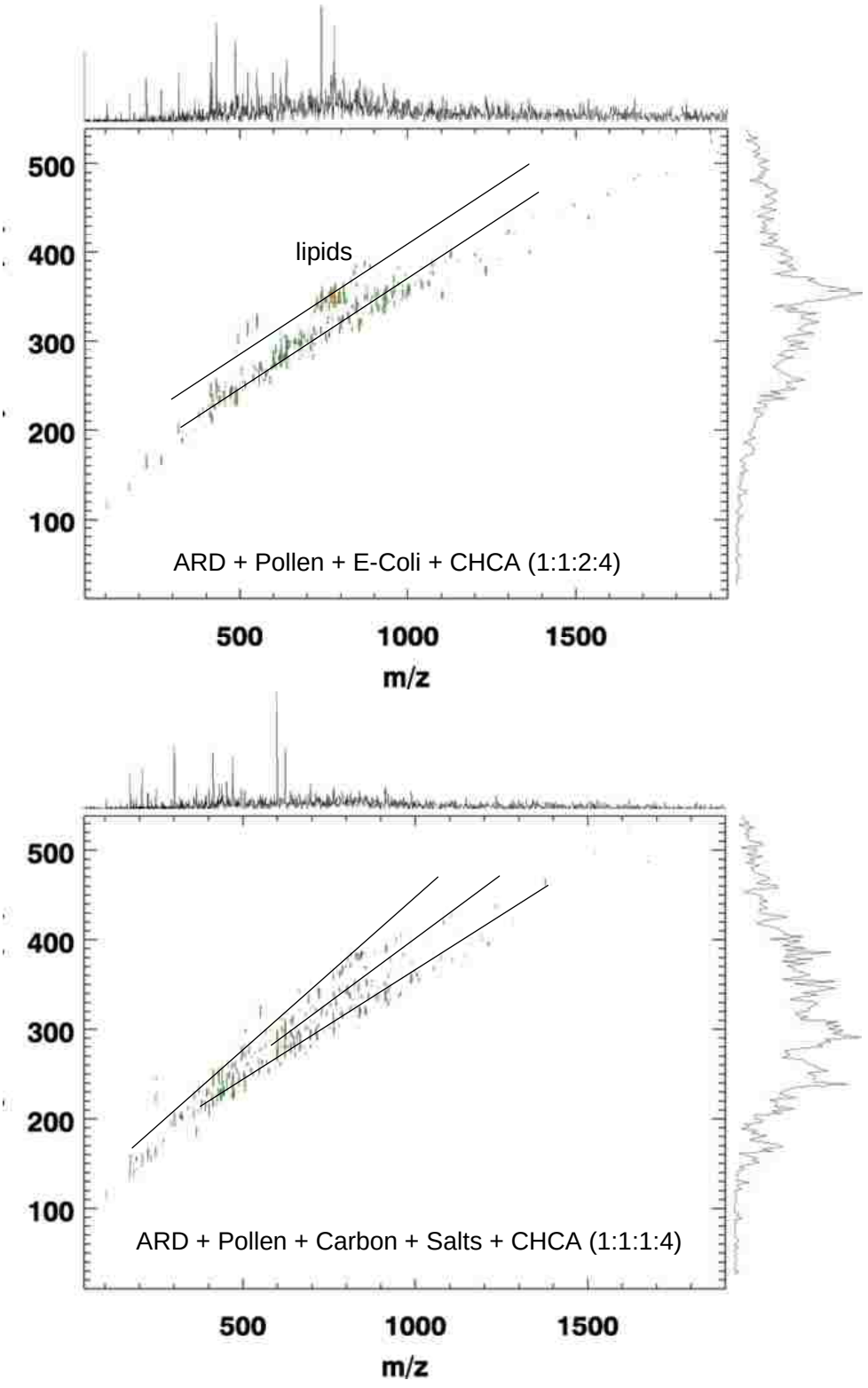


**Figure 7-8.** UV MALDI ion mobility mass spectra of potential bioaerosol interferant mixtures. The mixture of interferants contains Arizona road dust, pollens, and/or carbon black and salts (ammonium sulfate and sodium chloride).

### 7.3.4. Mixtures of Potential Bioaerosol Interferants

A mixture of potential bioaerosol interferants was simulated by mixing Arizona road dust, pollen, carbon black, and salts. Figure 7-8 shows the UV MALDI ion mobility mass spectra of the bioaerosol interferents with CHCA matrix mixed with *E. coli* strain W (top) and without bacteria (bottom). At least two trend lines could be observed from these complex mixtures. Although the integrated mass spectrum does not give rise to distinguishable peaks, it is likely that a data masking procedure that selects ions by ion mobility will improve the ability to resolve the various components. Overall, the MALDI IM-MS approach is an excellent way to separate complex biological mixtures and complex compound mixtures that may be found in atmospheric aerosol particles. The MALDI IM-MS data shows the potential of a two-dimensional separation, speed, and ease of IM-MS in particular.

## 7.4. Summary

A UV and IR MALDI ion mobility orthogonal time-of-flight mass spectrometer was evaluated for the analysis of bacteria, peptide standards, and simulated bioaerosol interferant mixtures. The ion mobility mass spectrometer has a mass resolving power of up to 3,500 and a sensitivity of 2 fmol for peptide standards. MALDI ion mobility mass spectra of *B. subtilis* and *E. coli* were obtained from the dried droplet sample preparations with mass peaks up to 10 kDa with CHCA and sinapinic acid using UV irradiation and with succinic acid and DHB using an IR irradiation. UV MALDI ion mobility mass spectra of *bacillus subtilis* with CHCA and SA matrices generated distinct double trend lines up to *m/z* 3,000. The upper trend line was assigned to bacterial lipids, and the bottom trend line was assigned to peptides and proteins. The mass range above 3,000 Da was dominated by protein peaks.

IR MALDI ion mobility MS was also demonstrated using bacterial species *E. coli* B strain and *bacillus subtilis* with DHB as a matrix. The MALDI ion mobility data for both

bacteria produced three distinct trend lines with a roughly constant ratio of mass to drift time, indicating that three different classes of compounds were desorbed and ionized. The top trend line was assigned to lipids, and the intermediate trend line was assigned to peptides and proteins. The weak bottom trend line that could not be observed with UV MALDI was most likely oligonucleotides, indicating that the IR MALDI ion mobility is more sensitive to this class of materials than UV MALDI ion mobility. There were a few distinct peaks belonging to lipid trend line in both mass spectra. Specifically, *bacillus subtilis* showed a few prominent peaks between 1,050 Da and 1,080 Da, which could be assigned to the alkali metal adducts of $C_{15}$-surfactin (lipopeptide).

The performance test of UV and IR lasers was carried out using a common DHB matrix that functions at both wavelengths. The mobility resolution of IR MALDI was slightly lower than the UV MALDI due to jitter in the electronic triggering of the IR laser. The IR laser is more sensitive and requires only a few laser shots due to the high rate of material removal compared to the UV laser.[14,82] The IR laser depletes sample quickly and requires frequent shifting of the laser spot. The IR laser can be used for matrix-free ionization, which is useful for bioaerosol detection.

A mixture of potential aerosol interferants were analyzed by UV MALDI ion mobility MS with a CHCA matrix. Although the integrated spectrum does not give rise to distinguishable peaks, it improves the ability to separate complex biological mixtures. The compact orthogonal TOF-MS needs to be improved in sensitivity, resolution, and detection limit to obtain better mass spectral information. However, the addition of ion mobility information to MALDI mass spectra has significantly improved the selectivity and specificity while maintaining the inherent speed of MALDI MS. This can lead to a more efficient technique for bacteria detection and recognition for military homeland security and other applications.

# CHAPTER 8. CONCLUSIONS AND FUTURE DIRECTIONS

The objective of the research presented in this dissertation is to develop methods and instrumentation for fast off-line analysis of bioaerosols in complex mixtures based on MALDI mass spectrometry. Test bioaerosol particles were generated from a nebulized bacterial solution and collected onto MALDI targets for off-line analysis. Bioaerosol particles collected on a matrix pre-coated target with post-collection solvent addition gave the most promise for off-line bioaerosol analysis, which were nearly identical to those obtained using the dried droplet method. However, signal could not be recovered efficiently if the bioaerosol particles were not properly mixed with matrix crystals without a proper post-treatment. The fact that solvent or matrix addition is necessary to obtain MALDI mass spectra of collected bioaerosol particles has important implications for portable and transportable instrumentation for bioaerosol detection. It will not only add complexity to the instrumentation but the added matrix will also increase a low mass spectral congestion.

A possible method for the field applications for off-line bioaerosol collection analysis is that the solvent is continuously sprayed on matrix pre-coated target during the bioaerosol particle collection. It will enhance mixing the bioaerosol particles to the matrix crystals more homogeneously, resulting improved mass spectra. By employing Taguchi experimental design, the complex experimental parameters, such as matrix, solvent, flow rate, and collection time, involved in the bioaerosol collection on bare or matrix pre-coated targets can be optimized systematically. With this technique, the sample preparation parameters and their interaction effects can be easily determined with the minimal experiments. It can also be used to find the best parameters for mass spectrometric analyses such as laser fluence, acceleration and extraction voltage, delay time, and reflectron voltage.

In this dissertation research, the silicon substrates were investigated compared to conventional stainless steel MADLI substrates for bioaerosol analysis. The silicon substrate decreases low mass background ion interferences and increases signal sensitivity, signal-to-noise ratio, and detection limit. The most promising result of the silicon targets is that the silicon targets perform up to ten times better shot-to-shot and spot-to-spot reproducibility than the stainless steel targets. These characteristics are important figures of merit for the applications of high-throughput and automated sample analysis as well as off-line bioaerosol analysis.

The principal challenge to mass spectrometry development in bioaerosol detection is in making the instrument portable while maintaining requisite speed, sensitivity, selectivity and specificity as well as eliminating complicated background signals. In transmission geometry MALDI mass spectrometry, a tight laser focus onto a sample from the back side of transparent target through a microscope objective lens is possible with UV or IR irradiation. The silicon wafer substrate developed in Chapter 3 is an excellent substrate for transmission geometry IR matrix-free LDI or IR MALDI for deposited bioaerosol particles analysis because the silicon wafer is transparent to IR wavelengths. In addition, the matrix-free IR LDI with UV laser post-ablation ionization approach will have a great potential for the bioaerosol particle analysis. The IR laser can ablate large amounts of material[14,82] while UV laser can ionize those desorbed particles efficiently,[186] eliminating complicated low mass interferences. This will enable a matrix-free soft ionization of deposited bioaerosol particles or biological tissues or cells by enhancing the ionization efficiency selectively.

MALDI ion mobility o-TOF MS was demonstrated for the identification of bacteria and complex bioaerosol mixtures by two-dimensional separation of ions according to their shapes and masses. The most promising aspect of the instrument is that the ion mobility can pre-separate the complex mixtures into the different classes of trend lines before the mass analysis to simplify

the resulting mass spectra. The instrument produced the separation of mobility trend lines for lipids, peptides and proteins, and nucleotides from bacterial species. A mixture of potential bioaerosol interferants was also separated into different trend lines although the integrated ion mobility mass spectra did not give rise to distinguishable peaks. In IM-MS, protein identification information is complemented by structural characterization data, which is difficult to obtain using conventional proteomic techniques. The addition of ion mobility information to bacteria and bioaerosol analysis by MALDI mass spectrometry will significantly improved the selectivity and specificity while maintaining the inherent speed and sensitivity of mass spectrometry. This can potentially lead to more efficient technique for bacteria and bioaerosol detection and recognition for homeland security applications.

The matrix-free IR LDI will be the basis for the future developments of the bioaerosol analysis. The matrix-free technique will have great advantages since it can eliminate low mass congestion by matrix ions. IR MALDI IM MS system is comparable in sensitivity and spectra quality to the UV based setup, while some additional information can be seen in two-dimensional ion mobility mass spectra obtained by IR laser. The compact orthogonal TOF mass analyzer of the MALDI ion mobility mass spectrometer needs to be optimized in order to further increase throughput, sensitivity, and resolution required for bioaerosol analysis. A direct aerosol inlet interface with ion mobility MALDI o-TOF MS will be investigated for real-time bioaerosol analysis.

The transmission geometry configuration enables a tight laser focusing without ion optic geometry restrictions, and the ion mobility can pre-separate the complex mixtures into different trend lines. By combining the two instrumental techniques, the off-line deposited bioaerosol particle analysis or on-line direct bioaerosol inlet analysis can be achieved from complex samples without sacrificing the performance of MALDI mass spectrometry. In addition, IR LDI

with UV laser post-ablation ionization approach can enable a soft ionization while minimizing low mass interferences for bioaerosol analysis. The compact orthogonal reflectron time-of-flight mass spectrometer can reduce the size of instrument but increases the accuracy and resolution of the ion signals. The ultimate goal of minimizing sample pre-treatment and maximizing sensitivity and selectivity for the bioaerosol analysis can be realized. Our primary application for this instrument is the off-line analysis of deposited bioaerosol particles, but the system is equally applicable to the analysis of single cells or micrometer resolution imaging of thin tissue sections.

## REFERENCES


1. Hinds, W. C., *"Aerosol Technology- Properties, Behavior, and Measurement"* John Wiley & Sons: New York, NY, **1982**, Chapter 1.

2. Suess, D. T.; Prather, K. A., Mass Spectrometry of Aerosols. *Chem. Rev.* **1999**, *99*, 3007–3036.

3. Hawley, R. J.; Eitzen, Jr. E. M., Biological weapons–a primer for microbiologists. *Annu. Rev. Microbiol*. **2001**, *55*, 235–253.

4. Klaassen, C. D., *"Casarett & Doull's Toxicology"* McGraw-Hill: New York, NY, **1996**, Chapter 28.

5. Walt, D. R.; Franz, D. R., Biological warfare detection. *Anal. Chem.* **2000**, *72*, 738A–746A.

6. *"Bioterrorism Agents/Diseases"* http://www.bt.cdc.gov/agent/agentlist-category.asp

7. Fatah, A. A.; Barrett, J. A.; Arcilesi, R. D.; Ewing, K. J.; Lattin, C. H.; Moshier, T. F., *"An Introduction to Biological Agent Detection Equipment for Emergency First Responders"* National Institute of Justice Guide 101-00, U.S. Department of Justice, December **2001**.

8. DOD, *"Chemical and Biological Defense Primer"* Department of Defense Chemical and Biological Defense Program, October **2001**, Washington, DC.

9. Fenselau, C., *"In Mass Spectrometry for the Characterization of Microorganisms"* Fenselau, C. Ed; American Chemical Society: Washington, DC, **1994**; Chapter 1.

10. Spurny, K. R., *"In Bioaerosols Handbook"* Cox, C. S., Wathes, C. M., Eds; CRC Press: Boca Raton, FL, **1995**; Chapter 12.

11. Nugent, P. G.; Cornett, J.; Stewart, I. W.; Parkes, H. C., Personal Monitoring of Exposure to Genetically Modified Microorganisms in Bioaerosols: Rapid and Sensitive Detection Using PCR. *J. Aerosol Sci*. **1997**, *28*, 525–538.

12. Jackson, S. N.; Murray, K. K., On-line matrix addition for detecting aerosol particles. *Anal. Chem*. **2002**, *74*, 4841–4844.

13. Steele, P. T.; Tobias, H. J.; Fergenson, D. P.; Pitesky, M. E.; Horn, J. M.; Czerwieniec, G. A.; Russell, S. C.; Lebrilla, C. B.; Gard, E. E.; Frank, M., Laser Power Dependence of Mass Spectral Signatures from Individual Bacterial Spores in Bioaerosol Mass Spectrometry. *Anal. Chem.* **2003**, *75*, 5480–5487.

14. Jackson, S. N.; Mishra, S.; Murray, K. K., Characterization of Coarse Particles Formed by Laser Ablation of MALDI Matrixes. *J. Phys. Chem. B* **2003**, *107*, 13106–13110.

15. Branscomb, L. M.; Klausner, R. D., (co-Chairs, National Research Council Committee on Science and Technology for Countering Terrorism), *"The Role of Science and Technology in Countering Terrorism"* **2002**, National Academies Press, Washington.

16. Spurny, K. R., *"Chemical Analysis of Bioaerosols"* in Cox CS, Wathies CM, Eds. *"Bioaerosols Handbook"* **1995**, CRC Press, Boca Raton, FL.

17. Hensel, A; Penzoldt, K. *"Biological and Biochemical Analysis of Bacteria and Viruses"* in Cox, C. S., Wathies, C. M., Eds. *"Bioaerosols Handbook"* **1995**, CRC Press, Boca Raton, FL.

18. Jensen, P. A.; Schafer, M. P., *"Sampling and Characterization of Bioaerosols"* NIOSH, Manual of Analytical Methods, **1998**.

19. Siuzdak, G., *"Mass Spectrometry for Biotechnology"* Academic Press: San Diego, CA, **1999**; Chapter 1 and 2.

20. Aebersold, R.; Goodlett, D. R. Mass Spectrometry in Proteomics, *Chem. Rev*. **2001**, *101*, 269-296.

21. Dass, C., *"Principles and Practice of Biological Mass Spectrometry"* John Wiley & Sons: New York, NY, **2001**, Chapter 2 and 3.

22. Barber, M.; Bordoli, R. S.; Sedgwick, R. D.; Tyler, A. N. Fast atom bombardment of solids as an ion source in mass spectrometry. *Nature,* **1981**, *293*, 270-275.

23. Karas, M.; Bahr, U.; Giebmann, U., Matrix-assisted laser desorption ionization mass spectrometry. *Mass Spectrom. Rev*. **1991**, *10*, 335–357.

24. Stahl B; Thurl S; Zeng J; Karas M; Hillenkamp F; Steup M; Sawatzki G., Oligosaccharides from human milk as revealed by matrix-assisted laser desorption/ionization mass spectrometry. *Anal. Biochem.* **1994**, *223*, 218-226.

25. Yau, P. Y.; Chan, T. W. Dominic; Cullis, Peter G.; Colburn, A. W.; Derrick, Peter J., Threshold fluences for production of positive and negative ions in matrix-assisted, laser desorption/ionization using liquid and solid matrixes. *Chem. Phys. Letters* **1993**, *202*, 93-100.

26. Fenn, J. B.; Mann, M.; Meng, C. K.; Wong, S. F.; Whitehouse, C. M., Electrospray Ionization-Principles and Practice. *Mass Spectrom. Rev*. **1990**, *9*, 37–70.

27. Thomson, J. J. On Rays of Positive Electricity. *Phil. Mag. Series 6*, **1907**, *13*, 561-575.

28. Pan, Y.; Cotter, R. J. Measurement of initial translational energies of peptide ions in laser desorption/ionization mass spectrometry. *Org. Mass Spectrom*. **1992**, *27*, 3-8.

29. Brown, R. S.; Lennon, J. J. Mass Resolution Improvement by Incorporation of Pulsed Ion Extraction in a Matrix-Assisted Laser Desorption/Ionization Linear Time-of-Flight Mass Spectrometer. *Anal. Chem*. **1995**, *67*, 1998-2003.

30. Vestal, M. L.; Juhasz, P.; Martin, S. A. Delayed extraction matrix-assisted laser desorption time-of-flight mass spectrometry. *Rapid Commun. Mass Spectrom.* **1995**, *9*, 1044-1050.

31. Boesl, U.; Neusser, H. J.; Weinkauf, R.; Schlag, E. W. Multiphoton mass spectrometry of metastables: direct observation of decay in a high-resolution time-of-flight instrument. *J. Phys. Chem*. **1982**, *86*, 4857-4863.

32. Kuehlewind, H.; Neusser, H. J.; Schlag, E. W. Production and unimolecular decay rate of internal energy selected molecular ions in a laser reflectron time-of-flight mass spectrometer. *J. Phys. Chem*. **1984**, *88*, 6104-6106.

33. Aberth, W. An imaging detector system for mass spectrometry. *Int. J. Mass Spectrom. Ion Processes* **1981**, *37*, 379-382.

34. Wiza, J. L. Microchannel plate detectors. *Nucl. Instrum. Methods* **1979**, *162*, 587-601.

35. Karas, M.; Bachmann, D.; Hillenkamp, F., Influence of the wavelength in high-irradiance ultraviolet laser desorption mass spectrometry of organic molecules. *Anal. Chem.* **1985**, *57*, 2935-2939.

36. Karas, M.; Bachmann, D.; Bahr, U.; Hillenkamp, F., Matrix-assisted ultraviolet laser desorption of non-volatile compounds. *Int. J. Mass Spectrom. Ion Processes* **1987**, *78*, 53–68.

37. Karas, M.; Hillenkamp, F., Laser desorption ionization of proteins with molecular masses exceeding 10,000 Daltons. *Anal. Chem.* **1988**, *60*, 2299–2301.

38. Tanaka, K.; Waki, H.; Ido, Y.; Akita, S.; Yoshida, Y.; Yoshida, T., Protein and polymer analyses up to *m/z* 100 000 by laser ionization time-of-flight mass spectrometry. *Rapid Commun. Mass Spectrom*. **1988**, *2*, 151–153.

39. Cotter, R. J., Laser desorption chemical ionization mass spectrometry. *Anal. Chem*. **1980**, *52*, 1767-1770.

40. Kirpekar F; Berkenkamp S; Hillenkamp F., Detection of double-stranded DNA by IR- and UV- MALDI mass spectrometry. *Anal. Chem.* **1999**, *71*, 2334-2339.

41. Schriemer, D. C.; Li, L., Detection of High Molecular Weight Narrow Polydisperse Polymers up to 1.5 Million Daltons by MALDI Mass Spectrometry. *Anal. Chem*. **1996**, *68*, 2721-2725.

42. Hurst, G. B.; Doktycz, M. J.; Britt, P. F.; Vass, A. A.; Buchanan, M. V, Detection and analysis of polymerase chain reaction products by mass spectrometry. *Proc. SPIE Int. Soc. Opt. Eng.* **1997**, *2985*, 120-128.

43. Anhalt, J. P.; Fenselau, C., Identification of bacteria using mass spectrometry. *Anal. Chem.* **1975**, *47*, 219–225.

44. Barshick, S. A.; Wolf, D. A.; Vass, A. A., Differentiation of Microorganisms Based on Pyrolysis-Ion Trap Mass Spectrometry Using Chemical Ionization. *Anal. Chem.* **1999**, *71*, 633–641.

45. DeLuca, S.; Sarver, E. W.; Harrington, P. B.; Voorhees, K. J., Direct analysis of bacterial fatty acids by Curie-point pyrolysis tandem mass spectrometry. *Anal. Chem.* **1990**, *62*, 1465–1472.

46. Weijman, A. C. M., Cell-wall composition and taxonomy of *Cephaloascus fragrans* and some Ophiostomataceae. *J. Microbiol. Serol.* **1976**, *42*, 315–324.

47. Madonna, A. J.; Voorhees, K. J.; Hadfield, T. L.; Hilyard, E. J., Investigation of Cell Culture Media Infected with Viruses by Pyrolysis Mass Spectrometry: Implications for Bioaerosol Detection. *J. Am. Soc. Mass Spectrom.* **1999**, *10*, 502–511.

48. Sinha, M. P.; Platz, R. M.; Friedlander, S. K.; Vilker, V. L., Characterization of bacteria by particle beam mass spectrometry. *Appl. Environ. Microbiol.* **1985**, *49*, 1366–1373.

49. Basile, F.; Beverly, M. B.; Voorhees, K. J.; Hadfield, T. L., Pathogenic bacteria: their detection and differentiation by rapid lipid profiling with pyrolysis mass spectrometry. *Trends Anal. Chem.* **1998**, *17*, 95–109.

50. Hendricker, A. D.; Abbas-Hawks, C.; Basile, F.; Voorhees, K. J.; Hadfield, T. L., Rapid chemotaxonomy of pathogenic bacteria using in situ thermal hydrolysis and methylation as a sample preparation step coupled with a field–portable membrane-inlet quadrupole ion trap mass spectrometer. *Int. J. Mass Spectrom.* **1999**, *190/191*, 331–342.

51. Spurny, K. R., *"In Bioaerosols Handbook"* Cox, C. S., Wathes, C. M., Eds; CRC Press: Boca Raton, FL, **1995**; Chapter 17.

52. Fenselau, C.; Demirev, P. A., Characterization of intact microorganisms by MALDI mass spectrometry. *Mass Spectrom. Rev.* **2001**, *20*, 157–171.

53. Demirev, P. A.; Ho, Y.; Ryzhov, V.; Fenselau, C., Microorganism identification by mass spectrometry and protein database searches. *Anal. Chem.* **1999**, *71*, 2732–2738.

54. Wahl, K. L.; Wunschel, S. C.; Jarman, K. H.; Valentine, N. B.; Petersen, C. E.; Kingsley, M. T.; Zartolas, K. A.; Saenz, A. J., Analysis of Microbial Mixtures by Matrix-Assisted Laser Desorption/Ionization Time-of-Flight Mass Spectrometry. *Anal. Chem.* **2002**, *74*, 6191–6199.

55. Yates, J. R., 3rd, Mass spectrometry. From genomics to proteomics. *Trends Genet*. **2000**, *16*, 5–8.

56. Jackson, S. N.; Mishra, S.; Murray, K. K., On-line laser desorption/ionization mass spectrometry of matrix-coated aerosols. *Rapid Commun. Mass Spectrom.* **2004**, *18*, 2041–2045.

57. Kim, J. K.; Jackson, S. N.; Murray, K. K., Matrix-assisted laser desorption/ionization mass spectrometry of collected bioaerosol particles. *Rapid Commun. Mass Spectrom*. **2005**, *19*, 1725–1729.

58. Bahr, U.; Karas, M.; Hillenkamp, F. Analysis of biopolymers by matrix-assisted laser desorption/ionization (MALDI) mass spectrometry. *Fresenius' J. Anal. Chem*. **1994**, *348*, 783-791.

59. Hillenkamp, F.; Karas, M.; Beavis, R. C.; Chait, B. T. Matrix-assisted laser desorption/ionization mass spectrometry of biopolymers. *Anal. Chem*. **1991**, *63*, 1193A-1203A.

60. Weickhardt, C.; Moritz, F.; Grotemeyer, J. Time-of-flight mass spectrometry: State-of the-art in chemical analysis and molecular science. *Mass Spectrom. Rev*. **1996**, *15*, 139-162.

61. Whittal, R. M.; Li, L. High-Resolution Matrix-Assisted Laser Desorption/Ionization in a Linear Time-of-Flight Mass Spectrometer. *Anal. Chem*. **1995**, *67*, 1950-1954.

62. Brown, R. S.; Lennon, J. J. Sequence-specific fragmentation of matrix-assisted laser-desorbed protein/peptide ions. *Anal. Chem*. **1995**, *67*, 3990-3999.

63. Fei, X.; Wei, G.; Murray, K. K. Aerosol MALDI with a Reflectron Time-of-Flight Mass Spectrometer. *Anal. Chem*. **1996**, *68*, 1143-1147.

64. Lindh, I.; Griffiths, W. J.; Bergman, T.; Sjovall, J. Electrospray/collision-induced dissociation of derivatized peptides: studies on a hybrid magnetic sector-orthogonal time-of-flight mass spectrometer. *Int. J. Mass Spectrom. Ion Processes* **1997**, *164*, 71-79.

65. Griffiths, W. J.; Yang, Y.; Sjoevall, J.; Lindgren, J. A. Electrospray/collision-induced dissociation mass spectrometry of mono-, di- and tri-hydroxylated lipoxygenase products, including leukotrienes of the B-series and lipoxins. *Rapid Comm. Mass Spectrom*. **1996**, *10*, 183-196.

66. Rohlfing, A.; Muthing, J.; Pohlentz, G.; Distler, U.; Peter-Katalinic, J.; Berkenkamp, S.; Dreisewerd, K. IR-MALDI-MS analysis of HPTLC-separated phospholipid mixtures directly from the TLC plate. *Anal. Chem*. **2007**, *79*, 5793-808.

67. Fay, L. B.; Newton, A.; Simian, H.; Robert, F.; Douce, D.; Hancock, P.; Green, M.; Blank, I. Potential of Gas Chromatography-Orthogonal Acceleration Time-of-Flight Mass

Spectrometry (GC-oaTOFMS) in Flavor Research. *J. Agric. Food Chem*. **2003**, *51*, 2708-2713.

68. Brown, R. S.; Lennon, J. J. Mass resolution improvement by incorporation of pulsed ion extraction in a matrix-assisted laser desorption/ionization linear time-of-flight mass spectrometer. *Anal. Chem*. **1995**, *67*, 1998-2003.

69. Vestal, M. L.; Juhasz, P.; Martin, S. A. Delayed extraction matrix-assisted laser desorption time-of-flight mass spectrometry. *Rapid Comm. Mass Spectrom*. **1995**, *9*, 1044-1050.

70. Kovtoun, S. V. Mass-correlated delayed extraction in linear time-of-flight mass spectrometers. *Rapid Comm. Mass Spectrom*. **1997**, *11*, 810-815.

71. Wang, B. H.; Dreisewerd, K.; Bahr, U.; Karas, M.; Hillenkamp, F. Gas-phase cationization and protonation of neutrals generated by matrix-assisted laser desorption. *J. Am. Soc. Mass Spectrom*. **1993**, *4*, 393-398.

72. Kaufmann, R.; Chaurand, P.; Kirsch, D.; Spengler, B. Post-source decay and delayed extraction in matrix-assisted laser desorption/ionization-reflectron time-of-flight mass spectrometry. Are there trade-offs? *Rapid Comm. Mass Spectrom*. **1996**, *10*, 1199-1208.

73. Jensen, O. N.; Podtelejnikov, A.; Mann, M. Delayed extraction improves specificity in database searches by matrix-assisted laser desorption/ionization peptide maps. *Rapid Comm. Mass Spectrom*. **1996**, *10*, 1371-1378

74. Tsarbopoulos, A.; Bahr, U.; Pramanik, B. N.; Karas, M. Glycoprotein analysis by delayed extraction and post-source decay MALDI-TOF-MS. *Int. J. Mass Spectrom. Ion Processes* **1997**, *169/170*, 251-261.

75. Amft, M.; Moritz, F.; Weickhardt, C.; Grotemeyer, J. Instrumental measures to enhance the mass resolution in matrix assisted laser desorption/ionization (MALDI) time-of-flight experiments: computational simulations and experimental observations. *Int. J. Mass Spectrom. Ion Processes* **1997**, *169/170*, 661-674.

76. Rousell, D. J.; Dutta, S. M.; Little, M. W.; Murray, K. K., Matrix-free infrared soft laser desorption/ionization. *J. Mass Spectrom.* **2004**, *39*, 1182–1189.

77. Bhattacharya, S. H.; Raiford, T. J.; Murray, K. K., Infrared laser desorption/ionization on silicon. *Anal. Chem.* **2002**, *74*, 2228–2231.

78. Woods, A. S.; Ugarov, M.; Jackson, S. N.; Egan, T.; Wang, H. Y. J.; Murray, K. K.; Schultz, J. A., IR-MALDI-LDI Combined with Ion Mobility Orthogonal Time-of-Flight Mass Spectrometry. *J. Proteome Res*. **2006**, *5*, 1484–1487.

79. Little, M. W.; Laboy, J.; Murray, K. K., Wavelength Dependence of Soft Infrared Laser Desorption and Ionization. *J. Phys. Chem.* **2007**, *111*, 1412–1416.

80. Ata, O. N.; Colak, S.; Copur, M.; Celik, C., Determination of the Optimum Conditions for Boric Acid Extraction with Carbon Dioxide Gas in Aqueous Media from Colemanite Containing Arsenic. *Ind. & Eng. Chem. Res.* **2000**, *39*, 488–493.

81. Hejazi, P.; Vasheghani-Farahani, E.; Yamini, Y., Supercritical fluid disruption of Ralstonia eutropha for poly(β-hydroxybutyrate) recovery. *Biotechnol. Prog*. **2003**, *19*, 1519–1523.

82. Jackson, S. N.; Kim, J. K.; Laboy, J. L.; Murray, K. K., Particle formation by infrared laser ablation of glycerol: implications for ion formation. *Rapid Commun. Mass Spectrom.* **2006**, *20*, 1299–1304.

83. Thomas, J. J.; Shen, Z.; Crowell, J. E.; Finn, M. G.; Siuzdak, G., Desorption/ionization on silicon (DIOS): a diverse mass spectrometry platform for protein characterization. *Proc. Natl. Acad. Sci. U. S. A.* **2001**, *98*, 4932–4937.

84. Thomas, J. J.; Shen, Z.; Blackledge, R.; Siuzdak, G., Desorption-ionization on silicon mass spectrometry: an application in forensics. *Anal. Chim. Acta* **2001**, *442*, 183–190.

85. Shen, Z.; Thomas, J.J.; Averbuj, C.; Broo, K. M.; Engelhard, M.; Crowell, J. E.; Finn, M. G.; Siuzdak, G., Porous Silicon as a Versatile Platform for Laser Desroption/Ionization Mass Spectrometry. *Anal. Chem*. **2001**; *73*, 612–619.

86. Cha, S.; Yeung, E. S. Colloidal Graphite-Assisted Laser Desorption/Ionization Mass Spectrometry and MSn of Small Molecules. 1. Imaging of Cerebrosides Directly from Rat Brain Tissue. *Anal. Chem*. **2007**, *79*, 2373-2385.

87. Dale, M. J.; Knochenmuss, R.; Zenobi, R. Graphite/Liquid Mixed Matrices for Laser Desorption/Ionization Mass Spectrometry. *Anal. Chem*. **1996**, *68*, 3321-3329.

88. Li, X.; Wilm, M.; Franz, T., Silicone/graphite coating for on-target desalting and improved peptide mapping performance of matrix-assisted laser desorption/ionization-mass spectrometry targets in proteomic experiments. *Proteomics* **2005**, *5*, 1460–1471.

89. Evans-Nguyen, K. M.; Tao, S.-C.; Zhu, H.; Cotter, R. J. Protein Arrays on Patterned Porous Gold Substrates Interrogated with Mass Spectrometry: Detection of Peptides in Plasma. *Anal. Chem*. **2008**, *ASAP Article*.

90. Xu, Y.; Watson, J. T.; Bruening, M. L. Patterned Monolayer/Polymer Films for Analysis of Dilute or Salt-Contaminated Protein Samples by MALDI-MS. *Anal. Chem*. **2003**, *75*, 185-190.

91. Hu, L.; Xu, S.; Pan, C.; Yuan, C.; Zou, H.; Jiang, G. Matrix-Assisted Laser Desorption/Ionization Time-of-Flight Mass Spectrometry with a Matrix of Carbon Nanotubes for the Analysis of Low-Mass Compounds in Environmental Samples. *Environ. Sci. Technol*. **2005**, *39*, 8442-8447.

92. Ugarov, M. V.; Egan, T.; Khabashesku, D. V.; Schultz, J. A.; Peng, H.; Khabashesku, V.

N.; Furutani, H.; Prather, K. S.; Wang, H.-W. J.; Jackson, S. N.; Woods, A. S. MALDI Matrices for Biomolecular Analysis Based on Functionalized Carbon Nanomaterials. *Anal. Chem*. **2004**, *76*, 6734-6742.

93. Xu, S.; Li, Y.; Zou, H.; Qiu, J.; Guo, Z.; Guo, B. Carbon Nanotubes as Assisted Matrix for Laser Desorption/Ionization Time-of-Flight Mass Spectrometry. *Anal. Chem*. **2003**, *75*, 6191-6195.

94. Schuerenberg, M.; Luebbert, C.; Eickhoff, H.; Kalkum, M.; Lehrach, H.; Nordhoff, E. Prestructured MALDI-MS Sample Supports. *Anal. Chem*. **2000**, *72*, 3436-3442.

95. Nordhoff, E.; Schurenberg, M.; Thiele, G.; Lubbert, C.; Kloeppel, K. D.; Theiss, D.; Lehrach, H.; Gobom, J., Sample preparation protocols for MALDI-MS of peptides and oligonucleotides using prestructured sample supports. *Int. J. Mass Spectrom*. **2003**, *226*, 163–180.

96. Gundry, R. L.; Edward, R.; Kole, T. P.; Sutton, C.; Cotter, R. J., Disposable Hydrophobic Surface on MALDI Targets for Enhancing MS and MS/MS Data of Peptides. *Anal. Chem*. **2005**, *77*, 6609–6617.

97. Wei, J.; Buriak, J. M.; Siuzdak, G., Desorption/Ionization Mass Spectrometry on Porous Silicon. *Nature* **1999**, *399*, 243–246.

98. Lowe, R.; Go, E.; Tong, G.; Voelcker, N. H.; Siuzdak, G., Monitoring EDTA and endogenous metabolite from serum with mass spectrometry. *Spectroscopy* **2005**, *19*, 137–146.

99. Kruse, R. A.; Rubakhin, S. S.; Romanova, E. V.; Bohn, P. W.; Sweedler, J. V., Direct assay of Aplysia tissues and cells with laser desorption/ionization mass spectrometry on porous silicon. *J. Mass Spectrom.* **2001**, *36*, 1317–1322.

100. Kruse, R. A.; Li, X.; Bohn, P. W.; Sweedler, J. V., Experimental Factors Controlling Analyte Ion Generation in Laser Desorption/Ionization Mass Spectrometry on Porous Silicon. *Anal. Chem*. **2001**, *73*, 3639–3645.

101. Luo, G.; Chen, Y.; Daniels, H.; Dubrow, R.; Vertes, A. Internal Energy Transfer in Laser Desorption/Ionization from Silicon Nanowires. *J. Phys. Chem. B* **2006**, *110*, 13381-13386.

102. Kim, Y.; Hurst, G. B.; Doktycz, M. J.; Buchanan, M. V., Improving Spot Homogeneity by Using Polymer Substrates in Matrix-Assisted Laser Desorption/Ionization Mass Spectrometry of Oligonucleotides. *Anal. Chem*. **2001**, *73*, 2617–2624.

103. Enebro, J.; Karlsson, S., Improved matrix-assisted laser desorption/ionisation time-of-flight mass spectrometry of carboxymethyl cellulose. *Rapid Commun. Mass Spectrom*. **2006**, *20*, 3693–3698.

104. Axelsson, J.; Hoberg, A. M.; Waterson, C.; Myatt, P.; Shield, G. L.; Varney, J.; Haddleton, D. M.; Derrick, P. J. Improved reproducibility and increased signal intensity in matrix-assisted laser desorption/ionization as a result of electrospray sample preparation. *Rapid. Commun. Mass Spectrom.* **1997**, *11*, 209-213.

105. Rosinke, B.; Strupat, K.; Hillenkamp, F.; Rosenbusch, J.; Dencher, N.; Krueger, U.; Galla, H. J., Matrix-assisted laser desorption/ionization mass spectrometry (MALDI-MS) of membrane proteins and non-covalent complexes. *J. Mass Spectrom.* **1995**, *30*, 1462–1468.

106. Gruic-Sovulj, I.; Ludemann, H. C.; Hillenkamp, F.; Weygand-Durasevic, I.; Kucan, Z.; Peter-Katalinic, J., Detection of noncovalent tRNA aminoacyl-tRNA synthetase complexes by matrix-assisted laser desorption/ionization mass spectrometry. *J. Biol. Chem*. **1997**, *272*, 32084–32091.

107. Moniatte, M.; Lesieur, C.; Ve´csey-Semje´n, B.; Buckley, J. T.; Pattus, F.; van der Goot, F. G.; van Dorsselaer, A., *Int. J. Mass Spectrom. Ion Processes* **1997**, *169/170*, 179–199.

108. Cohen, L. R. H.; Strupat, K.; Hillenkamp, F., Analysis of quaternary protein ensembles by matrix assisted laser desorption/ionization mass spectrometry. *J. Am. Soc. Mass Spectrom.* **1997**, *8*, 1046–1052.

109. Vogl, T.; Roth, J.; Sorg, C.; Hillenkamp, F.; Strupat, K., Calcium-induced noncovalently linked tetramers of MRP8 and MRP14 detected by ultraviolet matrix-assisted laser desorption/ionization mass spectrometry. *J. Am. Soc. Mass Spectrom.* **1999**, *10*, 1124–1130.

110. Strupat, K.; Sagi, D.; Schäfer, G.; Bönisch, H.; Peter-Katalinic, J., Oligomerisation and Substrate Binding studies of Adenylate Kinase from Sulpholobus Acidocaldarius by MALDI-MS. *Analyst* **2000**, *125*, 563–567.

111. Jarman, K. H.; Cebula, S. T.; Saenz, A. J.; Petersen, C. E.; Valentine, N. B.; Kingsley, M. T.; Wahl, K. L., An algorithm for automated bacterial identification using matrix-assisted laser desorption/ionization mass spectrometry. *Anal. Chem*. **2000**, *72*, 1217–1223.

112. Wang, B. H.; Biemann, K., Matrix-assisted laser desorp-tion/ionization time-of-flight mass spectrometry ofchemically modified oligonucleotides. *Anal. Chem.* **1994**, *66*, 1918–1924.

113. Gusev, A. I.; Wilkinson, W. R.; Proctor, A.; Hercules, D. M., Improvement of signal reproducibility and matrix/comatrixeffectsinmaldianalysis. *Anal. Chem.* **1995**, *67*, 1034–1041.

114. Latourte, L.; Blais, J. C.; Tabet, J. C.; Cole, R. B., Desorption Behavior and Distributions of Fluorinated Polymers in MALDI and Electrospray Ionization Mass Spectrometry. *Anal. Chem.* **1997**, *69*, 2742–2750.

115. Kim, Y; Hurst, G. B., Study of Matrix and Polymer Substrate in MALDI-TOF Mass Spectrometry of DNA. *Microchem. J.* **2001**, *70*, 219–228.

116. Masoud, Z. M.; Elmar, H.; Andreas, T., Qualitative and quantitative analysis of low molecular weight compounds by ultraviolet matrix-assisted laser desorption/ionization mass spectrometry using ionic liquid matrices. *Rapid Commun. Mass Spectrom.* **2004**, *18*, 141–148.

117. Medzihradszky, K. F.; Campbell, J. M.; Baldwin, M. A.; Falick, A. M.; Juhasz, P.; Vestal, M. L.; Burlingame, A. L., The Characteristics of Peptide Collision-Induced Dissociation Using a High-Performance MALDI-TOF/TOF Tandem Mass Spectrometer. *Anal. Chem.* **2000**, *72*, 552–558.

118. Luo G.; Marginean I.; Vertes A., Internal energy of ions generated by matrix-assisted laser desorption/ionization. *Anal. Chem.* **2002**, *74*, 6185–6190.

119. Vertes, A.; Luo, G.; Ye, L.; Chen, Y.; Marginean, I., Laser pulse length dependence of internal energy transfer in UV-MALDI-MS. *Appl. Phys. A* **2004**, *79*, 823–825.

120. Zhang, N.; Doucette, A.; Li, L., Two-layer sample preparation method for MALDI mass spectrometric analysis of protein and peptide samples containing sodium dodecyl sulfate. *Anal. Chem.* **2001**, *73*, 2968–2975.

121. Figueroa, I. D.; Torres, O.; Russell, D. H. Effects of the Water Content in the Sample Preparation for MALDI on the Mass Spectra. *Anal. Chem.* **2001**, *70*, 4527–4533.

122. Momcilovic, D.; Wittgren, B.; Wahlund, K. G.; Karlsson, J.; Brinkmalm, G., Sample preparation effects in matrix-assisted laser desorption/ionisation time-of-flight mass spectrometry of partially depolymerised methyl cellulose. *Rapid Commun. Mass Spectrom.* **2003**, *17*, 1116–1124.

123. Dai, Y.; Whittal, R. M.; Li, L., Two-Layer Sample Preparation: A Method for MALDI-MS Analysis of Complex Peptide and Protein Mixtures. *Anal. Chem.* **1999**, *71*, 1087–1091.

124. Vaidyanathan, S.; Winder, C. L.; Wade, S. C.; Kell, D. B.; Goodacre, R., Sample preparation in matrix-assisted laser desorption/ionization mass spectrometry of whole bacterial cells and the detection of high mass (>20 kDa) proteins. *Rapid Commun. Mass Spectrom.* **2002**, *16*, 1276–1286.

125. Preisler, J.; Hu, P.; Rejtar, T.; Karger, B. L., Capillary Electrophoresis-Matrix-Assisted Laser Desorption/Ionization Time-of-Flight Mass Spectrometry Using a Vacuum Deposition Interface. *Anal. Chem.* **2000**, *72*, 4785–4795.

126. Knochenmuss, R., Ion formation mechanisms in UV-MALDI. *Analyst* **2006**, *131*, 966–986.

127. Karas, M.; Krueger, R., Ion formation in MALDI: The cluster ionization mechanism. *Chem. Rev.* **2003**, *103*, 427–439.

128. Bantscheff, M.; Duempelfeld, B.; Kuster, B., An improved two-step calibration method for matrix-assisted laser desorption/ionization time-of-flight mass spectra for proteomics. *Rapid Commun. Mass Spectrom*. **2002**, *16*, 1892–1895.

129. Landry, F.; Lombardo, C. R.; Smith, J. W., A Method for Application of Samples to Matrix-Assisted Laser Desorption Ionization Time-of-Flight Targets That Enhances Peptide Detection. *Anal. Biochem*. **2000**, *279*, 1–8.

130. Laremore, T. N.; Murugesan, S.; Park, T.-J.; Avci, F. Y.; Zagorevski, D. V.; Linhardt, R. J. Matrix-Assisted Laser Desorption/Ionization Mass Spectrometric Analysis of Uncomplexed Highly Sulfated Oligosaccharides Using Ionic Liquid Matrices. *Anal. Chem*. **2006**, *78*, 1774-1779.

131. Zheng, J.; Li, N.; Ridyard, M.; Dai, H.; Robbins, S. M.; Li, L. Simple and Robust Two-Layer Matrix/Sample Preparation Method for MALDI MS/MS Analysis of Peptides. *J. Proteome Res*. **2005**, *4*, 1709-1716.

132. Hoteling, A. J.; Erb, W. J.; Tyson, R. J.; Owens, K. G. Exploring the Importance of the Relative Solubility of Matrix and Analyte in MALDI Sample Preparation Using HPLC. *Anal. Chem*. **2004**, *76*, 5157-5164.

133. McComb, M. E.; Perlman, D. H.; Huang, H.; Costello, C. E., Evaluation of an on-target sample preparation system for MALDI-TOF mass spectrometry in conjunction with normal-flow peptide HPLC for peptide mass fingerprint analyses. *Rapid Commun. Mass Spectrom*. **2007**, *21*, 44–58.

134. Taguchi, G., *"Introduction to quality engineering. Designing quality into products and processes"* American Supplier Institute: Dearbon, MI, 1986.

135. Shadpour, H.; Edrissi, M.; Zanjanchi, M. A., Preparation and characterization of $Co_xMn_mCr_nNi_kFe_{3-(x+m+n+k)}O_4$ ferrites and optimization of their structural and magnetic properties by Taguchi experimental design. *J. of Materials Science: Materials in Electronics* **2002**, *13*, 139–148.

136. Dai, Y.; Whittal, R. M.; Li, L. Confocal Fluorescence Microscopic Imaging for Investigating the Analyte Distribution in MALDI Matrixes. *Anal. Chem*. **1996**, *68*, 2494-2500.

137. Cohen, S. L.; Chait, B. T. Influence of Matrix Solution Conditions on the MALDI-MS Analysis of Peptides and Proteins. *Anal. Chem*. **1996**, *68*, 31-37.

138. Papac, D. I.; Wong, A.; Jones, A. J. S. Analysis of Acidic Oligosaccharides and Glycopeptides by Matrix-Assisted Laser Desorption/Ionization Time-of-Flight Mass Spectrometry. *Anal. Chem*. **1996**, *68*, 3215-3223.

139. Xiang, F.; Beavis, R. C. A method to increase contaminant tolerance in protein matrix-assisted laser desorption/ionization by the fabrication of thin protein-doped polycrystalline films. *Rapid Commun. Mass Spectrom*. **1994**, *8*, 199-204.

140. Xiang, F.; Beavis, R. C. Growing protein-doped sinapic acid crystals for laser desorption: an alternative preparation method for difficult samples. *Org. Mass Spectrom*. **1993**, *28*, 1424-1429.

141. Wu, K. J.; Odom, R. W. Matrix-Enhanced Secondary Ion Mass Spectrometry: A Method for Molecular Analysis of Solid Surfaces. *Anal. Chem*. **1996**, *68*, 873-882.

142. Bai, J.; Liu, Y. H.; Cain, T. C.; Lubman, D. M. Matrix-Assisted Laser Desorption/Ionization Using an Active Perfluorosulfonated Ionomer Film Substrate. *Anal. Chem.* **1994**, *66*, 3423-3430.

143. Mock, K. K.; Sutton, C. W.; Cottrell, J. S. Sample immobilization protocols for matrix-assisted laser-desorption mass spectrometry. *Rapid Commun. Mass Spectrom.***1992**, *6*, 233-238.

144. McCombie, G.; Staab, D.; Stoeckli, M.; Knochenmuss, R. Spatial and Spectral Correlations in MALDI Mass Spectrometry Images by Clustering and Multivariate Analysis. *Anal. Chem*. **2005**, *77*, 6118-6124.

145. Chaurand, P.; Norris, J. L.; Cornett, D. S.; Mobley, J. A.; Caprioli, R. M. New Developments in Profiling and Imaging of Proteins from Tissue Sections by MALDI Mass Spectrometry. *J. Proteome Res*. **2006**, *5*, 2889-2900.

146. Wilm, M.; Mann, M. Analytical Properties of the Nanoelectrospray Ion Source. *Anal. Chem*. **1996**, *68*, 1-8.

147. Nielsen, M. L.; Bennett, K. L.; Larsen, B.; Moniatte, M.; Mann, M. Peptide End Sequencing by Orthogonal MALDI Tandem Mass Spectrometry. *J. Proteome Res*. **2002**, *1*, 63-71.

148. Vorm, O.; Roepstorff, P.; Mann, M. Improved Resolution and Very High Sensitivity in MALDI TOF of Matrix Surfaces Made by Fast Evaporation. *Anal. Chem.* **1994**, 66, 3281-3287.

149. Kussmann, M.; Nordhoff, E.; Rahbek-Nielsen, H.; Haebel, S.; Rossel-Larsen, M.; Jakobsen, L.; Gobom, J.; Mirgorodskays, E.; Kroll-Kristensen, A.; Palm, L.; Roepstorff, P. Matrix-assisted laser desorption/ionization mass spectrometry sample preparation techniques designed for various peptide and protein analytes. *J. Mass Spectrom*. **1997**, *32*, 593-601.

150. Li, L.; Golding, R. E.; Whittal, R. M. Analysis of Single Mammalian Cell Lysates by Mass Spectrometry. *J. Am. Chem. Soc*. **1996**, *118*, 11662-11663.

151. Franze, T.; Weller, M. G.; Niessner, R.; Poeschl, U., Protein Nitration by Polluted Air. *Environ. Sci. Technol.* **2005**, *39*, 1673–1678.

152. Arnold, R. J.; Reilly, J. P., Observation of *Escherichia coli* Ribosomal Proteins and Their Posttranslational Modifications by Mass Spectrometry. *Anal. Biochem.* **1999,** *269,* 105–112.

153. Madonna, A. J.; Basile, F.; Ferrer, I.; Meetani, M. A.; Rees, J. L.; Voorhees, K. J., On-Probe Sample Pretreatment for the Detection of Proteins Above 15 kDa from Whole Cell Bacteria by Matrix-Assisted Laser Desorption/Ionization Time-of-Flight Mass Spectrometry. *Rapid Commun. Mass Spectrom.* **2000,** *14,* 2220–2229.

154. Ivleva, V. B.; Elkin, Y. N.; Budnik, B. A.; Moyer, S. C.; O'Connor, P. B.; Costello, C. E., Coupling Thin-Layer Chromatography with Vibrational Cooling Matrix-Assisted Laser Desorption/Ionization Fourier Transform Mass Spectrometry for the Analysis of Ganglioside Mixtures. *Anal. Chem.* **2004**, *76*, 6484–6491.

155. Li, L.; Garden, R. W.; Romanova, E. V.; Sweedler, J. V., In Situ Sequencing of Peptides from Biological Tissues and Single Cells Using MALDI-PSD/CID Analysis. *Anal. Chem.* **1999**, *71*, 5451–5458.

156. Shaw, E. I.; Moura, H.; Woolfitt, A. R.; Ospina, M.; Thompson, H. A.; Barr, J. R., Identification of Biomarkers of Whole *Coxiella burnetii* Phase I by MALDI-TOF Mass Spectrometry. *Anal. Chem*. **2004**, *76*, 4017–4022.

157. Williams, T. L.; Andrzejewski, D.; Lay, J. O., Jr.; Musser, S. M., Experimental factors affecting the quality and reproducibility of MALDI TOF mass spectra obtained from whole bacteria cells. *J. Am. Soc. Mass Spectrom.* **2003**, *14*, 342–351.

158. Jacobs, A.; Larsson, P. T.; Dahlman, O., Distribution of Uronic Acids in Xylans from Various Species of Soft- and Hardwood As Determined by MALDI Mass Spectrometry. *Biomacromolecules* **2001**, *2*, 979–990.

159. Shang, C.; Shibahara, T.; Hanada, K.; Iwafune, Y.; Hirano, H., Mass Spectrometric Analysis of Posttranslational Modifications of a Carrot Extracellular Glycoprotein. *Biochem.* **2004**, *43*, 6281–6292.

160. Price, N. P. J., Oligosaccharide Structures Studied by Hydrogen-Deuterium Exchange and MALDI-TOF Mass Spectrometry. *Anal. Chem*. **2006**, *78*, 5302–5308.

161. Leonard, R.; Petersen, B. O.; Himly, M.; Kaar, W.; Wopfner, N.; Kolarich, D.; van Ree, R.; Ebner, C.; Duus, J. O.; Ferreira, F.; Altmann, F., Two Novel Types of O- Glycans on the Mugwort Pollen Allergen Art v 1 and Their Role in Antibody Binding. *J. Biol. Chem*. **2005**, *280*, 7932–7940.

162. Van Baar, B. L. M., Characterisation of bacteria by matrix-assisted laser desorption/ionisation and electrospray mass spectrometry. *FEMS Microbiol. Rev*. **2000**, *24*, 193–219.

163. Stowers, M. A.; van Wuijckhuijse, A. L.; Marijnissen, J. C. M.; Scarlett, B.; van Baar, B. L. M.; Kientz, C. E., Application of matrix-assisted laser desorption/ionisation to on-line aerosol time-of-flight mass spectrometry. *Rapid Commun Mass Spectrom.* **2000**, *14*, 829–833.

164. Lay J. O., Jr., MALDI-TOF Mass Spectrometry of Bacteria. *Mass Spectrom. Rev.* 2001, **20**, 172–194.

165. Scholl, P. F.; Leonardo, M. A.; Rule, A. M.; Carlson, M. A.; Antoine, M. D.; Buckley, T. J., The Development of Matrix Assisted Laser Desorption/Ionization Time of Flight Mass Spectrometry for the Detection of Biological Warfare Agent Aerosols. *Johns Hopkins APL Technical Digest* **1999**, *20*, 343–351.

166. Bogan, M. J.; Agnes, G. R., MALDI-TOF-MS Analysis of Droplets Prepared in an Electrodynamic Balance: "Wall-less" Sample Preparation. *Anal. Chem.* **2002**, *74*, 489–496.

167. Siuzdak, G., Probing viruses with mass spectrometry. *J. Mass Spectrom.* **1998**, *33*, 203–211.

168. Claydon, M.A.; Davey, S.N.; Edwards-Jones, V.; Gordon, D.B., The rapid identification of intact microorganisms using mass spectrometry. *Nature Biotechnol.* **1996**, *14*, 1584–1586.

169. Loo, R. R. O.; Loo, J. A. Matrix-Assisted Laser Desorption/Ionization-Mass Spectrometry of Hydrophobic Proteins in Mixtures Using Formic Acid, Perfluorooctanoic Acid, and Sorbitol. *Anal. Chem*. **2007**, *79*, 1115-1125.

170. Arnold, R. J.; Reilly, J. P., Fingerprint Matching of *E. coli* Strains with Matrix-assisted Laser Desorption/Ionization Time-of-Flight Mass Spectrometry of Whole Cells using a Modified Correlation Approach. *Rapid Commun Mass Spectrom.* **1998**, *12*, 630–636.

171. Arnold, R. J.; Karty, J. A.; Ellington, A. D.; Reilly, J. P., Monitoring the Growth of a Bacteria Culture by MALDI-MS of Whole Cells". *Anal. Chem.* **1999**, *71*, 1990–1996.

172. Jones, J. J.; Stump, M. J.; Fleming, R. C.; Lay, J. O.; Wilkins, C. L., Investigation of MALDI-TOF and FT-MS Techniques for Analysis of *Escherichia coli* Whole Cells. *Anal. Chem.* **2003**, *75*, 1340–1347.

173. Stoeckli, M.; Farmer, T. B.; Caprioli, R. M., Automated Mass Spectrometry Imaging with a Matrix-Assisted Laser Desorption Ionization Time-of-Flight Instrument. *J. Am. Soc. Mass Spectrom.* **1999,** *10,* 67–71.

174. Li, L.; Garden, R. W.; Sweedler, J. V., Single-Cell MALDI: A New Tool for Direct Peptide Profiling. *Trends Biotechnol.* **2000,** *18,* 151–160.

175. Stoeckli, M.; Chaurand, P.; Hallahan, D. E.; Caprioli, R. M., Imaging Mass Spectrometry: A New Technology for the Analysis of Protein Expression in Mammalian Tissues. *Nat. Med.* **2001,** *7,* 493–496.

176. Chaurand, P.; Sanders, M. E.; Jensen, R. A.; Caprioli, R. M., Proteomics in diagnostic pathology: profiling and imaging proteins directly in tissue sections. *Am. J. Pathol.* **2004**, *165*, 1057–1068.

177. Savina, M. R.; Lykke, K. R., Microscopic Chemical Imaging with Laser Desorption Mass Spectrometry. *Anal. Chem*. **1997**, *69*, 3741.

178. Luxembourg, S. L.; Mize, T. H.; McDonnell, L. A.; Heeren, R. M. A., High-Spatial Resolution Mass Spectrometric Imaging of Peptide and Protein Distributions on a Surface. *Anal. Chem*. **2004**, *76*, 5339–5344.

179. Spengler, B.; Hubert, M., Scanning microprobe matrix-assisted laser desorption ionization (SMALDI) mass spectrometry: instrumentation for sub-micrometer resolved LDI and MALDI surface analysis. *J. Am. Soc. Mass Spectrom.* **2002**, *13*, 735–748.

180. Marsha C. Galicia; Akos Vertes; John H. Callahan., Atmospheric Pressure Matrix-Assisted Laser Desorption/Ionization in Transmission Geometry. *Anal. Chem.* **2002**, *74*, 1891–1895.

181. Vertes, A.; Balazs, L.; Gijbels, R., Matrix-assisted laser desorption of peptides in transmission geometry. *Rapid Commun. Mass Spectrom.* **1990**, *4*, 263–266.

182. Ehring, H.; Costa, C.; Demirev, P.; Sunqvist, B., Photochemical versus thermal mechanisms in matrix-assisted laser desorption/ionization probed by back side desorption. *Rapid Commun. Mass Spectrom.* **1996**, *10*, 821–824.

183. Schuerenberg, M.; Schulz, T.; Dreisewerd, K.; Hillenkamp, F., Matrix-assisted laser desorption/ionization in transmission geometry: instrumental implementation and mechanistic implications. *Rapid Commun. Mass Spectrom*. **1996**, *10*, 1873–1880.

184. Lennon, J. D., III; Glish, G. L., A MALDI probe for mass spectrometers. *Anal. Chem.* **1997**, *69*, 2525–2529.

185. Perez, J.; Petzold, C. J.; Watkins, M. A.; Vaughn, W. E.; Kenttamaa, H. I., Laser desorption in transmission geometry inside a Fourier-transform ion cyclotron resonance mass spectrometer. *J. Am. Soc. Mass Spectrom.* **1999**, *10*, 1105–1110.

186. Little, M. W.; Kim, .J. K.; Murray, K. K., Two-laser infrared and ultraviolet matrix-assisted laser desorption/ionization. *J. Mass Spectrom.* **2003**, *38*, 772–777.

187. Vestal, M. L. Methods of Ion Generation. *Chem. Rev*. **2001**, *101*, 361-376.

188. Zhang, H.; Cha, S.; Yeung, E. S. Colloidal Graphite-Assisted Laser Desorption/Ionization

MS and MSn of Small Molecules. 2. Direct Profiling and MS Imaging of Small Metabolites from Fruits. *Anal. Chem*. **2007**, *79*, 6575-6584.

189. Dreisewerd, K.; Lemaire, R.; Pohlentz, G.; Salzet, M.; Wisztorski, M.; Berkenkamp, S.; Fournier, I. Molecular Profiling of Native and Matrix-Coated Tissue Slices from Rat Brain by Infrared and Ultraviolet Laser Desorption/Ionization Orthogonal Time-of-Flight Mass Spectrometry. *Anal. Chem*. **2007**, *79*, 2463-2471.

190. Vogel, A.; Lorenz, K.; Horneffer, V.; Huettmann, G.; von Smolinski, D.; Gebert, A. Mechanisms of laser-induced dissection and transport of histologic specimens. *Biophys. J*. **2007**, *93*, 4481-4500.

191. Allwood, D. A.; Dreyfus, R. W.; Perera, I. K.; Dyer, P. E., UV Optical Absorption of Matrices Used for Matrix-assisted Laser Desorption/Ionization. *Rapid Commun. Mass Spectrom.* **1996**, *10*, 1575–1578.

192. Xu, J; Whitten, W. B.; Ramsey, J. M., Space Charge Effects on Resolution in a Miniature Ion Mobility Spectrometer. *Anal. Chem.* **2000**, *72*, 5787–5791.

193. Xu, J; Whitten, W. B.; Ramsey, J. M., A miniature ion mobility spectrometer. *Int. J. Ion Mobil. Spectrom.* **2002**, *5*, 207–214.

194. Xu, J; Whitten, W. B.; Ramsey, J. M., Pulsed-Ionization Miniature Ion Mobility Spectrometer. *Anal. Chem.* **2003**, *75*, 4206–4210.

195. Clemmer, D. E.; Jarrold, M. F., Ion mobility measurements and their applications to cluster and biomolecules. *J. Mass Spectrosc.* **1997**, *32*, 577–592.

196. Wu, C.; Siems, W. F.; Klasmeier, J.; Hill, H.H., Separation of isomeric peptides using electrospray ionization/highresolution ion mobility spectrometry. *Anal. Chem.* **2000**, *72*, 391–395.

197. Wyttenbach, T.; Kemper, P. R.; Bowers, M. T., Design of a new electrospray ion mobility mass spectrometer. *Int. J. Mass Spect.* **2001**, *212*, 13–23.

198. Couterman, A. E.; Clemmer, D. E., Large anhydrous polyalanine ions: evidence for extended helices and onset of a more compact state. *J. Am. Chem. Soc.* **2001**, *123*, 1490–1498.

199. Ruotolo, B. T.; Gillig, K. J.; Woods, A. S.; Egan, T. F.; Ugarov, M. V.; Schultz, J. A.; Russell, D. H., Analysis of phosphorylated peptides by ion mobility-mass spectrometry. *Anal. Chem.* **2004**, *76*, 6727–6733.

200. Stone, E. G.; Gillig, K. J.; Ruotolo, B. T.; Russell, D. H., Optimization of a matrix-assisted laser desorption ionization-ion mobility-surface induced dissociation-orthogonal-time-of-flight mass spectrometer: Simultaneous Acquisition of Multiple correlated MS1and MS2 Spectra. *Int. J. Mass Spect.* **2001**, *212*, 519–531.

201. Becker, C. H.; Jusinski, L. E.; Moro, L., Infrared laser-induced desorption of neutral organic compounds from frozen aqueous solution followed by single photon ionization. *Int. J. Mass Spectrom. Ion Processes* **1990**, *95*, R1–R4.

202. Jarrold, M. F., Peptides and proteins in the vapor phase. *Annu. Rev. Phys. Chem*. **2000**, *51*, 179–207.

203. Wu, C.; Siems, W. F.; Asbury, G. R.; Hill, H. H., Jr., Electrospray Ionization High-Resolution Ion Mobility Spectrometry-Mass Spectrometry. *Anal. Chem.* **1998**, *70*, 4929–4938.

204. Ruotolo, B.T.; Gillig, K.J.; Stone, E.G.; Russell, D.H.; Fuhrer, K.; Gonin, M.; Schultz, J.A., Analysis of protein mixtures by matrix-assisted laser desorption ionization-ion mobility-orthogonal-time-of-flight mass spectrometry. *Int. J. Mass Spectrom*. **2002**, *219*, 253–263.

205. Stone, E. G.; Gillig, K. J.; Ruotolo, B.; Fuhrer, K.; Gonin, M.; Schultz, A.; Russell, D. H., Surface-Induced Dissociation on a MALDI-Ion Mobility-Orthogonal Time-of-Flight Mass Spectrometer: Sequencing Peptides from an "In-Solution" Protein Digest. *Anal. Chem*. **2001**, *73*, 2233–2238.

206. Henderson, S. C.; Valentine, S. J.; Counterman, A. E.; Clemmer, D. E., ESI/Ion Trap/Ion Mobility/Time-of-Flight Mass Spectrometry for Rapid and Sensitive Analysis of Biomolecular Mixtures. *Anal. Chem.* **1999**, *71*, 291–301.

207. Gillig, K. J.; Ruotolo, B.; Stone, E. G.; Russell, D. H.; Fuhrer, K.; Gonin, M.; Schultz, A. J., Coupling High-Pressure MALDI with Ion Mobility/Orthogonal Time-of-Flight Mass Spectrometry. *Anal. Chem*. **2000**, *72*, 3965–3971.

208. Woods, A. S.; Ugarov, M.; Egan, T.; Koomen, J.; Gillig, K. J.; Fuhrer, K.; Gonin, M.; Schultz, J. A., Lipid/Peptide/Nucleotide Separation with MALDI-Ion Mobility-TOF MS, *Anal. Chem*. **2004**, *76*, 2187–2195.

209. Jackson, S. N.; Ugarov, M.; Egan, T.; Post, J. D.; Langlais, D.; Schultz, J. A.; Woods, A. S., MALDI-ion mobility-TOFMS imaging of lipids in rat brain tissue. *J. Mass Spectrosc.* **2007**, *42*, 1093–1098.

210. Ruotolo, B. T.; Verbeck, G. F., IV; Thomson, L. M.; Woods, A. S.; Gillig, K. J.; Russell, D. H., Distinguishing between Phosphorylated and Nonphosphorylated Peptides with Ion Mobility-Mass Spectrometry. *J. Proteome Res*. **2002**, *1*, 303–306.

211. McLean, J. A.; Russell, D. H., Sub-Femtomole Peptide Detection in Ion Mobility-Time-of-Flight Mass Spectrometry Measurements. *J. Proteome Res*. **2003**, *2*, 427–430.

212. Madonna, A. J.; Voorhees, K. J.; Taranenko, N. I.; Laiko, V. V.; Doroshenko, V. M., Detection of cyclic lipopeptide biomarkers from Bacillus species using atmospheric pressure matrix-assisted laser desorption/ionization mass spectrometry. *Anal. Chem.* **2003**,

*75*, 1628–1637.

213. Koumoutsi, A.; Chen, X. H.; Henne, A.; Liesegang, H.; Hitzeroth, G.; Franke, P.; Vater, J.; Borriss, R., Structural and functional characterization of gene clusters directing nonribosomal synthesis of bioactive cyclic lipopeptides in Bacillus amyloliquefaciens strain FZB42. *J. Bacteriol.* **2004**, *186*, 1084–1096.

## APPENDIX A. CALIBRATION STANDARD KITS

The peptides and proteins mass information in the calibration standard kits purchased from Bruker Daltonics, Inc. These kits were used for an external calibration for all mass spectra obtained in this research, otherwise, it is noted in the description.

| **Peptide calibration standard** | **$[M+H]^+$ Mono isotopic** | **$[M+H]^+$ Average** |
|---|---|---|
| Angiotensin II | 1,046.5418 | 1,047.19 |
| Angiotensin I | 1,296.6848 | 1,297.49 |
| Substance P | 1,347.7354 | 1,348.64 |
| Bombesin | 1,619.8223 | 1,620.86 |
| ACTH clip 1-17 | 2,093.0862 | 2,094.43 |
| ACTH clip 18-39 | 2,465.1983 | 2,466.68 |
| Somatostatin 28 | 3,147.4710 | 3,149.57 |
| **Protein calibration standard I** | **$[M+2H]^{2+}$ Average** | **$[M+H]^+$ Average** |
| Insulin | | 5,734.51 |
| Ubiquitin I | | 8,565.76 |
| Cytochrome c | 6,180.99 | 12,360.97 |
| Myoglobin | 8,476.65 | 16,952.30 |
| **Protein calibration standard II** | **$[M+2H]^{2+}$ Average** | **$[M+H]^+$ Average** |
| Trypsinogen | | 23,982 |
| Protein A | 22,307 | 44,613 |
| Albumin-Bovine (BSA) | approx. 33.3 kDa | approx. 66.5 kDa |

## APPENDIX B. LETTERS OF PERMISSION



John Wiley & Sons Ltd
The Atrium, Southern Gate, Chichester,
West Sussex, PO19 8SQ, UK

Tel: +44 (0)1243 770649 (direct)
Fax: +44 (0)1243 770620 (direct)
Email: permreq@wiley.co.uk

# FAX MESSAGE

| | |
|---|---|
| **To:** | Jae-Kuk Kim, Professor Kermit Murray's Research Group<br>Department of Chemistry, Louisiana State University<br>232 Choppin Hall, Baton Rouge, LA 70803<br>USA |
| **Fax No:** | **001 225 578 3458** /001 225 578 4424 |
| **Our Ref:** | |
| **Your Ref:** | |
| **From:** | Duncan James, Permissions Coordinator |
| **Date:** | **10 October 2007** |
| **No. of pages:** | **4** *(including this page)* |

Dear Jae-Kuk Kim

**RE: Attached permission requests**

Thank you for your permission requests.

Permission is hereby granted to reproduce the articles requested as part of the specified thesis. The articles may be incorporated into the specified thesis only and may not be stored separately or made available independently from the thesis in any way.

Any third party material is expressly excluded from this permission. If any material appears within these articles with credit to another source, authorisation from that source must be obtained.

This permission does not include the right to grant others permission to reproduce this material. Please note that Wiley does not permit the placing of journal articles into open-access repositories.

Proper credit must be given to our publication.

Credit must include the following components:
Title of the Work, Author(s) and/or Editor(s) Name(s). Copyright year. © John Wiley & Sons Limited. Reproduced with permission.

Yours sincerely

Duncan James.

*Duncan James*
Permissions Coordinator

Subject: Copyright Permission Request for Dissertation

To Copyright Permission Department:

I am sending this letter to you to formally request permission to use texts and figures from a publication under one of your journals in which I am the author/co-author. The information will be used in my dissertation for graduating with a Ph.D. in Chemistry at Louisiana State University. I am trying to finish the dissertation by September 28, 2007 so if possible, I am requesting the permission by this date. Louisiana State University requires copyright permission from the publisher to use a published article as a chapter or in part of dissertation. The following information identifies which article I am referring and contact information is listed below.

Little, Mark W.; Kim, Jae-Kuk; Murray, Kermit K. Two-laser infrared and ultraviolet matrix-assisted laser desorption/ionization., Journal of Mass Spectrometry, 2003, 38(7), 772-777. Publisher: John Wiley & Sons Ltd., CODEN: JMSPFJ, ISSN: 1076-5174.

Louisiana State University uses the Electronic Thesis/Dissertation (ETD) system to display finished dissertations to others outside of the university through UMI/ProQuest publication services. More information about this process can be found at the following website.

http://etd.lsu.edu/submit/letter.htm

Thank you in advance for your help and I'm looking forward to hearing you soon.

Sincerely,

Jae-Kuk Kim
Prof. Kermit Murray's Research Group
Department of Chemistry
Louisiana State University
232 Choppin Hall
Baton Rouge, LA 70803
Office: 225-578-3385
Fax: 225-578-3458
Email: jkim13@lsu.edu

Subject: Copyright Permission Request for Dissertation

To Copyright Permissions Department:

I am sending this letter to you to formally request permission to use texts and figures from a publication under one of your journals in which I am the author/co-author. The information will be used in my dissertation for graduating with a Ph.D. in Chemistry at Louisiana State University. I am trying to finish the dissertation by September 28, 2007 so if possible, I am requesting the permission by this date. Louisiana State University requires copyright permission from the publisher to use a published article as a chapter or in part of dissertation. The following information identifies which article I am referring and contact information is listed below.

Kim, Jae-Kuk; Jackson, Shelley N.; Murray, Kermit K. Matrix-assisted laser desorption/ionization mass spectrometry of collected bioaerosol particles., Rapid Communications in Mass Spectrometry, 2005, 19(12), 1725-1729. Publisher: John Wiley & Sons Ltd., CODEN: RCMSEF, ISSN: 0951-4198.

Louisiana State University uses the Electronic Thesis/Dissertation (ETD) system to display finished dissertations to others outside of the university through UMI/ProQuest publication services. More information about this process can be found at the following website.

http://etd.lsu.edu/submit/letter.htm

Thank you in advance for your help and I'm looking forward to hearing you soon.

Sincerely,

Jae-Kuk Kim
Prof. Kermit Murray's Research Group
Department of Chemistry
Louisiana State University
232 Choppin Hall
Baton Rouge, LA 70803
Office: 225-578-3385
Fax: 225-578-3458
Email: jkim13@lsu.edu

Subject: Copyright Permission Request for Dissertation

To Copyright Permissions Department:

I am sending this letter to you to formally request permission to use texts and figures from a publication under one of your journals in which I am the author/co-author. The information will be used in my dissertation for graduating with a Ph.D. in Chemistry at Louisiana State University. I am trying to finish the dissertation by September 28, 2007 so if possible, I am requesting the permission by this date. Louisiana State University requires copyright permission from the publisher to use a published article as a chapter or in part of dissertation. The following information identifies which article I am referring and contact information is listed below.

Jackson, Shelley N.; Kim, Jae-Kuk; Laboy, Jorge L.; Murray, Kermit K. Particle formation by infrared laser ablation of glycerol: implications for ion formation., Rapid Communications in Mass Spectrometry, 2006, 20(8), 1299-1304. Publisher: John Wiley & Sons Ltd., CODEN: RCMSEF, ISSN: 0951-4198.

Louisiana State University uses the Electronic Thesis/Dissertation (ETD) system to display finished dissertations to others outside of the university through UMI/ProQuest publication services. More information about this process can be found at the following website.

http://etd.lsu.edu/submit/letter.htm

Thank you in advance for your help and I'm looking forward to hearing you soon.

Sincerely,

Jae-Kuk Kim
Prof. Kermit Murray's Research Group
Department of Chemistry
Louisiana State University
232 Choppin Hall
Baton Rouge, LA 70803
Office: 225-578-3385
Fax: 225-578-3458
Email: jkim13@lsu.edu

**From:** Jae-Kuk Kim [mailto:jkim13@lsu.edu]
**Posted At:** 13 September 2007 22:13
**Posted To:** Microsoft Office Outlook Embedded Message
**Conversation:** Copyright Permission Request for Dissertation
**Subject:** Copyright Permission Request for Dissertation

To Whom It May Concern:

I am writing this email to you to formally request permission to use texts and figures from a publication under one of your journals in which I am the author/co-author. The information will be used in my dissertation for graduating with a Ph.D. in Chemistry at Louisiana State University. I am trying to finish the dissertation by September 28, 2007 so if possible, I am requesting the permission by this date. A reply to this email granting permission is all that is required by LSU for dissertation. The following information identifies which article I am referring and contact information is listed at the end of this email.

Hamed Shadpour; Jae-Kuk Kim; Jifeng, Chen. Orthogonal array design for minimizing loss of vitamin $B_9$ in bread., Nutrition and Food Science, 2007, 37(2), 105-114.

Louisiana State University uses the Electronic Thesis/Dissertation (ETD) system to display finished dissertations to others outside of the university through UMI/ProQuest publication services. More information about this process can be found at the following website.

http://etd.lsu.edu/submit/letter.htm

If this email has reached to a wrong person at your publishing company, please reply me with the correct instructions for copyright permission or for ward the email to the correct party. Thank you in advance for your help and I'm looking forward to hearing you soon.

Sincerely,

Jae-Kuk Kim
Department of Chemistry
Louisiana State University
232 Choppin Hall
Baton Rouge, LA 70803
Office: 225-578-3385
Fax: 225-578-3458
Email: jkim13@lsu.edu

**From:** Emily Hall [mailto:EHALL@emeraldinsight.com]
**To:** Jae-Kuk Kim [mailto:jkim13@lsu.edu]
**Sent:** Tuesday, September 18, 2007 3:55 AM
**Subject:** RE: Copyright Permission Request for Dissertation

Dear Jae-Kuk Kim,

Many thanks for your email to permissions@emeraldinsight.com. Please allow me to introduce myself, my name is Emily Hall and I am the point of contact here at Emerald for Permissions, Translations and e-Prints.

As you are the author of this article, then from Emerald's perspective, you do not need formal permission to reuse your own work. However I appreciate that some institutions require formal permission, so for this reason I have included the following statement

**Emerald Group Publishing Limited grants Jae-Kuk Kim permission to reuse his article as detailed below within his dissertation and any other thesis, dissertations or publications of which he is either the author or editor free of charge.**
**Hamed Shadpour; Jae-Kuk Kim; Jifeng, Chen. Orthogonal array design for minimizing loss of vitamin $B_9$ in bread., Nutrition and Food Science, 2007, 37(2), 105-114.**

Good luck with your dissertation,

Kind regards,

Emily Hall
Business Development Manager: Permissions
**Emerald Group Publishing Limited**
***The world's leading publisher of management journals and databases***
---
Tel: +44 (0)1274 785230
Fax: +44 (0)1274 785201
Web: **http://www.emeraldinsight.com**

Emerald Group Publishing Limited
Howard House
Wagon Lane
Bingley
BD16 1WA
*VAT number: GB 665 3593 06*
---

**Karen Buehler**

RECEIVED

APR - 9 2008

ACS COPYRIGHT OFFICE

**From:** Jae-Kuk Kim [jkim13@lsu.edu]
**Sent:** Tuesday, April 08, 2008 7:57 PM
**To:** Copyright
**Subject:** Copyright Permission Request for Dissertation

To Copyright Permission Department:

I am sending this letter to you to formally request permission to use a figure from a publication under one of your journals. The information will be used in my dissertation for graduating with a Ph.D. in Chemistry at Louisiana State University. I am trying to finish the dissertation by April 17, 2008 so if possible, I am requesting the permission by this date. Louisiana State University requires copyright permission from the publisher to use a published article in part of dissertation. The following information identifies which article I am referring and contact information is listed below.

Permission requested to use Figure 1 and the figure caption in page 3008 in the article below.

Suess, David T.; Prather, Kimberly A. Mass Spectrometry of Aerosols. Chemical Reviews (Washington, D. C.) (1999), 99(10), 3007-3035. Publisher: American Chemical Society, CODEN: CHREAY ISSN: 0009-2665

Louisiana State University uses the Electronic Thesis/Dissertation (ETD) system to display finished dissertations to others outside of the university through UMI/ProQuest publication services. More information about this process can be found at the following website.

http://etd.lsu.edu/submit/letter.htm

Thank you in advance for your help and I'm looking forward to hearing you soon.

Sincerely,

Jae-Kuk Kim
Prof. Kermit Murray's Research Group
Department of Chemistry
Louisiana State University
232 Choppin Hall
Baton Rouge, LA 70803
Office: 225-578-3385
Fax: 225-578-3458
Email: jkim13@lsu.edu

**PERMISSION TO REPRINT IS GRANTED BY THE AMERICAN CHEMICAL SOCIETY**

**ACS CREDIT LINE REQUIRED. Please follow this sample: Reprinted with permission from (reference citation). Copyright (year) American Chemical Society.**

**APPROVED BY:** C. Arleen Courtney 4/15/08
**ACS Copyright Office**

☐ **If box is checked, author permission is also required. See original article for address.**

## VITA

Jae-Kuk Kim was born in Kimhae, South-Korea. He had received a Bachelor of Science degree from the department of chemistry, Changwon National University, South-Korea, in February 1997. During his undergraduate study, he had served at the military service; Artillery Corps., from 1992 to 1994 and honorably discharged on December 29, 1994. After graduation, he had extended his study in analytical chemistry with his advisor Dr. Yong-Ill Lee and received a Master of Science degree in February 1999,

He had been employed by the Basic Science Research Institute (BSRI) of Changwon National University in 1999 and worked on instrumentation of low-pressure inductively coupled plasma atomic emission spectrometry (LP-ICP-AES) and laser (1064nm, Nd:YAG) ablation for the determination of transition metals in zinc-based die casting alloys. He had also been employed by Korea Electrotechnology Research Institute (KERI) in 2000 and had investigated the optimum composition of the complex anode/cathode of lithium polymer batteries (LPB) for cellular phone industry.

After a couple of years of employment experiences, he had decided to extend his study at the doctoral program for chemistry at Louisiana State University in 2001 with his advisor Dr. Kermit Murray. During his doctoral program, he worked in the Mass Spectrometry Facility (MSF) at LSU for three years when he gained experience in management and maintenance of a number of mass spectrometers and in analyses of a variety of sample types from industry, hospitals, and universities. He is currently a member of the American Chemical Society (ACS) and the American Society of Mass Spectrometry (ASMS). He has presented his research at seven conferences during the degree program and he co-authored four reviews and was the primary author on one publication. He is currently a candidate for the degree of Doctor of Philosophy in chemistry, which will be awarded at the Summer 2008 Commencement.